



UNIVERSITAT POLITÈCNICA DE CATALUNYA
BARCELONATECH
Escola d'Enginyeria de Barcelona Est

MASTER THESIS

Master's Degree in Advanced Material Science and Engineering

**PATTERNED POLYMERIC SCAFFOLDS FOR
CARDIOVASCULAR APPLICATIONS**



Author: Clàudia Iglesias
Director: Dr. Marta Pegueroles
Co-Director: Victor Chausse
Semester: June 2021



ABSTRACT

Coronary artery disease (CAD) is the principal cause of death in the world. It is the result of plaque accumulation which narrows and blocks artery's lumen. As a solution, percutaneous intervention is a revolutionary technique which introduces a catheter that delivers a balloon at the site of the vessel narrowing. Tubular cardiovascular scaffolds, called stents, are integrated in percutaneous intervention as a support to give the mechanical strength needed to stenotic arteries to allow the blood flow. Generally, these stents are inert and remain into de body of the patient forever.

New generation stents are bioresorbable stents (BRSs) that create a temporary mechanical support to prevent restenosis and vascular recoil. These BRSs would ideally disappear once its main function has been served. In this work, we have fabricated polymeric BRSs by 3D printing. To that end, two different polymers were used for obtaining two different conditions of stents: high molecular PLLA and a PLLA-PCL copolymer. Stents manufacture was carried out by 3D printing through solvent-cast direct-writing (SC-DW) and it has been developed a new 3D printer accessory in order to decrease evaporation rate of the ink while printing. Additionally, patterned BRSs were produced when printed onto micropatterned rotating mandrel in order to obtain an increased endothelial cell adhesion.

Two other concerns of biodegradable materials for stents are presented: the control of degradation rate and the effects of sterilization on physical-chemical and mechanical properties. Therefore, the current project presents an accelerated degradation assay in alkaline medium over 10 days of degradation, which showed an effective and fast way to study hydrolysis erosion of stents. The evaluation of the degradation assay was in the following aspects: changes of morphology, thermal properties and changes in crystallinity, as well as mechanical properties.

Furthermore, BRSs were sterilized through two different methods: gamma radiation and ethylene oxide. After the sterilization process, characterization analysis was performed in order to evaluate their thermal and crystallinity properties, molecular weight changes as well as mechanical properties.

The results of the project are: (1) a new method to improve manufacturing efficiency of stents through 3D printing; (2) the design of a fast and effective accelerated degradation assay and; (3) the selection of the proper sterilization method in order to avoid damage on biodegradable stents properties.



ACKNOWLEDGEMENTS

In the first place, I would like to express my sincere gratitude to Dr. Marta Pegueroles for the opportunity to carry out my master thesis at the Biomaterials, Biomechanics and Tissue Engineering (BBT) research group. For her support, advices and always guiding me along the project.

My grateful thanks to Ph.D Student Victor Chausse, for his constant help as well as for providing me the necessary information and the ideas of this project. I have learnt a lot from him and I really appreciate his patience as well as all the useful critiques and the discussions we made about this research work.

I would also like to thank Ms. Meritxell Molmeneu for her help with the compression testing machine and other laboratory assistance. Thanks to Dr. Inna Keridou, not only for carrying out the NMR analysis but also for her help understanding the results. Dr. Jordi Bou for providing GPC analysis and Mr. Quim Albó for his help building the solvent trap used in this project.

I would also like to extend my thanks to all the members of the BBT research group that have always being very kind and have helped me with all my questions at the laboratory. To all my AMASE-ing colleagues of the master who have always being present, no matter if they are in Luleå, Saarbrücken, Nancy or Barcelona.

Finally, I wish to thank my family and boyfriend to always support and encourage me throughout my study.



GLOSSARY

CAD: Coronary artery disease

PCI: Percutaneous intervention

BMS: Bare metallic stents

DES: Drug-eluting stents

BRS: Bioresorbable stent

PLA: Poly-Lactic Acid

PLLA: Poly-L-Lactic Acid

PDLA: Poly-D-Lactic Acid

M_w: Weight average molecular weight

M_n: Number average molecular weight

PCL: Poly(ϵ -caprolactone)

PLCL: Poly (L-lactide-co- ϵ -caprolactone)

SC-DW: Solvent-cast direct writing

ΔP : Applied extrusion pressure

Q: Flow rate

τ_w : Wall shear stress

$\dot{\gamma}_{New}$: Newtonian shear rate

$\dot{\gamma}_w$: Wall shear rate

n: Rabinowitch-Mooney correction parameter

η_{app} : Apparent viscosity

NaOH: Sodium hydroxide

T_m: Melting temperature

T_g: Glass transition temperature

ΔH_m: Fusion enthalpy

ΔH_m[°]: Fusion enthalpy for 100% crystalline polymer

SEM: Scanning electron microscopy

OM: Optical microscopy

DSC: Differential scanning calorimetry

GPC: Gel permeation chromatography/ Size exclusion chromatography

NMR: Nuclear magnetic resonance

ATR-FTIR: Infrared spectroscopy

γ-sterilization: Gamma radiation sterilization

EtO-sterilization: Ethylene oxide sterilization

Index

ABSTRACT	_____	
ACKNOWLEDGEMENTS	_____	II
GLOSSARY	_____	IV
1. PROJECT PROPOSAL AND OBJECTIVES	_____	1
2. INTRODUCTION	_____	3
2.1. Coronary arteries.....		3
2.2. Coronary artery disease (CAD).....		5
2.3. Medical solutions.....		6
2.4. Cardiovascular stents.....		7
2.4.1. Bare metal stents (BMS).....		7
2.4.2. Drug Eluding Stents (DES).....		8
2.4.3. Bioresorbable stents (BRSs).....		9
2.5. Resorbable materials used in bio-resorbable stents.....		10
2.5.1. Poly (L-lactide) (PLLA).....		10
2.5.2. Poly (L-lactide-co- ϵ -caprolactone) (PLCL).....		11
2.6. BRS design considerations.....		13
2.6.1. Strut diameter.....		13
2.6.2. Recoil.....		13
2.6.3. Resorption time.....		13
2.7. Degradation evaluation for BRS.....		14
2.8. Additive Manufacturing of stents.....		17
2.9. Micropatterned surfaces in stents.....		19
2.10. Sterilization of medical devices made of polymers.....		21
3. MATERIALS AND METHODS	_____	23
3.1. Chemicals and materials.....		23
3.2. Stents fabrication.....		23
3.2.1. Polymer-based ink preparation.....		23
3.2.2. 3D Printing of stents.....		23
3.3. Sterilization of stents.....		26
3.3.1. γ -radiation sterilization.....		26
3.3.2. Ethylene oxide sterilization.....		26
3.4. Characterization techniques.....		27

3.4.1.	Ink characterization	27
3.4.2.	Stents characterization.....	29
4.	RESULTS AND DISCUSSION	36
4.1.	Rheology of the ink	36
4.2.	3D printed stents.....	40
4.3.	3D printed patterned stents	44
4.4.	Accelerated degradation study of the stents	48
4.4.1.	Stents appearance.....	48
4.4.2.	Optical Microscope (OM)	49
4.4.3.	Scanning electron microscopy (SEM).....	50
4.4.4.	pH evolution	54
4.4.5.	% of mass loss.....	54
4.4.6.	Molecular weight.....	55
4.4.7.	Composition change (NMR)	57
4.4.8.	Thermal properties and crystallinity changes.....	59
4.4.9.	Mechanical properties.....	60
4.5.	Stents sterilization technique evaluation	64
4.5.1.	Fourier transformed infrared spectroscopy (ATR-FTIR)	64
4.5.2.	Thermal properties changes	65
4.5.3.	Molecular weight.....	67
4.5.4.	Mechanical properties.....	68
5.	CONCLUSIONS	70
6.	FUTURE WORKS	72
7.	COSTS	73
8.	REFERENCES	74
9.	ANNEX	81

1. PROJECT PROPOSAL AND OBJECTIVES

A new generation of stents made of biodegradable materials that present promising results in solving atherosclerotic problems would be of great benefit for the society. The final goal of BRSs is to recover blood flow after atherosclerosis and facilitate stent surface endothelialisation to finally reabsorb and recover a functional artery. For this reason, previous studies of the Biomaterials, Biomechanics and Tissue Engineering research group analysed the surface modification of *poly-L-Lactic acid* (PLLA) films by patterning and functionalization in order to ameliorate cell response. Patterning and functionalization resulted in improved cell migration of PLLA films. Also, solvent-cast direct-writing (SC-DW) technique has been already showed to be a promising way for polymeric stents manufacturing.

Therefore, the aim of this project is to produce bioresorbable stents (BRSs) with a micropatterned structure made of PLLA or poly(l-lactide-co- ϵ -caprolactone) (PLCL) through SC-DW 3D printing. Additionally, two other objectives are presented: the study of the degradation rate of BRSs and the evaluation of sterilization techniques without damaging material's properties. Thus, degradation studies of BRSs as well as stents characterization techniques before and after sterilization process will be carried out.

The objectives of the present study are defined below:

A. Polymeric ink characterization studies.

The rheology of the polymeric ink solutions used for 3D printing will be evaluated since is an important parameter for SC-DW technology. Injectability assay will be carried out for both developed inks used: PLLA and PLCL. The rheological study will determine apparent viscosity, apparent shear stress and apparent shear rate parameters.

B. Identification of suitable design strategies to avoid fast solvent evaporation.

The polymeric ink is obtained after dissolution of the polymer with a solvent, chloroform; then, fast solvent evaporation during 3D Printing may cause some defects such as less strong junctions between the struts of the stents as well as no completely patterning definition. For this reason, a solvent trap will be designed and built as a 3D Printer accessory with a chloroform reservoir. With this oversaturated chloroform atmosphere, a reduction of solvent evaporation is expected.

C. BRSs fabrication by 3D printing with a modified setup for printing on a cylinder and physico-chemical characterization.

Stents with and without a patterning morphology will be produced in order to study different of the BRSs major concerns.

D. Accelerated degradation study of BRSs.

The design and the performance of an accelerated assay for the stents will be carried out.

E. Evaluation of BRSs properties after sterilization.

Gamma and ethylene oxide sterilization of stents will be done in external and specialised companies. After that, different evaluation methods will be performed.

2. INTRODUCTION

Coronary artery disease (CAD) is the principal cause of death in the world. European Cardiovascular Disease Statistics from 2017 [1], reported 3.9 million deaths a year, or 45% of all deaths. By comparison with the next most common cause of death, cancer, it accounts for just under 1.1 million of deaths in men and just under 900000 deaths in women. Also, it has an annual cost of around € 60 billion corresponding to treatment costs, the informal care costs and productivity losses [2].

CAD is developed when the arteries of the heart cannot deliver enough blood flow to the tissue heart. The decrease of blood flow blocks the delivery of oxygen and nutrients needed for the proper organs operation. CAD is caused by the growth of a plaque material made up of fatty deposits such as cholesterol through the artery. It leads to a progressive narrowing of the lumen of the artery that allows blood flow [2]. Tubular cardiovascular scaffolds called stents are currently the most widely used solution for CAD treatment. They are introduced into coronary arteries to compress the plaque and fully restore blood flow. Stents implantation showed a revolutionary change in coronary artery diseases, however, some challenges are still present. Therefore, research for new solutions for cardiovascular scaffolds are an important issue of global interest.

2.1. Coronary arteries

There are two main coronary arteries called the right coronary artery and the left coronary artery which originate separately from the base of the aorta. Each main coronary artery is 2-4 mm wide and they travel through the surface of the heart and divide into smaller branches that penetrate in the muscular walls of the heart and provide a network of more vessels that allow the blood and therefore the oxygen needed to every cell of the heart [3].

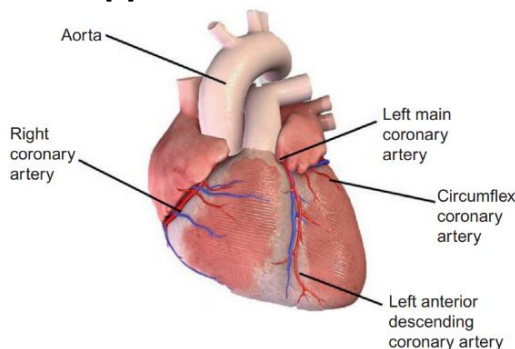


Figure 1. Coronary arteries and the aorta [3].

Left coronary artery is a short vessel that divides into the left anterior descending artery and the left circumflex artery. Right coronary artery gives rise to many branches, its main branch being the posterior descending artery, which travel through the groove between the two ventricles at the back [3].

The coronary artery wall involves three different layers; the inner layer which is called intima, the middle layer called media, and the outer one named the externa as can be shown in *Figure 2*.

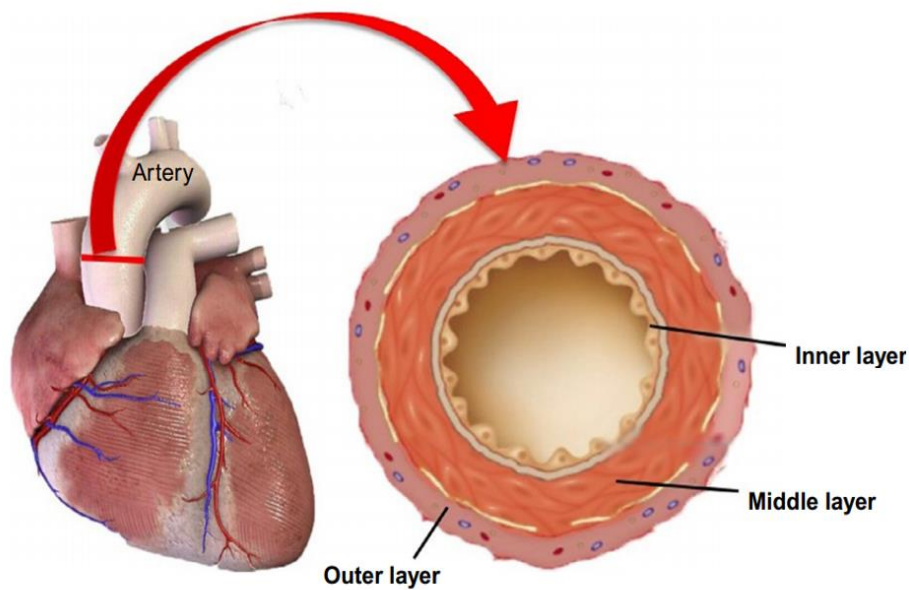


Figure 2 Cross-section of an artery showing inner, middle, and outer layers [3].

- TUNICA INTIMA. It is composed by monolayer of endothelial cells and connective tissue. This layer covers the luminal surface of the arteries.
- TUNICA MEDIA. The middle layer is composed by smooth muscle cells and elastic fibres. The connective tissue is full of collagen, elastin and other elastic fibres. Smooth muscle cells are able to contract and relax. The thickness of the media comprises ranges between 125 and 350 μm . When an atherosclerotic episode occurs, the media is thinner and ranges around 16 and 190 μm .
- TUNICA EXTERNA. The adventitia is composed by fibrous tissue, thus, it is mostly elastin and collagen fibres and fibroblasts. The thickness of the outer layer comprises ranges between 0.1-1 [3].

2.2. Coronary artery disease (CAD)

Atherosclerosis is the result of plaque accumulation which narrows and blocks artery's lumen. Since coronary arteries transport blood to the heart tissue, atherosclerosis can origin serious problems. The reduction of the oxygen and nutrients that arrive to the heart muscle can lead to a heart attack and possibly death. In order to clinically identify this problem, the diameter of the lumen of the artery can be measured with an angiography system. When plaques narrow the artery by more than 60-70 %, patients are at higher risks for acute coronary syndrome [4].

Figure 3 shows atherosclerotic lesion development. Adhesion and migration of monocytes occur at the beginning of atherosclerotic plaque formation. Then, these cells transform into tissue macrophages, which ingest lipids and form fatty deposits. Platelets adhesion generate proliferation of smooth muscle cells in the tunica intima. Then, an atheroma layer is formed by monocytes, lipids, platelets, smooth muscle cells and fibrous connective tissues. These can lead to the progressive narrowing of the lumen of the artery and if no treatment is applied, endothelium can become vulnerable to rupture causing myocardial infarction or potentially stroke.

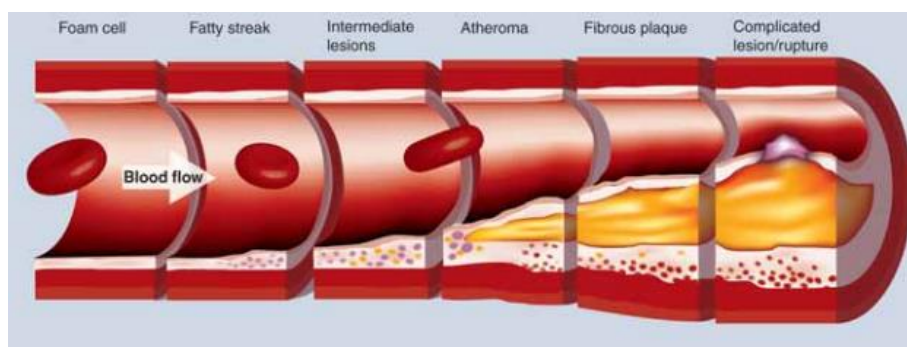


Figure 3. Atherosclerotic lesion development in the artery [5].

Therefore, atherosclerosis can generate two main complications that are defined below:

- STENOSIS. Stenosis is the continuous narrowing of the artery due to a slow growth of the artery. These can lead to the final obstruction of the artery [6].
- THROMBOSIS. Thrombosis is the formation of a blood clot inside the vessel. It is formed when the stability of the atheroma is weakened due to the digestion of the fibrous cap by matrix metalloproteinases. This lead to the plaque rupture, erosion and occlusion of the vessel [3][5].

2.3. Medical solutions

In order to prevent atherosclerosis at early stages, one may introduce lifestyle changes or medicines. Healthy lifestyles changes comprise recommendations such as a proper healthy weight, being physically active or quitting smoking. Some medicines can help to lower blood pressure and decrease the heart's workload or to control high blood cholesterol.

However, when the vessel is damaged is necessary to perform a revascularization procedure. Revascularization means the process where the blood flow is restored. Then, two methods can be performed depending on the severity of atherosclerosis: coronary artery bypass graft or percutaneous coronary intervention (PCI). The first one is performed in patients with complex multivessel disease and diverts blood around narrowed or clogged artery in the heart by using a blood vessel from another part of the body. The second one is used in patients with a less complex disease and consists on the introduction of a catheter that delivers a balloon at the site of the vessel narrowing. This balloon is inflated under pressure, compressing the plaque of fatty deposits in order to fully restore blood flow [2]. *Figure 4* shows the procedure of a percutaneous coronary intervention with a balloon.

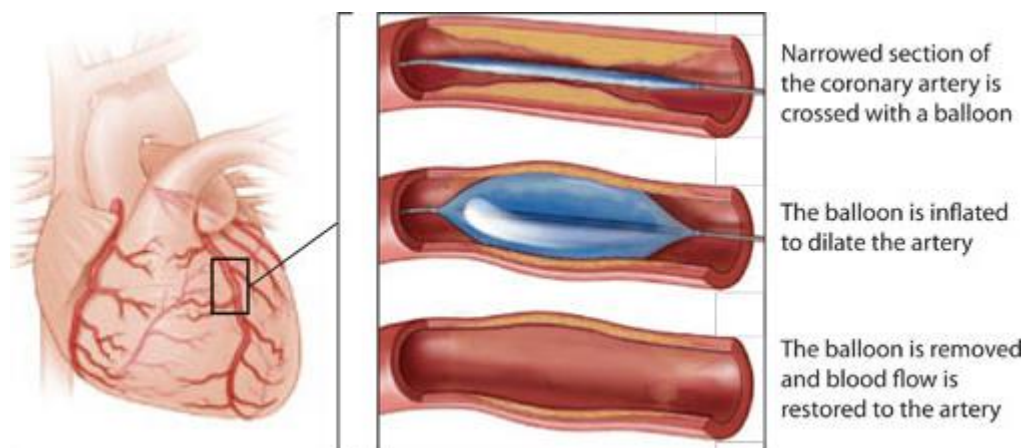


Figure 4. Procedure for percutaneous intervention (PCI) of a balloon [3].

PCI was first performed in the late 1970s and revolutionized the management of coronary artery disease, providing an effective, quick and safe method for many patients. However, there were still some limitations in balloon angioplasty like the decrease in coronary flow during or immediately the intervention (acute vessel closure), removal of the balloon so that arteries returned to their original size (elastic recoil), and the recurrence of a treated coronary artery stenosis over time (restenosis).

Therefore, a scaffold support was proposed as a solution to prevent acute vessel occlusion and restenosis issues after balloon dilatation. These cardiovascular scaffolds called stents, give the mechanical strength needed to the stenotic arteries until the risk of closure is fully removed. *Figure 5* shows the scheme for the coronary stent implantation.

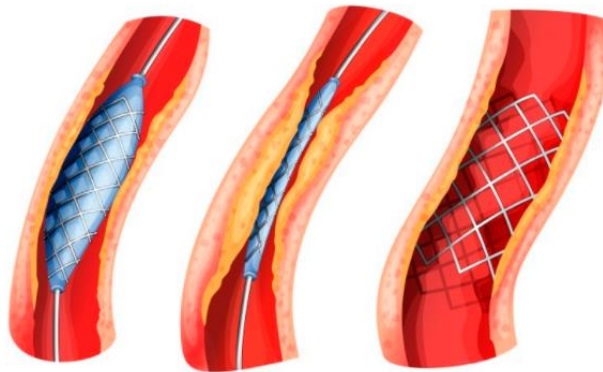


Figure 5. Implantation of a coronary stent for PCI [7].

2.4. Cardiovascular stents

Stents can be divided in 3 different types depending on its generation: bare metal stents (BMS), drug eluting stents (DES), and bioresorbable stents (BRS) [8].

2.4.1. Bare metal stents (BMS)

First, metallic intracoronary stents were used in 1980 as a solution to the coronary artery disease. These BMS represented a really advance in the treatment of coronary artery disease. After balloon angioplasty, a structure remains in the artery walls preventing the artery from restenosis. BMS are generally made of stainless steel and cobalt-chromium alloys for balloon-expandable, and nickel-titanium alloys for self-expanding stents [8].

A metallic stent should have the properties of good flexibility and deliverability, low thrombogenicity, strong radial force, good radio-opacity under X-ray imaging, and good biocompatibility to ensure low rates of neointimal hyperplasia and stent thrombosis during long term follow-up.

In the pre-stent era the occurrence of restenosis ranged between 32–55 % of all angioplasties, and decrease to successively 17–41 % in the BMS era [9]. But it had also some drawbacks such as increased risk of thrombosis due to the high mechanical stress during implantation that destroys the endothelium and restenosis due to the over-proliferation of smooth muscle cells (also called in-stent restenosis).

2.4.2. Drug Eluting Stents (DES)

The introduction of (DES) heralded a major technological breakthrough and had the objective to reduce in-stent restenosis due to smooth muscle cells over-proliferation by providing localised drug delivery. DES have a metal scaffold and the polymer which coats the stent acting as a drug reservoir allowing slow release and the drug. The polymer can be durable or bioresorbable. Durable polymers used are Parylene C, poly(butyl methacrylate) PBMA, poly(ethylene-co-vinyl acetate) PEVA, poly(Styrene-block-IsoButylene-block-Styrene) SIBS or polycarbonate (PC) while biodegradable polymers used were copolymers made of lactic acid stereoisomers and polyglycolide [10]. On the first-generation of DES, stainless steel stents with a strut thickness greater than 130 μm and a polymer coating with antiproliferative drug were used while in the second-generation DES, the platform was changed to metal alloys such as cobalt-chromium or platinum-chromium, which allowed the decrease in strut thickness and more flexibility [11]. DES, especially from second generation, decreased restenosis rate achieving values around 10 % compared with values of 17–41 % for BMS [9].

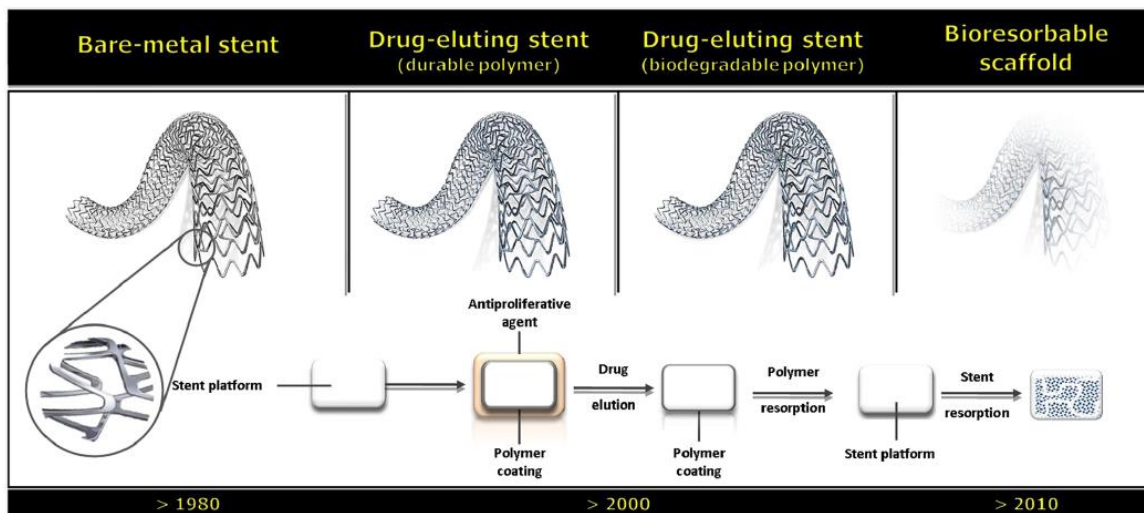


Figure 6. Stents evolution overview [12].

However, it was reported an increased risk of death and myocardial infarction related to late stent thrombosis because of delayed endothelialisation of stent. Late stent thrombosis usually occurs one year after stent implantation because the stent is not completely covered by endothelial cells. The endothelialisation is delayed due to the antiproliferative drug delivered by the stent that inhibits endothelial cell migration to the stent and thus, the inert material is exposed to the blood flow. Then patients should undergo to dual-platelet therapy for more than one year to minimize late stent thrombosis [8]. Finally, BRSs were proposed as a solution to DES drawbacks (*See Figure 6*).

2.4.3. Bioresorbable stents (BRSs)

BRSs are composed by a platform made of a bioresorbable material, coated with a polymer and an antiproliferative drug. Permanent metallic stents drawbacks led to fully BRSs investigations during last decade, representing the fourth revolution in interventional cardiology. The aim is to create a temporary mechanical support in the vessel in order to prevent restenosis and vascular recoil and, at the same time, the degradation of the stent is taking place in order to eliminate the long-term risks related with permanent scaffolds [12].

As permanent metallic DES, BRS provide the local drug delivery and mechanical support in the first 12 months but also are able to reabsorb completely after 24 to 36 months. Then, normal luminal diameter and vasomotor function are restored over years without any possible late inconvenience, which means that the need of long-term dual antiplatelet therapy is significantly reduced.

Recent investigations have shown the advantages of using polylactic acid polymer (PLA) stents, moreover some challenges still exist for first generation PLA BRS. First one, the radial force of a BRS is weaker than the force of DES, so recoil can be a problem because of the rapid absorption. Thus, struts thickness has to be bigger than the other stents generations to maintain radial strength and this might result in incomplete expansion and reduced lumen diameter after implantation. Higher strut thickness of the stents can cause higher flow disturbance on the artery which produce higher probability of thrombotic events [8].

2.5. Resorbable materials used in bio-resorbable stents

Materials used for BRS have to tolerate the biomechanical and biological burdens imposed on a temporary function. Some of the principal materials options for the structure or coating used on stents are: poly(L-lactide) (PLLA), poly(D-lactide) (PDLA), poly(D,L-lactide) (PDLLA), salicylate (SA)/poly anhydride, poly(D,L-lactide-co-glycolide) (PLGA), desaminotyrosine polycarbonate polymer (PTD-PC), cross linked polyester, cross linked polyurethane and magnesium [13].

PLA and its enantiomers are by far the most common bioresorbable material seen in the BRS stent technology because of its mechanical properties, biocompatibility and biodegradability [13].

2.5.1. Poly (L-lactide) (PLLA)

Poly-lactic acid (PLA) is a thermoplastic polymer produced from renewable resources such as sugarcane and corn starch. Currently, it is one of the biopolymers most used in the industry of packaging, biomedical applications such as degradable implants, sutures and scaffolds. PLA exists as two enantiomers (L- and D-). On *Figure 7* both chemical structures of PLA are shown. PLLA is semi-crystalline and has a high mechanical strength, whereas PDLA is essentially amorphous [14].

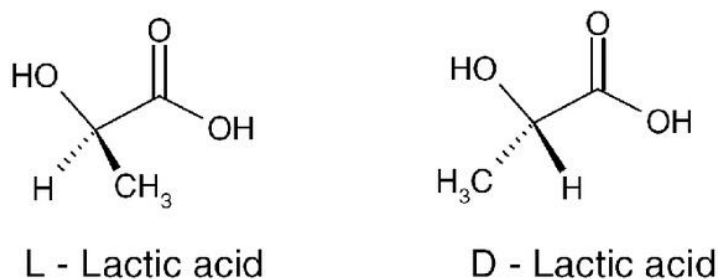


Figure 7. Stereoisomers of lactic acid [14].

PLA can be synthesized through ring-opening polymerization of lactide dimer or direct condensation polymerization of lactic acid monomers. Ring-opening polymerization is mainly used when it comes to high-scale production as it achieves high molecular weight required in structural applications [15]. Molecular weight (M_w , M_n) will be an important consideration not only because of its strength but also for processing and degradation control. Polymerisation of L-lactide or D-lactide results in isotactic, semi-crystalline polymer named PLLA or PDLA respectively. Polymerization of the monomer (D,L-lactide) results in atactic amorphous polymer poly(D,L-lactide) (PDLLA). With different compositions of D- and L-isomer, the physical properties and biodegradability of PLA can be modified.

Due to the CH₃ groups, PLA is highly hydrophobic and therefore has a low degradation rate and a high modulus. Its glass transition temperature (T_g) is typically around 60 °C, it has a low strain rate (5-10 %), a tensile strength around 50-60 MPa and a modulus of generally 2.5 GPa. Because of these characteristics, it accomplishes with the load-bearing orthopaedic requirements as well as cardiovascular applications [13].

PLA can be degraded through different mechanisms such as hydrolysis, oxidation, thermal, microbial, enzymatic, chemical and photodegradative mechanisms. These mechanisms primarily cause main and side chain scissions. In the body, hydrolytic degradation occurs as the polymer is in contact with tissue fluids and the amorphous areas of the polymeric network start to degrade. Degradation considerations are very important when designing an implant structure, also, depending on the shape of the implant, the degradation profile can be greatly influenced.

PLLA in its semi-crystalline form is composed of crystalline lamellae with amorphous tie chains to link these regions (See Figure 8). The amorphous areas would be more susceptible to water penetration.

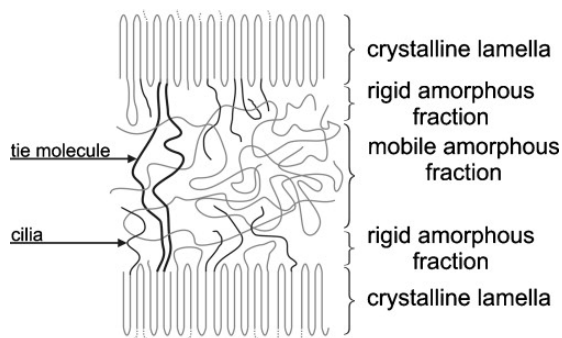


Figure 8. Schematic structure of semi-crystalline polymers [16].

2.5.2. Poly (L-lactide-co-ε-caprolactone) (PLCL)

Poly(ε-caprolactone) (PCL) is a biodegradable, semi-crystalline thermoplastic polyester with a T_m ranging between 57 and 64°C and a T_g of -60°C. It has a tensile strength of 16 MPa and a tensile modulus of 0.4 GPa. This much lower glass-transition temperature helps its biodegradability despite its high degree of crystallinity. Like PLA, it is biodegradable, biocompatible and nontoxic, but it has a slower degradation rate than PLA. PCL is synthesized by ring-opening polymerization of ε-caprolactone monomer with some catalyst like dibutyltin dilaurate. This polymer is one of the softest aliphatic polyesters with a high strain at break. It has high mobility of chain segments and low intermolecular

interactions as a result of a very low melting and glass transition temperature. At low M_w can be either viscous, liquids or hard waxes, while at high M_w it is soft and flexible with low melting point and low glass transition temperature. It is miscible with a variety of polymers and it has no color, thus, it is highly used to be copolymerized with other polymers in order to tune the material properties [13].

One of the main drawbacks of PLLA is its low elongation at break due to the high glass transition temperature and crystallinity. By copolymerization with lower glass-transition temperature polymers, such as PCL, PLA become more flexible. PLCL chemical structure based in PLA and PCL segments, is seen in the image below (Figure 9) [13][17].

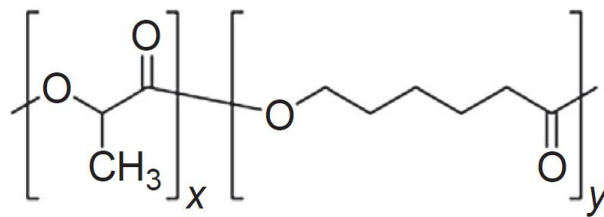


Figure 9. PLCL copolymer chemical structure [17].

There are two main possibilities structures of this copolymer: randomized copolymers and block copolymers. Randomized copolymer consists of a random sequence of PLA and PCL while block copolymers will consist of PLA blocks and PCL blocks.

Copolymerization of lactide (LA) with ϵ -caprolactone (ϵ -CL) is mainly used in order to control mechanical properties, degradation rate and controlled drug-release properties. When synthesizing statistical copolymers, depending on the polymerization conditions and the relative rates of incorporation of each comonomer, copolymers exhibit different chain microstructures following different distributions of sequences. Random PLCL synthesis can be obtained through determined amounts of LA and ϵ -CL simultaneously added in a controlled temperature oil bath [17].

The main application of this copolymer is in structural devices which may add flexibility to their structure. By increasing the caprolactone composition, a considerable reduction of the brittleness in the copolymer can be seen.

Actually, it is reported that there is an increase in the elongation at break and a decrease in Young's modulus as the composition of CL increases as well as a reduction in the T_g [17].

2.6. BRS design considerations

In order to achieve a proper PLLA based stent design, it has to be taken into account the mechanical properties of the building material that will be related with some other properties such as the final stent strut thickness, stent geometry, stent radial strength, recoil behavior and the performance of the device over time [18].

2.6.1. Strut diameter

Thinner struts lead to more flexible devices and reduced cross sectional profiles. Also it is associated with reduced restenosis cases. Too much thickness can create laminar flow disruptions that are associated with increased rates of scaffold thrombosis. Localized turbulent flow increases endothelial shear stress, which negatively affects re-endothelialisation and neointimal coverage of the stent struts, leading to late stent thrombosis. However, it has to be combined with enough thickness in order to have the mechanical properties needed. Therefore, the clear design challenge on stents is to reduce stent strut thickness as much as possible. Therefore, mechanical properties of polymers like PLA would be the limiting factor [2][18] .

2.6.2. Recoil

Stents have to be expanded radially onto the balloon until their maximum diameter. Afterwards, when the balloon is removed the diameter may suffer a little variation, due to elastic recoil. Minimum elastic recoil of a stent has been the focus of attention of the scientists in order to prevent lumen loss and restenosis. Radial strength of the scaffolds is the most important property of a stent in the elastic recoil issues. Big recoils generate flow disruptions, leading to stent restenosis or stent dislodgement and migration along the vessel. On the other hand, recoil of the stent must be resisted to allow the natural tissue to heal properly without reoccurrence of a blockage. BRS present some challenges with gradual losses in radial strength and the ability to resist constructive remodeling long before the stent is fully absorbed. [13].

2.6.3. Resorption time

The functional time is defined as the period of time in which the degradable polymer can maintain its functionality under application conditions, while the disappearance time is the period of time in which the polymer totally degrade. After their functional time, BRS lose their mechanical properties as a result

of the degradation of the material. This degradation process is related to the polymers characteristics and can be monitored by mass loss or molar mass changes [2][18].

In *Figure 10*, a general behavior of the stents over degradation is shown. At time zero the stent is deployed in the human body, therefore, the molecular weight and mass of the stent are at maximum. The first three months correspond to the revascularization period (in red) in which the drug content is released in a controlled rate. M_w of the stent decreases with the stent implantation time. After that, scaffold support decreases followed by mass loss. Finally, in the resorption stage, the molecular weight of the polymer is further reduced by shortening chain oligomers which can be resorbed by the body until the stent fully disappears [18].

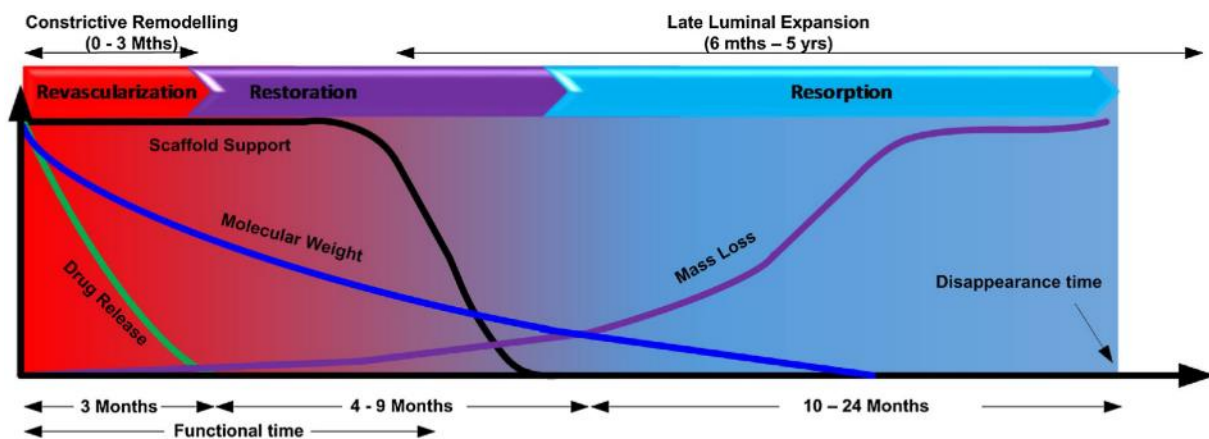


Figure 10. Variation of stents variables over degradation [18].

Although a time of 24 months is shown in the scheme, the real timeframe will depend on the material, design and physiological environment. There are discrepancies regarding the optimal degradation time, though a 6-12 month window seems to be the target for most of the stent developers.

2.7. Degradation evaluation for BRS

Bioresorbable polymers are broadly studied in the medical field for applications where the medical device has to be degraded after accomplishing with its application. Therefore, there is a need to study and evaluate the behavior of these materials and their degradation mechanisms in the body [19]. Actually, the control of its hydrolytic degradation and biodegradation is fundamental for medical applications.

After exposure to moisture, two different types of hydrolysis occur for PLLA: homogeneous or bulk hydrolysis and heterogeneous or surface erosion [20]. The first one occurs simultaneously throughout the entire specimen. Thus, the decrease in M_w , the reduction and in mechanical properties occurs simultaneously throughout the entire specimen. In the second one, hydrolysis occurs in the region near the surface and therefore the core of the material keeps not affected [21]. Thus, a highly decrease on molecular weight will determine bulk hydrolysis while high mass loss will determine surface erosion hydrolysis [22].

Bulk erosion can proceed also with autocatalysis mechanisms on PLA. Autocatalytic degradation results from the hydrolytic cleavage of the ester bonds forming new acidic carboxyl end groups. As the degradation proceeds the soluble oligomers produced close to the surface can escape, while those in the centre cannot diffuse out of the polymer. This results in a higher internal acidity, with the carboxyl end groups catalysing the ester hydrolysis reaction, and a differentiation between the surface and interior degradation rates [23]. *Figure 11* shows the scheme with the different degradation mechanisms of PLA [21].

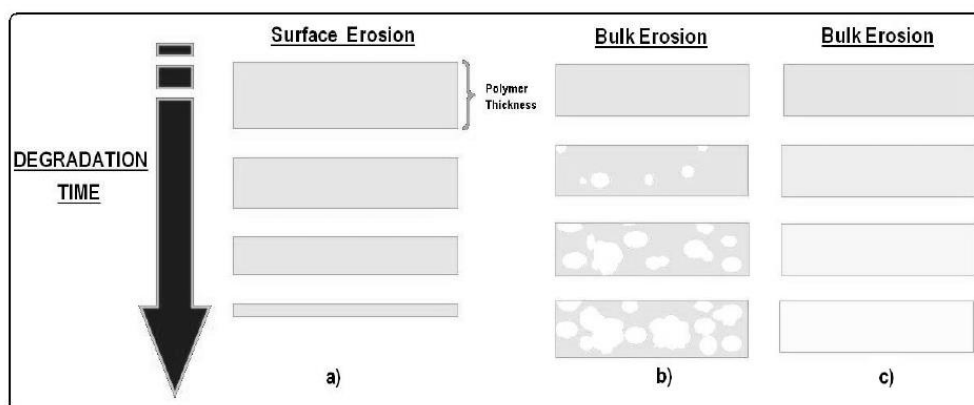


Figure 11. Schematic process of three types of PLA degradation: (a) surface degradation, (b) bulk degradation with autocatalysis and (c) bulk degradation without autocatalysis [21].

There is a general consensus that degradation *in vivo* of PLLA, like all aliphatic polyesters, occurs through random bulk hydrolysis mechanisms of the hydrolytically unstable ester linkage in the polymer's backbone [23]. Then, the degradation products are ultimately metabolized to carbon dioxide and water that are finally eliminated from the body.

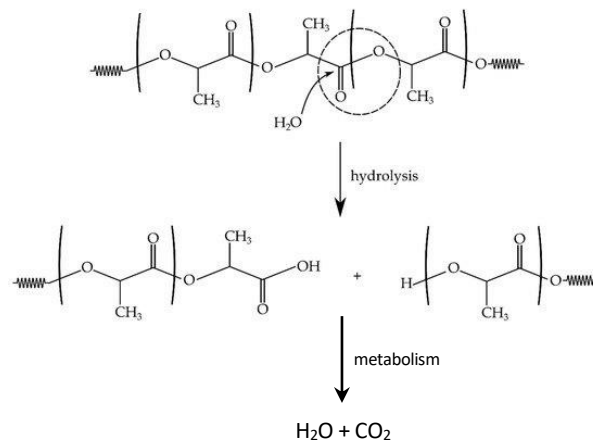


Figure 12. Schematic representation of hydrolysis fragmentation of ester groups of PLA chains with water presence [74].

According to the literature PLA hydrolysis occurs in two stages [23][24]. At the beginning water molecules or corporal fluids interact with the ester linkages of the amorphous areas of the polymer. After that, second stage is characterized by the onset of mass loss and attack of the less accessible crystalline regions.

Li et al. [25] studied degradation of PLLA in a buffer solution at a temperature of 37°C and concluded that degradation occurred more rapidly in the centre than in the surface showing that bulk autocatalytic degradation was the predominant mechanism. Weir et al. [23] studied degradation of PLLA *in vitro* and *in vivo* and bulk degradation without autocatalysis was observed. Then, they concluded that perhaps as polymer crystallinity increases, the importance of the autocatalysis degradation mechanism become less significant.

Depending on the material and its application, degradation assays mimicking physiological conditions can take around 1-5 years or even more. Therefore, accelerating this evaluation process would be obviously beneficial for the study of biomaterials. Some techniques have been studied in order to perform accelerated hydrolysis assays. For example, with the introduction of applied strain [26], introducing enzymes to the degradation medium [27], increasing the temperature of degradation medium [28] or varying pH [21].

Weir et al. [28] studied degradation of PLLA with increased temperature after their studies in non-accelerated conditions. They concluded that degradation at 50°C showed similar mechanisms of bulk degradation to the *in vitro* and *in vivo* degradation mechanisms reported at 37°C.

On the other hand, the use of a solution of sodium hydroxide (NaOH) as the degradation media seems to be an easy and effective way to perform degradation studies of polymers. Woodard et al. [29] reported a comparison of nonaccelerated degradation assay of PCL-PLLA films over 56 weeks in PBS media and an accelerated degradation assay in a solution of NaOH 1M during 120 hours. Also, Lam et al. [22] made a comparison between PCL degradation on PBS media and in NaOH 5M. Both obtained hydrolysis mechanisms in all the conditions, however, nonaccelerated conditions presented bulk erosion behavior while accelerated conditions showed surface erosion mechanisms.

2.8. Additive Manufacturing of stents

Additive Manufacturing, also called 3D Printing, is the technology that enables the creation of three-dimensional objects (3D) by adding layer-upon-layer of material under computer control. This technology represents a solution to the drawbacks of the conventional technologies such as the customization of the design depending on the patient. The main 3D Printing technologies used are Inkjet, Stereolithography (SL), Selective Laser Sintering (SLS), Fused Filament Fabrication (FFF) and solvent-cast direct writing (SC-DW). FFF is a reported technique for the BRS manufacture [30].

FFF, also known as Fused Deposition Modelling (FDM), consists on the extrusion of a hot thermoplastic. The print head is moved under computer control to print the desired geometry. The advantages of this techniques are the relation between cost and efficiency to produce a thermoplastic object, short lead times due to the high availability, the possibility of allowing the production of multi-material objects and the wide range of thermoplastics that can be used. Regarding its drawbacks, one can find the low resolution compared to other 3D printing techniques, the need of a post-processing to soften surfaces for visible layer lines and the anisotropy due to the layer adhesion mechanisms [31].

In general, FFF machines follow Cartesian Coordinates which makes difficult to print tubular geometries. Thus, an innovative technique was reported [30] where some drawbacks of FFF could be avoided. This method consists on the implementation of a rotating mandrel, achieving a 3D printed cylindrical structure following the scheme of *Figure 13*.

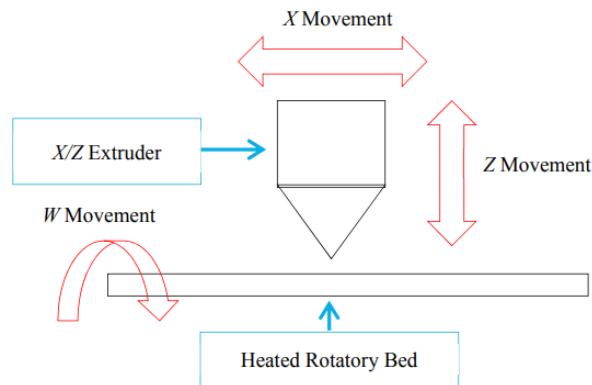


Figure 13. Scheme of 3D Printing process using a rotating mandrel for the manufacture of cylindrical stents [30].

On the other hand, SC-DW technique employs a computer-controlled translation stage, which moves an ink-deposition nozzle, to create materials with controlled architecture and composition. Since it is a process that does not use temperature to melt the polymer, a specific ink rheology and viscoelastic properties are required. Also, the rigidity of the filament after extrusion must increase in order to show shape retention. Polymeric ink is composed by a solution of the polymer in a solvent that evaporates post extrusion. While the solvent evaporates, the diameter of the filament decreases and its rigidity gradually increases with time because of higher polymer concentration. Therefore, the extruded filament changes from fluid-like to solid-like. This enables the creation of different complex geometries [17].

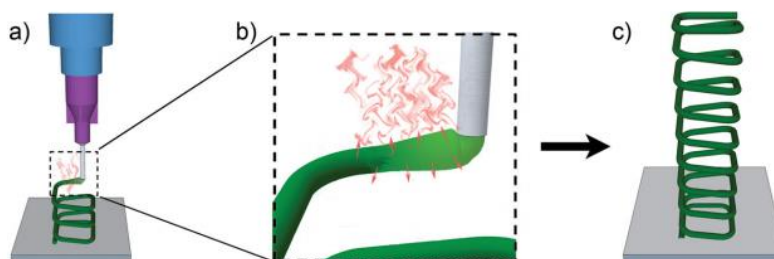


Figure 14. Scheme of SC-DW process with a thermoplastic solution. (a) Deposition of the polymer, (b) solvent evaporation and (c) example of the final product [17].

In order to have a proper SC-DW process, the selection of the solvent and the polymer concentration is important to ensure the correct ink rheological behavior and the fast solvent evaporation. Also, the speed of the extrusion nozzle and the applied pressure on the solution must be studied to achieve the desired linear flow rate [32].

In the current study, stents will be printed implementing a rotatory Cartesian platform using SC-DW. Thanks to this technique, personalized stents can be achieved by 3D-printing and avoiding temperature during the manufacture process. This prevents the polymer to degrade, resulting in higher crystallinity and better mechanical properties of the stents than with others methodologies. Among other advantages, SC-DW is a fast fabrication process, is seamless and presents low cost.

2.9. Micropatterned surfaces in stents

The control of cell behaviour is a topic of great interest in the science community from biomaterials, cellular biosensors to tissue engineering. S. Chen et al. [33] reported that micropatterned surfaces are essential not only for the construction of biosurface devices but also to investigate the interactions between cells and the extracellular matrix. Also, tissue engineering applications require cells to be placed into specifically places to generate organized structures and the use of micropatterned surfaces can make that happen.

Regarding cardiovascular diseases, many studies have focused on modifying blood-contacting surfaces of cardiovascular devices in order to promote endothelial cell adhesion, migration and proliferation, and finally build an endothelial layer on the surfaces. The creation of this endothelial layer throughout the cardiovascular device gives an anticoagulant surface, which would constitute the most efficient way to solve some of the risks that cardiovascular devices can generate, such as thrombosis or restenosis [34]. Endothelial cells are aligned and elongated in the native endothelium in the direction of blood flow. Then, mimicking the original alignment with a patterned topography in nanoscale or microscale should improve cells adhesion. The patterned structure can increase the hydrophilicity of the device and therefore, with the presence of cell-binding ligands and other biomolecules, adhesion, migration and proliferation of the cells may be favored.

The third generation of DES wants to solve the in-stent restenosis problem with the addition of drugs in the polymeric stents such as Sirolimus, Everolimus or Paclitaxel which control restenosis by impeding neointimal growth. However, this medicines also delay endothelialization, leading to late stent thrombosis and late in-stent restenosis. Then, surface modification through surface texturing can help to achieve endothelialization [34].

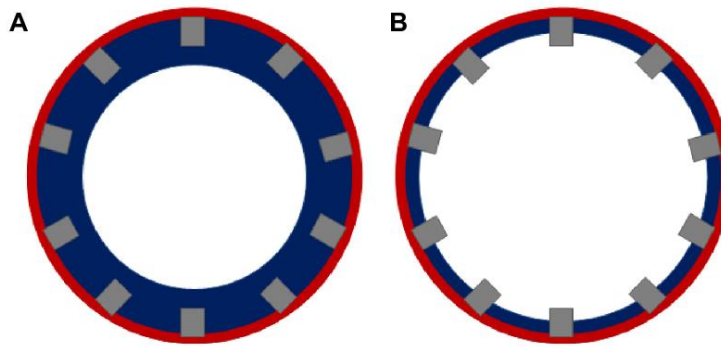


Figure 15. Stent strut coverage (A) A well-expanded stent with proper stent coverage of endothelialization layer (B) Poor neointimal stent coverage creating a risk for stent thrombosis. In red the arterial wall, in blue neointimal coverage and in grey stent strut

Regarding BMS surfaces studies, it has been shown that in-stent restenosis can be decreased by surface endothelialization of the stent which prevents from thrombogenicity. With the purpose of increase surface endothelialization, Y. Shen et. al. [35] investigated the effect of micropatterning in nitinol alloy stents since the smooth surface of this material difficult the adhesion of the endothelial cells to the stent showing that patterned surfaces could enhance cell adhesion compared with smoother surfaces.

Furthermore, E. Saleh et. al. [36] studied functional nanoarchitectures modifying the drug eluting stent surface in order to optimize duration and conditions for endothelium healing through the DES. S. Choudhary et. al. [37] created nanostructured titanium and CoCrMo for stents, showing increased endothelial and vascular smooth muscle cell adhesion on nanostructured compared with the conventional materials.

Therefore, creation of patterning of cardiovascular stents showed potential results for the improvement of the endothelialization process.

2.10. Sterilization of medical devices made of polymers

Sterilization is a process where a material is made free of contamination from living microorganisms, bacteria, yeasts and viruses. When sterilizing biodegradable scaffolds, it would be very important to choose the right technique taking into account that structural and biochemical properties have to be maintained after the treatment. Furthermore, polymers will be more sensitive than other materials such as metals due to their nature and their chemical properties. Sterilizations techniques can be divided in general into several categories: heat, irradiation, plasma, chemical sterilization and others novel techniques [38]. For polymers sterilization, four main sterilization techniques are generally used: gamma irradiation (γ), electron beam, ethylene oxide (EtO) and plasma.

On *Table 1*, advantages and disadvantages of the most used sterilization techniques for polymers are briefly discussed:

Table 1. Most used sterilization techniques for polymers [38].

TECHNIQUE	METHOD	ADVANTAGES	DISADVANTAGES
Gamma	Irradiation	High penetration ability, low temperature, effective, easy to control and no residues presented.	Can induce structural properties changes, dose rate is lower than electron beams. It requires long time.
Electron beam	Irradiation	Low temperature, easy to control, no residue, fast	Can induce structural properties changes, it is needed an electron accelerator and it has low penetration ability.
Ethylene Oxide	Chemical treatment	Effective and low temperature.	Can induce structural properties changes, leave toxic residues, it is flammable, explosive and carcinogenic.
Plasma	Plasma	Low temperature, improved cell interaction, increasing wettability on surface of biodegradable polymers and fast process.	May cause changes in chemical and mechanical properties of polymers and it can leave reactive species.

Many studies have focused on comparing between gamma irradiation and EtO on PLA samples since they are currently the most commonly used sterilization methods in the medical device technology [39][40].

Radiation sterilization is a fast sterilization process, requiring only one dose between 8-45 kGy to destroy microbial load on medical devices. Gamma rays are usually emitted by ^{60}Co source that has an energy around 1.2 MeV and are highly penetrating, therefore making a possible sterilization of densely packaged materials. Gamma rays cause ionization of cellular components, especially nucleic acids that cause the death of microorganisms because its high energy but not that high to impart radioactivity to the sterilized material [41]. Gamma radiation typical cycle consist on: (i) loading the product to be sterilized into the processing container, (ii) dosimeters are placed into the chamber so that the samples

are exposed to radiation field such as Cobalt 60 during a period of time, and (iii) dosimeters are analysed in order to confirm the proper sterilization[42].

A dose of 8 kGy is used in polymers since higher doses can produce damage to the material. The interaction of gamma sterilization with a polymer can cause crosslinking, chain scission and hydrogen evolution which will influence the chemical and physical properties of the material. In fact, both mechanisms occur at the same time but one of them will dominate the other [43]. The result of recombination, crosslinking and chain scission will be different depending on the polymer, the chemical composition, morphology of the polymer, absorbed dose or storage conditions [42]. With crosslinking conditions, a higher molecular weight and more branched polymer will cause the alteration of mechanical properties while chain scission will result in low molecular weight and change in crystallinity and density.

Ethylene oxide is a colour less gas with a boiling temperature of 10.4 °C at 760 mm of mercury. Sterilization processes with EtO are carried out at low temperatures (around 30-60 °C), which make this technique the ideal for materials that are sensitive to moisture and temperature. It usually takes about 2.5 hours excluding the EtO removal step, which can take approximately 8 hours. A typical EtO sterilization cycle consists on: (i) initial evacuation and nitrogen dilution in order to remove oxygen, (ii) conditioning of temperature and moisture, (iii) EtO injection and dwell time, (iv) EtO removal and nitrogen washes, and (v) air bleed in order to remove residual EtO in the sample [42].

However, it is reported in the literature that it can leave harmful residues in the implant if the degassing step is not well performed. Actually, the American Health Industry Manufacturers Association and the American National Institute for Occupational Safety and Health (NIOSH) have set guidelines of 25–250 ppm as the maximum EtO residual concentration in medical devices post-EtO sterilization, with recommended range of 10–25 ppm. Given these restrictions, aeration of scaffolds after EtO sterilization is mandatory in order to remove residual EtO [25].

Despite the advantages of these techniques for polymers sterilization, it is clear that there are still some challenges to achieve and huge drawbacks can appear depending on the conditions. Therefore, a study of the sterilized samples would be important in order to be sure that the polymer has not lost its properties or that no toxic residual appeared in the medical device.

3. MATERIALS AND METHODS

3.1. Chemicals and materials

PLLA (Purabsorb® PL 65; inherent viscosity IV=6.95 dl/g, Mw=1675000 g/mol) and PLCL (Purabsorb® PL 9538; inherent viscosity IV= 3.81 dl/g, Mw=700000 g/mol) were purchased from Corbion (Netherlands). Chloroform (≥99.5%) was obtained from Sigma-Aldrich (USA) and Sodium hydroxide pellets from PanReac (Spain).

3.2. Stents fabrication

3.2.1. Polymer-based ink preparation

Two printable inks were obtained in order to compare two different conditions of stents. The first one, by dissolution of PLLA pellets in chloroform at a 10% ratio (w/v) and the second one, by dissolution of PLCL pellets in chloroform at a 12.5% ratio (w/v). Each dissolution was placed into a medium size (25 ml) speed mixer polypropylene recipient, which was then sealed with a coverage of paraFilm®. The recipient was properly set in a Dual Asymmetric Centrifuge (SpeedMixer™, AC 150.1 FVZ, FlackTek, Germany) at 3500 rpm for 5 minutes. The dissolution process in the SpeedMixer was repeated until no solid pellet was seen in the mixture.

The obtained ink was introduced in 3cc cartridges (Optimum®, Nordson, USA) with a nozzle of 250 µm of diameter in order to do the 3D printing step explained in the next chapter.

3.2.2. 3D Printing of stents

Stents were manufactured by means of solvent-cast direct-write (SC-DW) technique. A commercial fused deposition modelling (FDM) 3D printer was previously modified in order to be able to extrude the polymeric solution in chloroform. The model of the 3D printer is BCN 3D+ and it was provided by BCN 3D technologies. Following previous studies in the research group, the printer's y axis was substituted by introducing a rotating steel mandrel of 3 mm of diameter in order to print cylindrical structures. For the stents with patterning, a modified steel rod with linear micropattern was used so that the pattern could be transferred to the inner surface of the stents (*See Figures 16 and 17*). These steel rods were modified through a direct laser interference patterning (DLIP) thanks to a collaboration

with the group of Prof. Franck Mücklich from the University of Saarbrücken (Germany) [44]. The patterned area of the mandrels was limited by the printing range of 24 cm. Morphology presented nano and microscale patterning of a height in the profile of 800 nm. The nanopatterning was placed in the parallel direction of the cylinder length, while a perpendicular or parallel micropatterning was used in order to analyse results with two types of morphologies. For the DLIP process, a fluence of 1960 mJ/cm² and a number of shots of 8.3 had been used.

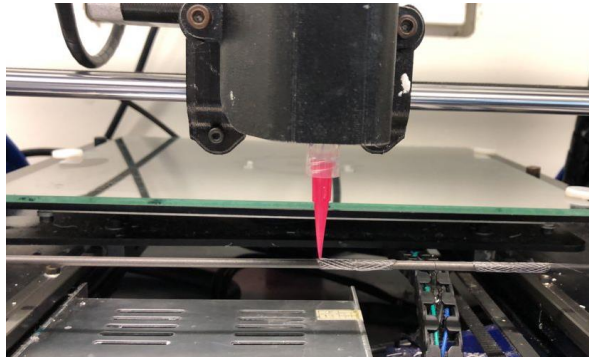


Figure 16. 3D printing of the stents using a rotating mandrel.

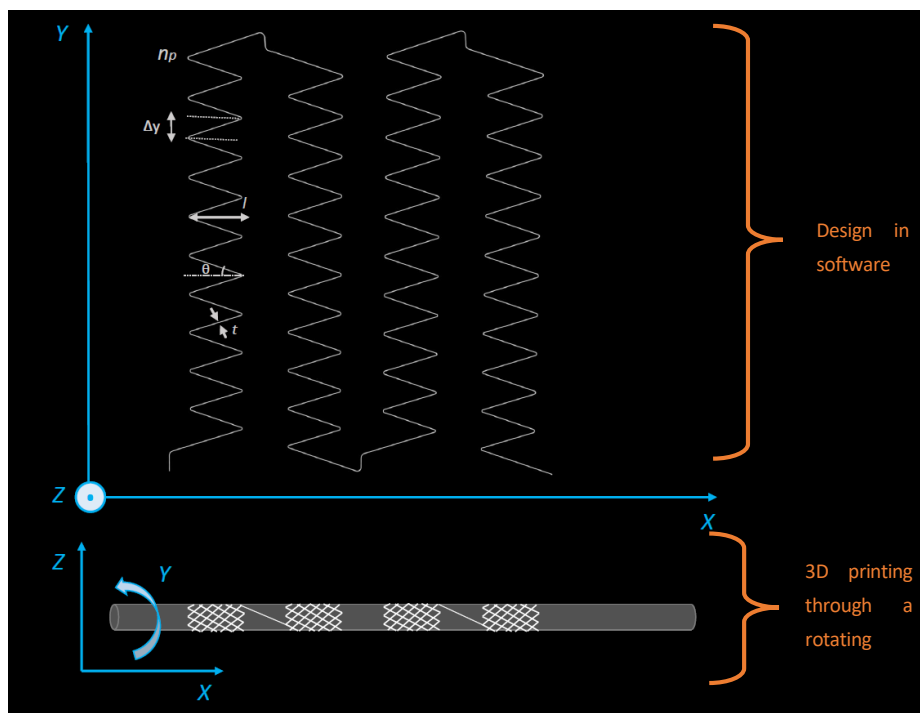


Figure 17. Scheme of the 3D printing process for the manufacturing of four stents of $n_p=10$.

The 3D printer followed the design of rhombic cells as can be seen in Figure 17. The draw was designed in order to obtain 4 stents for each cylinder. The design parameters were length (l), stent diameter (d), strut thickness (t), number of peaks (n_p) and number of revolutions (n_r). Stent length was set to 30 mm

and stent diameter was determined by the 3 mm diameter of the mandrel. Following the scheme of *Figure 17*, stents were printed with 10 peaks since was the most optimized condition obtained in previous investigations of the research group. The stents were printed at a speed of $4 \text{ mm}\cdot\text{s}^{-1}$.

In order to avoid fast solvent evaporation while printing, a solvent trap was designed and built as a 3D printer accessory with a chloroform reservoir. The design was calculated to fit with the exact printer dimensions. The material selection was evaluated in order to have easy processability, good chloroform resistance, present transparency and low cost. Thus, polyethylene terephthalate (PET) layers of 5 mm were used. Also, a Teflon tape was used in the gap where the nozzle moved (*See Figure 18*) in order to keep the trap closed as much as possible. *Figures 19 and 20* show the solvent trap drawings done through AutoCAD.

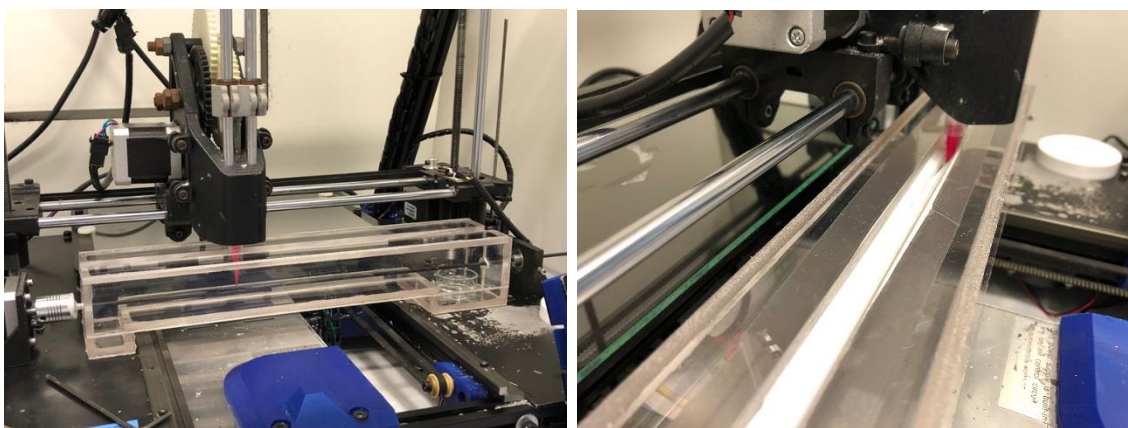


Figure 18. Solvent trap and 3D printer setup.

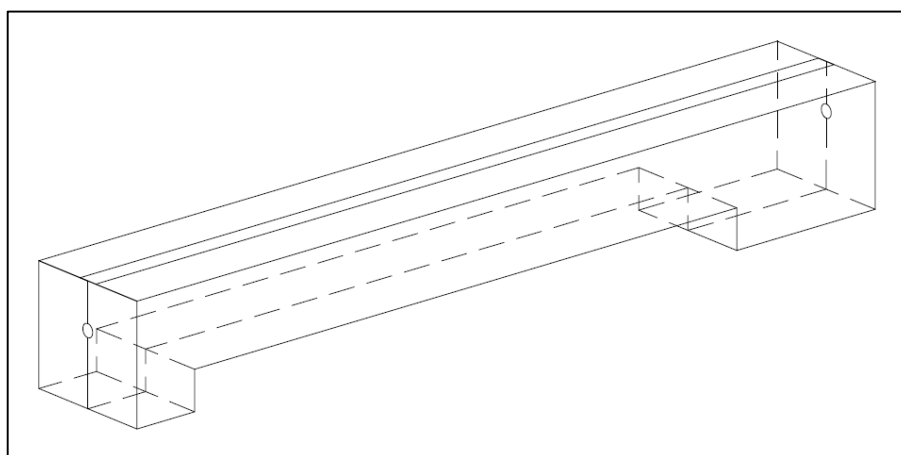


Figure 19. Solvent trap drawing in three-dimensional view done with AutoCAD.

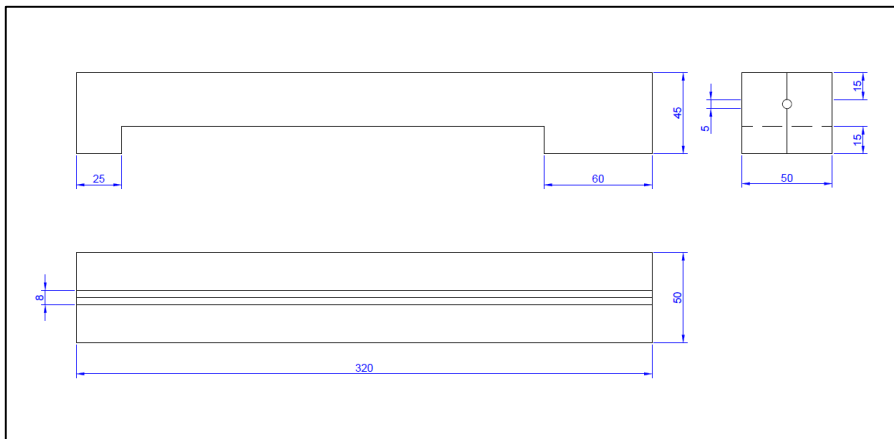


Figure 20. Solvent trap drawing dimensions done with AutoCAD.

Finally, stents underwent thermal treatment in the oven at 80°C for 12 hours in order to ensure the complete evaporation of the residual chloroform as well as to increase their crystallinity.

3.3. Sterilization of stents

3.3.1. γ -radiation sterilization

PLLA and PLCL stents were placed in packed self-seal sterilization pouches in order to be prepared to be placed in a gamma beam irradiation chamber. In this study γ -sterilization was performed at Aragogamma, S.L. company (Barcelona, Spain) that are qualified with the standards certifications for ISO13485/ISO1137 compliance. A source of ^{60}Co γ -sterilization at a dose of 8kGy was used as ray irradiation. For more details of the radiation sterilization guidelines of ISO1137 can be consulted [45].

3.3.2. Ethylene oxide sterilization

PLLA and PLCL stents were placed in packed self-seal sterilization pouches in order to be prepared to be placed in a ethylene oxide (EtO) sterilization chamber. In this study, EtO-sterilization was performed at Soadco company (Andorra) according to the standards ISO 11135. For more details of the development, validation and routine control of EtO sterilization guidelines of ISO1135 can be consulted [46].

3.4. Characterization techniques

3.4.1. Ink characterization

The rheology of the ink was determined through the injectability test. This test consists on the extrusion of the ink in the same syringe used in the 3D printer and a capillary tip (Blue general purpose tip from Nordson with diameter $d_{\text{tip}}=410 \mu\text{m}$ and length $l_{\text{tip}}=12.7 \text{ mm}$) with a controlled rate and using a compression setup (Bionix 858 Test System, MTS, USA).



Figure 21. Injectability test setup.

A personalized assembly had to be used in order to press the piston and hold the syringe. This assembly consisted on a PMMA cylinder with a PMMA disc on the top with a hole in the centre of the same diameter than the syringe so that the syringe could be introduced on it. Also, a metal piston was placed in order to press the plunger tip (see Figures 21 and 22 for the setup scheme).

The test was carried out testing the different rates that the 3D printer can achieve (from $1 \text{ mm}\cdot\text{s}^{-1}$ to $60 \text{ mm}\cdot\text{s}^{-1}$). During the test, load force versus extension was monitored. The test was stopped when force load was stabilized, meaning that the steady state had been reached.

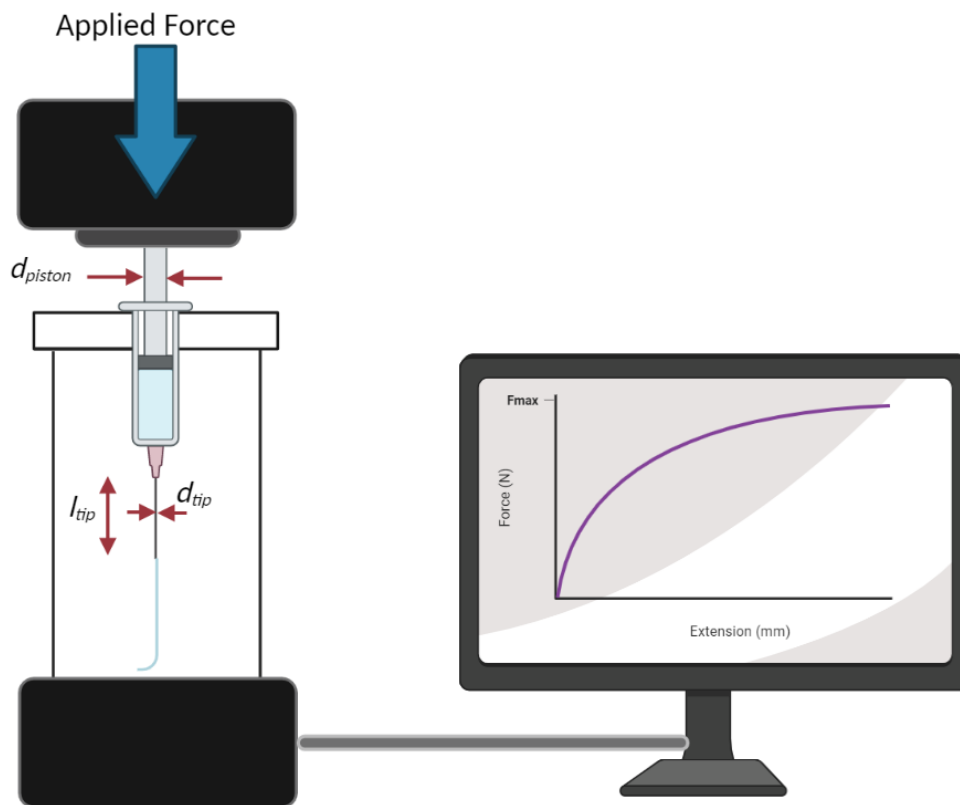


Figure 22. Scheme of the injectability parameters and motoring of compression machine.

The required extrusion force (F) for each speed was determined in order to be used to calculate next equations:

$$\Delta P = \frac{F}{S_{piston}} \quad (1)$$

Where ΔP is the extrusion applied pressure and the S_{piston} is the piston's surface, with a diameter of 9.6 mm.

The process related wall shear stress (τ_w) was determined with Equation 2.

$$\tau_w = \Delta P \cdot \frac{d_{tip}}{4 \cdot l_{tip}} \quad (2)$$

The dimensions of the tip for the assay were chosen so that l_{tip}/d_{tip} ratio was 31 following the literature [47]. With a high value of L/D, Bagley correction could be avoided [32][47][48].

The printing flow rate (Q) for each speed was calculated as *Equation 3*, where v is the printing speed in $\text{mm}\cdot\text{s}^{-1}$, and S_{tip} is the surface of the capillary tip in mm^2 .

$$Q = v \cdot S_{tip} \quad (3)$$

In order to calculate the wall shear rate ($\dot{\gamma}_w$) (*Equation 5*), the Newtonian shear rate ($\dot{\gamma}_{New}$) was first determined through Equation 4:

$$\dot{\gamma}_{New} = \frac{4 \cdot Q}{\pi \cdot r^3} \quad (4)$$

Where r is the radius of the assay nozzle (0.205mm).

Then, Non-Newtonian effects were taken into account with the Robinowitch-Mooney correction (*Equation 5*), where n corresponds to the slope of logarithmic plot of \bar{C}_w versus $\dot{\gamma}_{New}$ (*Equation 6*). \bar{C}_w is in units of s^{-1} and $\dot{\gamma}_w$ is in kPa.

$$\dot{\gamma}_w = \dot{\gamma}_{New} \cdot \frac{3n+1}{4n} \quad (5)$$

$$n = \frac{d \cdot \log(\bar{C}_w)}{d \cdot \log(\dot{\gamma}_{New})} \quad (6)$$

Finally, apparent viscosity was calculated following next equation ($\text{Pa}\cdot\text{s}$):

$$\eta_{app} = \frac{\bar{C}_w}{\dot{\gamma}_w} \quad (7)$$

Then, rheological curve for each ink was obtained by plotting shear rate in X axis against shear stress in Y axis.

3.4.2. Stents characterization

3.4.2.1. Optical microscopy

Stents were observed through optical microscopy (OM) to measure strut thickness. An Olympus BX51 microscope (Olympus, Japan) was used with magnifications of x5 and x10. To determine strut thickness, 10 measures of stents filaments were measured using AnalysisDocu software (Tableau, Seattle). Also, stents were radially cut and vertically hold with the angle needed to have the strut

perfectly perpendicular to the microscope lenses (see Figure 23) in order to measure the inner diameter of the struts. Next scheme shows how the sample was displaced onto the OM for measuring.

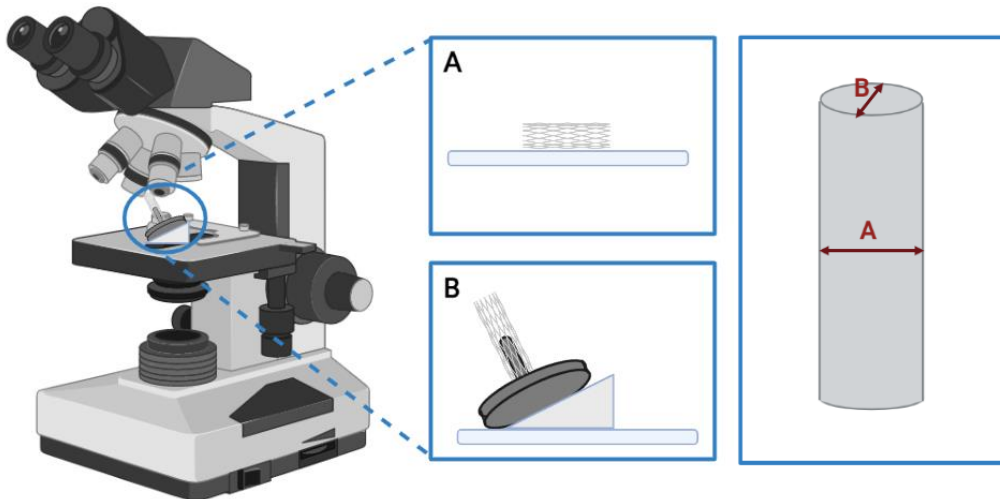


Figure 23 Scheme of OM setup. (A) Strut thickness, (B) Inner diameter of the stent.

3.4.2.2. Scanning electron microscopy (SEM)

SEM is a technique that generates the image of a sample by scanning it with a beam of electrons. Electrons interact with different atoms on the surface of the sample to generate various signals, revealing information about the morphology and composition of the sample surface [49].

The acceleration voltage applied in SEM is usually in the range of a few to 30 keV. The creation of SEM images is made by collecting secondary low energy electrons (SE) or backscattered electrons (BSE). The secondary electron detector provides the information about the contrast of the topographic contrast, which makes it a suitable method for estimating surface roughness and characterizing local topography properties. BSE carry relatively high energy and are emitted from the deeper part of the sample [50].

As preparation of samples, samples are coated with gold or platinum in order to provide a conductive and a protective layer to the samples under high voltage. The holder with the sample is screwed onto the exchange rod, and then the electron column is connected to the SEM by creating a vacuum [51].

Scanning electron microscopy (SEM) was used in order to examine stent's morphology with a JEOL JSM-7001F equipment (Jeol, Japan). Samples were prepared cutting axially the cylindrical stents so that the stent could be placed as a flat sample in the holder. Also, samples were coated with platinum-palladium so that a conductive surface was achieved.



Figure 24. Laboratory SEM.

3.4.2.3. Differential scanning calorimetry (DSC)

DSC is a technique that studies the response of polymers to heating and variables such as melting temperature, glass transition temperature and percentage of crystallinity can be obtained from this method. DSC set-up is composed of a measurement chamber and a computer. There are two pans that are heated, one for the sample and the other for the reference. The system monitors the temperature and regulates the rate at which temperature changes. For the collection of the heat flux data, the system varies the heat provided to one of the pans in order to keep the temperature of both pans the same, and the difference in heat output of the two pans is recorded, obtaining the plot between the difference in heat (q) versus temperature (T). Samples should weigh between 5 and 15 mg [52].

Thermal properties of all the conditions were examined by DSC using a DSC2920 equipment from TA instruments (USA). Under controlled nitrogen atmosphere, samples were heated to 250°C at a scanning rate of 10°C·min⁻¹, and maintained at the final temperature for 1 minute.

Percentage of crystallinity (X_c) was calculated through the *Equation 8*, where ΔH_m and ΔH_{cc} are the melting enthalpy and the cold crystallization enthalpy respectively in units of J·g⁻¹, ω is the mass fraction of the polymer and ΔH_m° is a reference value that represents the heat of melting if the polymer were

100% crystalline in units of $\text{J}\cdot\text{g}^{-1}$. PLCL copolymer used has only a 5% of random PCL, then, PCL parts will be not able to crystallize and the X_c of this copolymer will correspond to PLA chains [17]. Thus, same value of $93 \text{ J}\cdot\text{g}^{-1} \Delta H_m^\circ$ corresponding to PLA was used for both conditions (PLLA and PLCL) [53].

$$X_c(\%) = \frac{\Delta H_m + \Delta H_c}{\Delta H_m^0} \cdot \frac{100}{\omega} \quad (8)$$

3.4.2.4. Mechanical tests

The mechanical properties of the stents were carried out adapting the setup and test conditions of a rheometer (Discovery HR-2, TA instruments). Samples were radially compressed at 25% and 50% of the diameter between the two parallel flat plates of the machine so that the radial force was obtained. The upper plate moved vertically at a speed of $1 \text{ mm}\cdot\text{min}^{-1}$. Also, initial and final diameter of the stents were obtained. With this data, elastic recovery was calculated with *Equation 9*, where d_f is the final diameter and d_i is the initial diameter.

$$\text{Elastic recovery (\%)} = \frac{d_f}{d_i} \cdot 100 \quad (9)$$



Figure 25. Compression test of the stents.

3.4.2.5. Accelerated degradation

Stents were immersed in 10 ml of a solution of 0.1M NaOH in individual sealed glass vials maintained at 37°C . The NaOH concentration was established based on previous studies [54][55][56]. Prior to immersion, stent's mass was measured.

After 2, 4, 7 and 10 days of immersion, stents were extracted for analysis. Stents were dried in the oven at 37°C during 24 hours and weighted for each time point. Evaluation methods for the accelerated degradation were morphology changes through OM (following *Chapter 3.4.2.1*) and SEM (following *Chapter 3.4.2.2*), % mass loss, pH changes, molecular weight changes through gel permeation chromatography (GPC), molar ratio changes of the monomer units in the case of the copolymer via

Nuclear Resonance Magnetic (NMR), thermal changes through DSC (following *Chapter 3.4.2.3*) and mechanical properties changes through a compression test (following *Chapter 3.4.2.4*).

% Mass loss

Mass loss was determined through *Equation 10*, where m_i is the initial mass and m_f is the final mass.

$$\text{Mass loss (\%)} = \frac{m_f - m_i}{m_i} \cdot 100 \quad (10)$$

Gel permeation chromatography (GPC)

GPC (or size exclusion chromatography, SEC) technique is used to determine molecular weight distribution of polymers. The equipment is composed by chromatography columns that are filled with microporous gel called the stationary phase, a solvent pump, sample injector, thermostat column department and a refractive index detector. When the solution of the polymer arrives into the column, the small polymeric chains are retained into the cavities of the gel, and therefore, it takes more time for them to get out of the column. On the contrary, higher polymer chains will appear much faster in the detector signal since they are not able to be retained in the small cavities. The recorded data show a spectra of the detector signal and the elution volume. Therefore, it is a technique that separates by size, and not by chemical interactions [57].

GPC is based on the separation of molecules of different sizes in solution, thus, it was used in order to determine the molecular weight of the degraded stents per each time point and also in sterilized stents in order to see if any differences appeared. A 1260 Infinity series (Agilent Technologies, Santa Clara, CA, USA) equipment was used. The separation was carried out in an Agilent PL HFIP gel column (USA) using Hexafluoro-2-propanol (HFIP) containing 0.05 M of sodium trifluoroacetate as eluent. Sample concentration used for analysis was 2 mg/ml. The used flow was 0.3 ml/min and the injection volume was 10 μ L. Molecular weights were calculated after calibration with PMMA standards from Sigma-Aldrich (Darmstadt, Germany), the molecular weight calibration range was between 2.7 million to 2000 Dalton. Chemstation Software (Agilent Technologies) was used in order to do the calculations.

Nuclear magnetic resonance (NMR)

NMR is a technique that studies the molecular structure of the materials by observing and analysing the interaction of nuclear spins when a magnetic field is applied. The equipment consists of a superconducting magnet, a spectrometer, a control system and a detector [58].

NMR spectroscopy was used to determine the chemical composition of PLCL per time point. Proportion between lactide and caprolactone monomers acid was analysed in order to see how this proportion was modified as the copolymer was degraded.

Spectra was recorded with a Bruker NMR Ascend 400 spectrometer of 400 MHz spectrometer, using Chloroform-d (99.80%) + 0.03% (v/v) TMS (CDCl_3) as solvent. Data was analysed with Topspin software. Sample amount used was around 5 mg for each sample in order to obtain a dissolution about 0.7ml (approximate height of 5 cm).

3.4.2.6. Fourier transform infrared spectroscopy (FTIR)

Fourier transform infrared spectroscopy (FTIR) is a technique to characterize and identify organic molecules. In the attenuated total reflectance mode (ATR-FTIR) this kind of spectroscopy has a distance penetration of radiation of around 1 μm .

This methodology gives information about chemical bonding interactions between structures when samples are put in contact with a crystal that acts like the internal reflection element (IREs) of the system, such as zinc selenide or germanium. During the process, the sample is in contact with the crystal allowing total internal reflection. Infrared rays arrive at the crystal which give rise to an evanescent wave that at each reflection continues beyond the surface of the crystal and penetrates the sample. Spectrum obtained have the absorption peaks that are characteristic for each type of chemical bonds, functional groups and chemical structure of polymers [59].

The presence or absence of specific functional groups and the chemical structure of polymer materials will give information about the samples. If ATR-FTIR shows any differences of the frequency of absorption bands or in the band intensities, it means that changes in the chemical structure or environment around the sample happened [60].

Sterilization techniques in polymeric devices can be harmful for the polymer chemical structure. Furthermore, regarding EtO sterilization, residual toxicity of EtO has a major concern since very restricted compositions are mandatory in order to accomplish the standards of Safety and Health Institutions [38].

Therefore, ATR-FTIR of EtO sterilized stents were carried out, in order to see possible chemical composition modifications and show if residual EtO compound remained in the samples.

Evaluation of chemical composition modification of the sterilized techniques was done by reflectance (ATR-FTIR). The resolution of the spectra was 2 cm^{-1} with a total of 64 scans. A Germanium crystal was used and a range of wavelength from 4000 to 400 cm^{-1} was measured.

3.4.2.7. Statistical analysis

Values were analysed as means and standard deviations and analysed through 1-way analysis variance (ANOVA) and Tukey test using Minitab software. The significance level used was a p value of <0.05 .

4. RESULTS AND DISCUSSION

4.1. Rheology of the ink

PLLA and PLCL inks were characterized through the injectability test obtaining the required extrusion force in *Table 2* for each printing speed ranged from 1 to 60mm·s⁻¹.

Table 2. Extrusion force required during the rheology characterization of PLLA and PLCL ink.

Printing speed (mm·s ⁻¹)	Extrusion force (N)	
	PLLA	PLCL
1	51.5 ± 5.8	24.8 ± 1.6
2	68.8 ± 6.8	38.2 ± 1.8
3	78.6 ± 7.9	46.9 ± 1.0
4	85.5 ± 7.4	55.0 ± 2.6
5	90.1 ± 7.7	59.5 ± 1.9
10	119.8 ± 12.0	83.9 ± 6.7
15	135.8 ± 11.8	96.6 ± 5.1
20	146.4 ± 11.3	106.6 ± 5.6
25	153.0 ± 11.2	114.9 ± 4.4
30	158.5 ± 11.0	123.2 ± 4.6
40	163.8 ± 8.4	135.2 ± 5.3
50	167.9 ± 6.5	144.7 ± 5.6
60	172.5 ± 7.3	154.8 ± 5.8

Then, apparent shear stress (τ_w), apparent shear rate ($\dot{\gamma}_w$) and apparent viscosity (η_{app}) values were obtained with *Equations 1-7* for PLLA and PLCL inks shown in *Table 3* and *Table 4* respectively.

The shear rate values were corrected for the non-Newtonian effects. *Figure 26* shows the value for n determined as the slope of the log-log plot of τ_w against $\dot{\gamma}_{New}$ which corresponds to the Rabinowitch-Moone parameter. Thus, a value of 0.2991 for PLLA and 0.4305 for PLCL was determined.

Table 3. Rheological parameters for PLLA ink.

τ_w (Apparent Shear stress) [kPa]	$\log(\tau_w)$ [kPa]	$\dot{\gamma}_w$ Apparent shear rate (s^{-1})	η_{app} (apparent viscosity) [Pa·s]
5.74 ± 0.65	0.76 ± 0.05	8.85 ± 0.43	651.63 ± 102.82
7.68 ± 0.76	0.88 ± 0.04	17.70 ± 0.86	435.70 ± 62.83
8.76 ± 0.88	0.94 ± 0.04	26.55 ± 1.29	331.51 ± 47.81
9.53 ± 0.83	0.98 ± 0.04	35.41 ± 1.71	270.41 ± 35.79
10.05 ± 0.86	1.00 ± 0.04	44.26 ± 2.14	228.00 ± 29.58
13.36 ± 1.34	1.12 ± 0.04	88.51 ± 4.28	151.60 ± 21.84
15.14 ± 1.31	1.18 ± 0.04	132.77 ± 6.43	114.54 ± 15.04
16.32 ± 1.26	1.21 ± 0.03	177.03 ± 8.57	92.57 ± 11.36
17.06 ± 1.24	1.23 ± 0.03	221.28 ± 10.71	77.39 ± 9.14
17.68 ± 1.22	1.25 ± 0.03	265.54 ± 12.85	66.82 ± 7.67
18.26 ± 0.93	1.26 ± 0.02	354.05 ± 17.13	51.74 ± 5.00
18.72 ± 0.73	1.27 ± 0.02	442.57 ± 21.42	42.41 ± 3.62
19.24 ± 0.81	1.28 ± 0.02	531.08 ± 25.70	36.33 ± 3.22

Table 4. Rheological parameters for PLCL ink.

τ_w (Apparent Shear stress) [kPa]	$\log(\tau_w)$ [kPa]	$\dot{\gamma}_w$ Apparent shear rate (s^{-1})	η_{app} (apparent viscosity) [Pa·s]
2.77 ± 0.18	0.44 ± 0.03	9.65 ± 0.08	286.68 ± 17.79
4.25 ± 0.20	0.63 ± 0.02	19.31 ± 0.15	220.29 ± 9.26
5.23 ± 0.11	0.72 ± 0.01	28.96 ± 0.23	180.43 ± 3.00
6.14 ± 0.29	0.79 ± 0.02	38.62 ± 0.31	158.90 ± 6.76
6.63 ± 0.22	0.82 ± 0.01	48.27 ± 0.39	137.42 ± 3.89
9.35 ± 0.75	0.97 ± 0.03	96.55 ± 0.77	96.83 ± 7.30
10.77 ± 0.56	1.03 ± 0.02	144.82 ± 1.16	74.34 ± 3.58
11.88 ± 0.62	1.07 ± 0.02	193.10 ± 1.54	61.54 ± 2.99
12.81 ± 0.49	1.11 ± 0.02	241.37 ± 1.93	53.07 ± 1.87
13.73 ± 0.52	1.14 ± 0.02	289.65 ± 2.31	47.42 ± 1.70
15.07 ± 0.59	1.18 ± 0.02	386.20 ± 3.08	39.03 ± 1.55
16.14 ± 0.62	1.21 ± 0.02	482.75 ± 3.85	33.43 ± 1.32
17.27 ± 0.65	1.24 ± 0.02	579.29 ± 4.62	29.81 ± 1.21

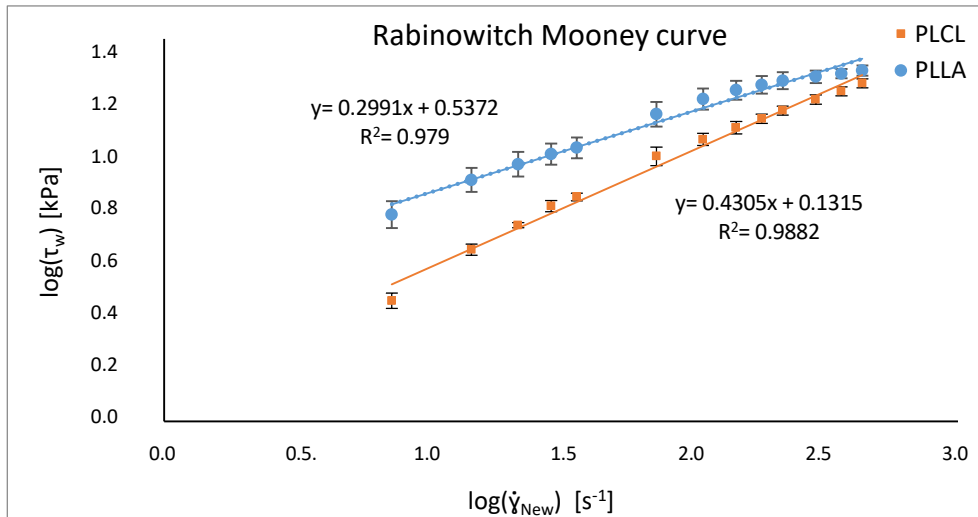


Figure 26. Graph for the obtention of the correction factor “n” of Non-Newtonian fluids through the Rabinowitch Mooney curve for PLLA and PLCL ink.

As expected in a Non-Newtonian fluid, the relationship of the shear stress (τ_w) and the shear rate ($\dot{\gamma}_w$) shows data with no linear behaviour as can be seen in *Figure 27*. Indeed, a visco-plastic behaviour with shear-thinning can be determined from the flow curves.

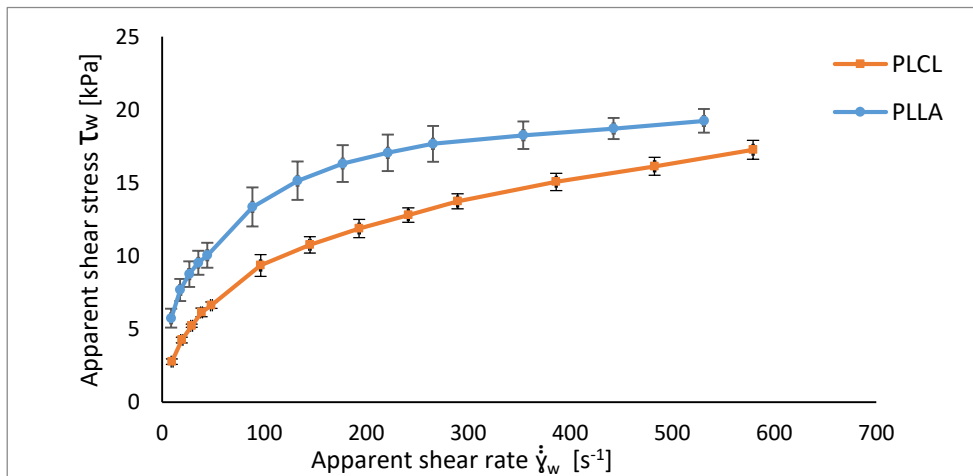


Figure 27. Apparent shear stress versus apparent shear rate for PLLA and PLCL ink.

In general, shear-thinning tendency is the most common behaviour type of time-independent non-Newtonian fluid in engineering applications [61]. As can be seen in *Figure 28* it is defined by the apparent viscosity η_{app} (determined as the division of τ_w and $\dot{\gamma}_w$) that gradually decreases when increasing the shear rate. These means that the material extrusion at higher rates was more easily processed [62]. Rheological properties of PLA depend on temperature, molecular weight and shear

rate [32]. With a higher inherent viscosity and higher molecular weight of the PLLA raw material used compared to the PLCL raw material used, it makes sense that the apparent viscosity of PLLA ink has higher values than PLCL ink. However, at higher values of $\dot{\gamma}_w$ the viscosity of both becomes closer. Probably because at higher rates the molecules of the polymer are more oriented, thus, the number of entanglements between the polymer chains decreases and it makes easier to the fluid to flow for both polymers [47][63] as can be seen in *Figure 29*.

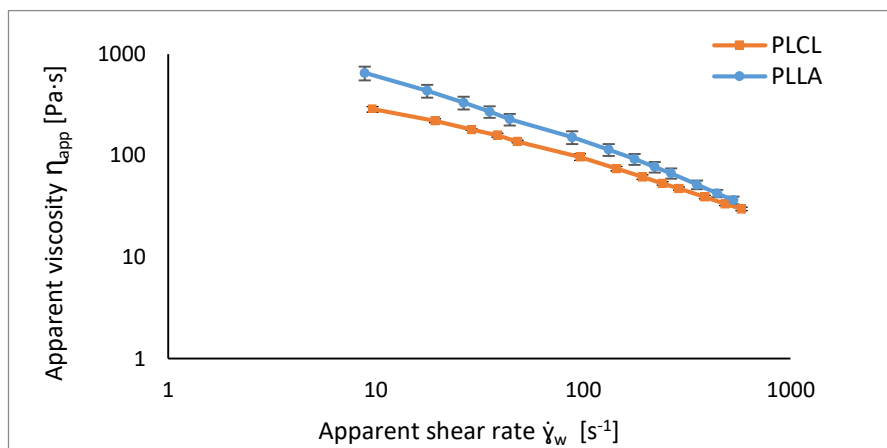


Figure 28. Apparent viscosity versus printing apparent shear rate for PLLA and PLCL ink.

Figure 29 shows viscosity versus the printing speed. Printing speed of $4 \text{ mm}\cdot\text{s}^{-1}$ is used during 3D printing. Values of viscosity obtained at this speed are $270.4 \pm 35.8 \text{ Pa}\cdot\text{s}$ for PLLA and $158.9 \pm 6.76 \text{ Pa}\cdot\text{s}$ for the PLCL. The higher viscosity of PLLA compared with PLCL is attribute to its higher value of molecular weight of the raw material.

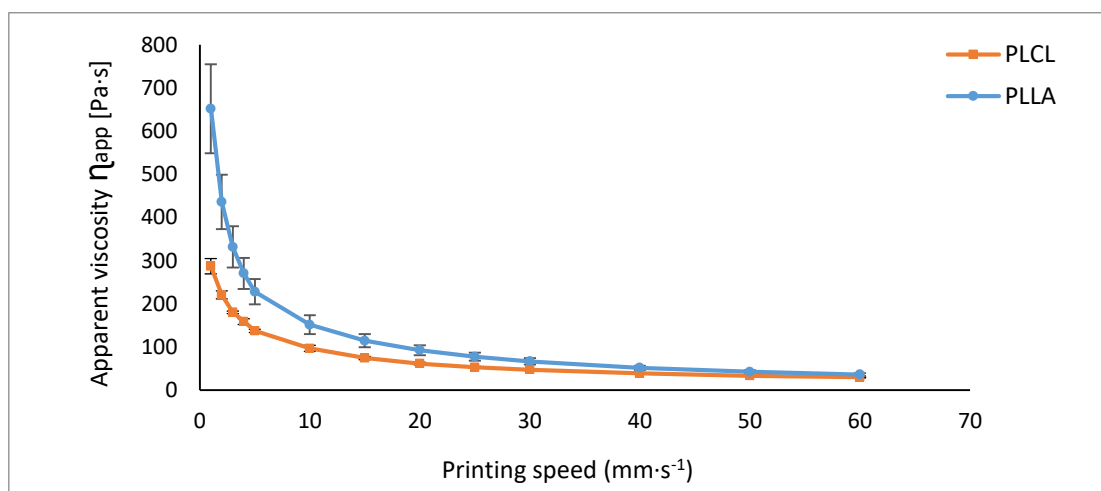


Figure 29. Apparent viscosity versus printing speed for PLLA and PLCL ink.

4.2. 3D printed stents

PLLA and PLCL stents of 10 peaks were successfully obtained by SC-DW 3D printing. Stents surface was analysed through OM and also strut thickness was measured for stents made of both ink types. Unions between struts acquired a more planar or squared morphology at the centre of the stents in comparison to the unions on the edges. This more squared morphology indicates that the filament of the first printed strut was not completely solidified when the second strut was printed above. Unions between struts are the more susceptible points to be broken under compression tests. With these behaviour, a good union between struts has been created which will be positive in order to have good mechanical properties.

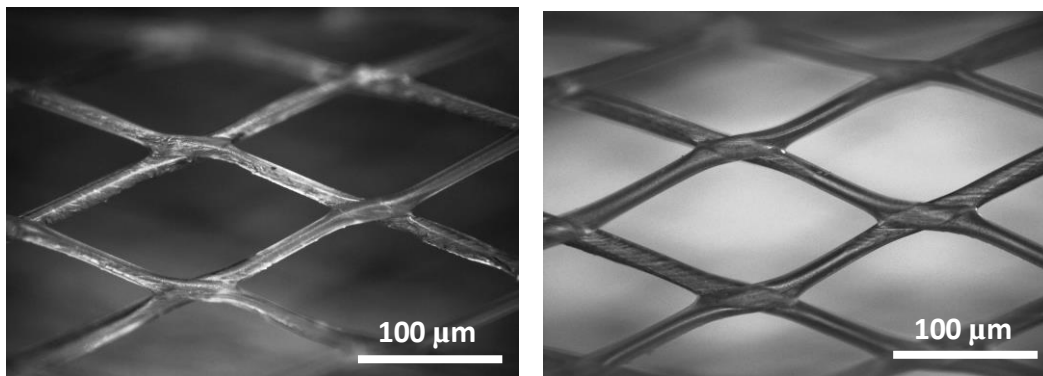


Figure 30 Stents surface images of PLLA (left) and PLCL (right).

Regarding strut thickness, clearly differences were found (*Table 5*) between PLLA and PLCL. PLLA showed a lower value than PLCL. PLLA presented approximately a thickness of 120.98 µm while PLCL presented approximately a value of 151.59 µm although molecular weight of PLLA is much higher. This is because different ratio of polymer/solvent had to be used in order to achieve a good behaviour of printability for the two different inks. A lower quantity of chloroform was used for the PLCL ink, thus, more quantity of polymer was dissolved in the same volume of the solution extruded through the nozzle, and therefore, when the chloroform evaporated, higher amount of polymer is deposited in the struts of PLCL compared with the struts of PLLA.

Table 5 Strut thickness, transversal section and mass of each fabricated stent condition.

Stents	Strut thickness (μm)	Transversal section (mm^2)	Mass (mg)
PLLA	120.98 ± 0.29	$4.38 \cdot 10^{-2} \pm 0.73 \cdot 10^{-2}$	7.43 ± 0.58
PLCL	151.59 ± 7.23	$6.79 \cdot 10^{-2} \pm 0.52 \cdot 10^{-2}$	10.40 ± 1.58

Taking into account design consideration of *Chapter 2.6.1*, a compromise between a reduction in stent strut thickness for avoiding laminar flow disruption as well as enough thickness in order to have good mechanical properties make a limiting factor when producing stents of polymer instead of metal [13]. Thinner metallic stents have struts thickness ranging from 60 up to 100 μm [2]. Some studies showed the differences regarding stents with strut thickness of 50 μm and strut thickness of 140 μm showing less ratio of restenosis in patients with thinner stents [2]. Thickness values between 150 and 200 μm of strut for PLLA stents have been found in the literature [13][64], which indicates that the SC-DW 3D printed stents present good results taking into consideration the difficulties for having thin strut thickness and maintaining mechanical properties with PLA stents. However, other investigations have tried to reduce strut thickness reporting values of PLLA around 150 μm for the first generation of stents and 120 μm and less than 99 μm for the second generation of BRs [65].

Figure 31 shows SEM images for PLLA stents and *Figure 32* shows SEM images for PLCL. At magnification of x15 it can be seen in both conditions that junctions on the centre of the stents are more welded since they adopted a more squared geometry. The reason of that is the geometry of the design: the areas of the middle of the stents were more rapidly done and therefore one strut was still not dry when the other was printed above. In general, the junctions between struts will be weakly spots in compression forces, therefore, is a good think that the unions appeared to have a strong junction. On PLLA, at a magnification of 100 μm , it can be seen a texture like orange peel. It could be produced due to a not perfect linear flow in some moments while printing. Also the presence of cavities at higher resolution confirmed the fast solvent evaporation. Different morphologies of these cavities are observed comparing PLLA to PLCL stents.

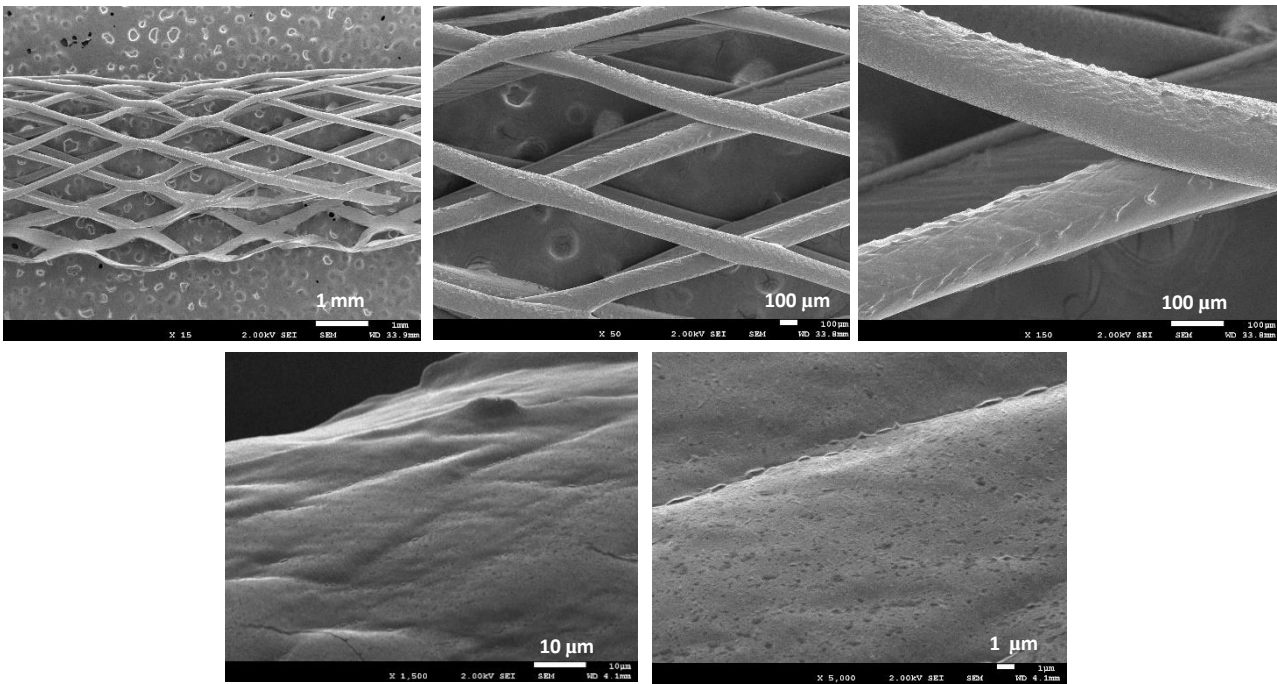


Figure 31. SEM images of PLLA stents.

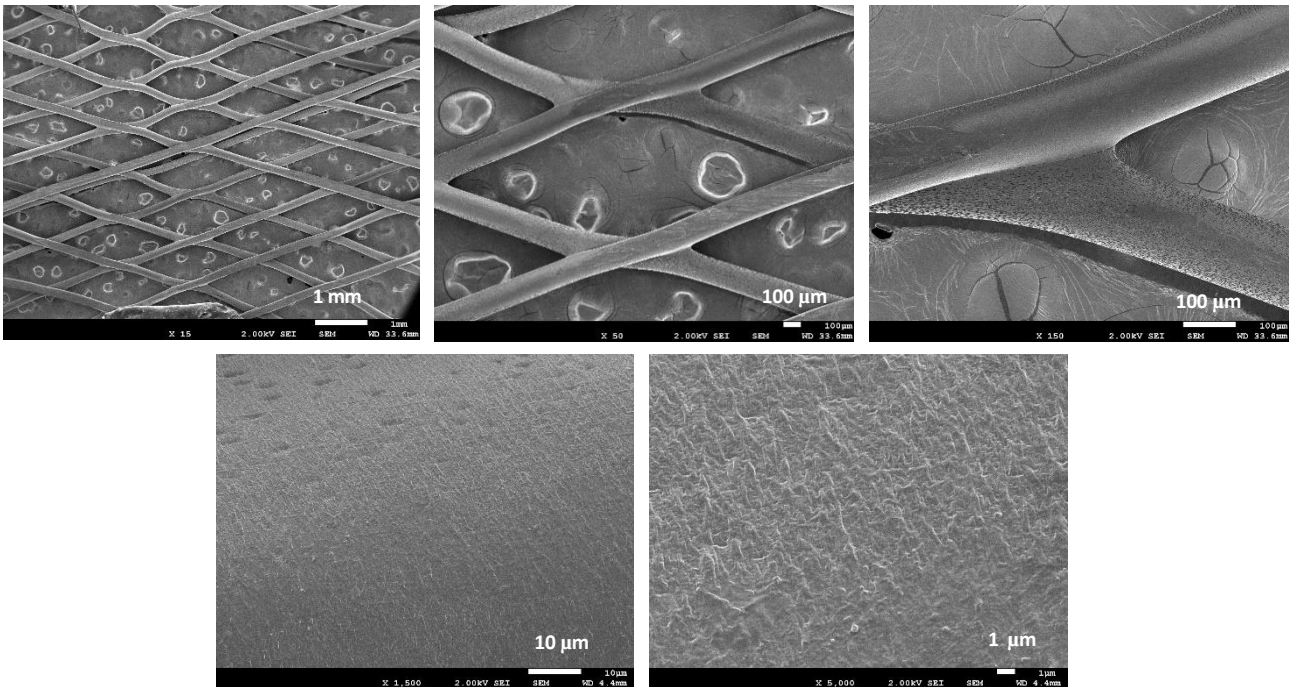


Figure 32. SEM images of PLCL stents.

Thermal properties of both fabricated stents are summarized in *Table 6*. Higher values of glass transition temperature (T_g), melting temperature (T_m), melting enthalpy ΔH_m and percentage of crystallinity for PLLA stents were obtained. These results were expected since the main reason to synthesize a copolymer of PLLA and PCL is to reduce the low flexibility of PLLA due to the high T_g and crystallinity. Thanks to adding a lower T_g polymer (PCL), it makes easier to the polymer chains to move, thus, it is easier to crystallize or to melt so the process is done at lower temperatures [13]. In other words, T_g and percentage of crystallization decrease. Therefore, with same geometry conditions it can be said that PLCL would present more flexibility compared with PLLA.

Table 6. Thermal properties of PLLA and PLCL stents.

Sample	T_g (°C)	T_m (°C)	ΔH_m (J·g ⁻¹)	Crystallinity (%)
PLLA	69.99 ± 2.06	178.70 ± 0.27	24.90 ± 0.70	26.78 ± 0.76
PLCL	59.88 ± 0.72	162.41 ± 0.28	18.27 ± 1.90	23.60 ± 2.71

Mechanical properties of the stents were examined through a compression test and force values at 25% and 50% of compression diameter and elastic recovery were determined as can be seen in *Table 7*. Higher values of the mechanical properties were found for the PLCL stents but also very similar values of the elastic recovery were found, although a higher standard deviation for PLLA stents make no significant differences regarding the flexibility of both stents. After seen thermal properties (*Table 6*) higher values of mechanical properties would be expected for PLLA since higher percentage of crystallinity was found for PLLA. However, not only crystallinity has to be taken into consideration, but also geometrical factors such as the strut thickness of stents (*See Table 7*). Then, it is shown how an increase of the strut thickness is related with higher values of the mechanical properties. Also, it is interesting to see the effect of the material regarding the elastic recovery. Although there is higher presence of material in PLCL stents which enhance the mechanical properties, no significant differences were found in terms of flexibility. This shows the presence of PCL in the copolymer.

Finally, it can be said that the results obtained are in accordance with the literature [66] and none stent of both conditions broke.

Table 7. Mechanical properties of PLLA and PLCL stents.

Sample	Force at 25% compression [N·mm ⁻¹]	Force at 50% compression [N·mm ⁻¹]	Elastic recovery (%)
PLLA	0.039 ± 0.008	0.075 ± 0.015	94.73 ± 1.34
PLCL	0.045 ± 0.009	0.091 ± 0.018	95.25 ± 0.86

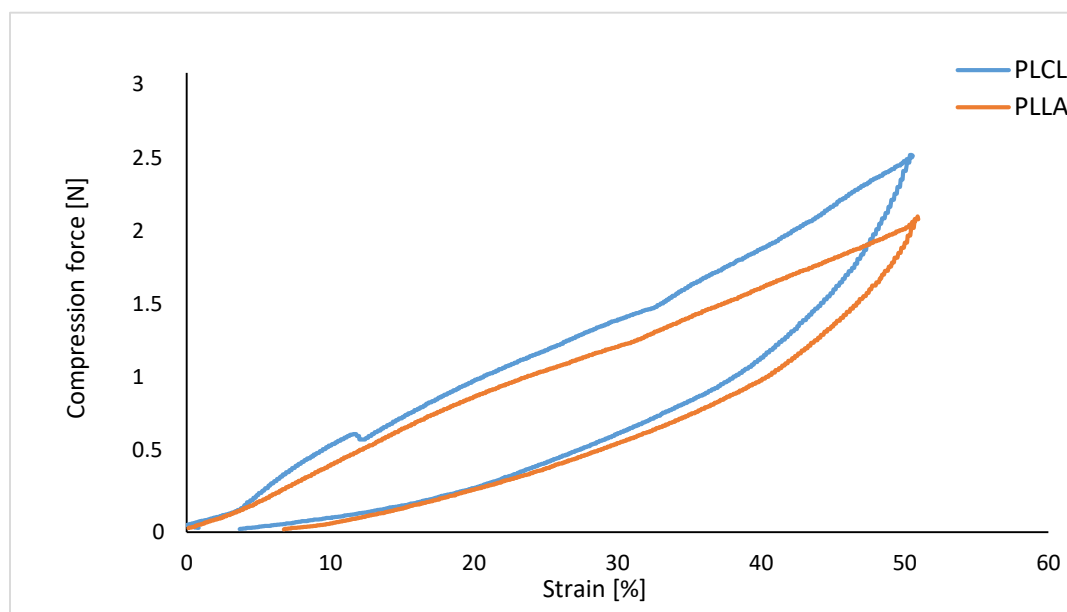


Figure 33. Compression curves for PLLA and PLCL stents.

4.3. 3D printed patterned stents

PLLA and PLCL inner patterned stents were successfully produced by 3D printing and analysed by SEM. Three different conditions were analysed for PLLA and PLCL stents: perpendicular micro-patterning, parallel micro-patterning and also another condition of parallel micro-patterning but creating a saturated atmosphere of chloroform during the 3D printing process. In *Annex A* is showed the solvent trap design that was created for the purpose of decrease solvent evaporation ratio during 3D printing. For each condition, magnifications of x15, x500, x1500 and x5000 are showed in *Figures 34 to 39*.

It can be seen that the laser-induced periodic surface structure was successfully imaged onto the stent inner surface. This was achieved for both, parallel and perpendicular orientations. Therefore, PLLA ink

and PLCL can penetrate and reproduce properly surface geometry and these structures are preserved after heat treatment. However, some differences were seen between PLLA and PLCL ink.

Comparing PLLA and PLCL stents without the solvent trap, PLCL presented more homogeneous patterning in the images. This result was expected after seen properties of both samples where PLCL stents presented higher values of mass as well as a better behaviour while 3D Printing. Therefore, it seems that the evaporation rate of chloroform is lower in the PLCL stents manufacturing, which makes easier to the ink to completely acquire the textured form. Then, it is interesting to see what happens when a solvent trap is added to the 3D printing process. Comparing parallel micro-patterning of PLLA without trap (*Figure 35*) and PLLA with trap (*Figure 36*), it is evident that more homogeneous behaviour of the patterning is seen when adding this accessory in the 3D printer.

Therefore, it is demonstrated that solvent evaporation of PLLA decreased when creating a oversaturated atmosphere of chloroform, which helped to the ink to have more time to consolidate the structure. On the other hand, when adding the solvent trap to the PLCL stents (*See Figure 38 and 39*) no big differences were seen. Actually, an homogeneous behaviour is seen in both conditions which is not surprising since PLCL already presented a better evaporation rate. For this reason, in PLLA samples an improvement on the 3D printing efficiency is successfully obtained.

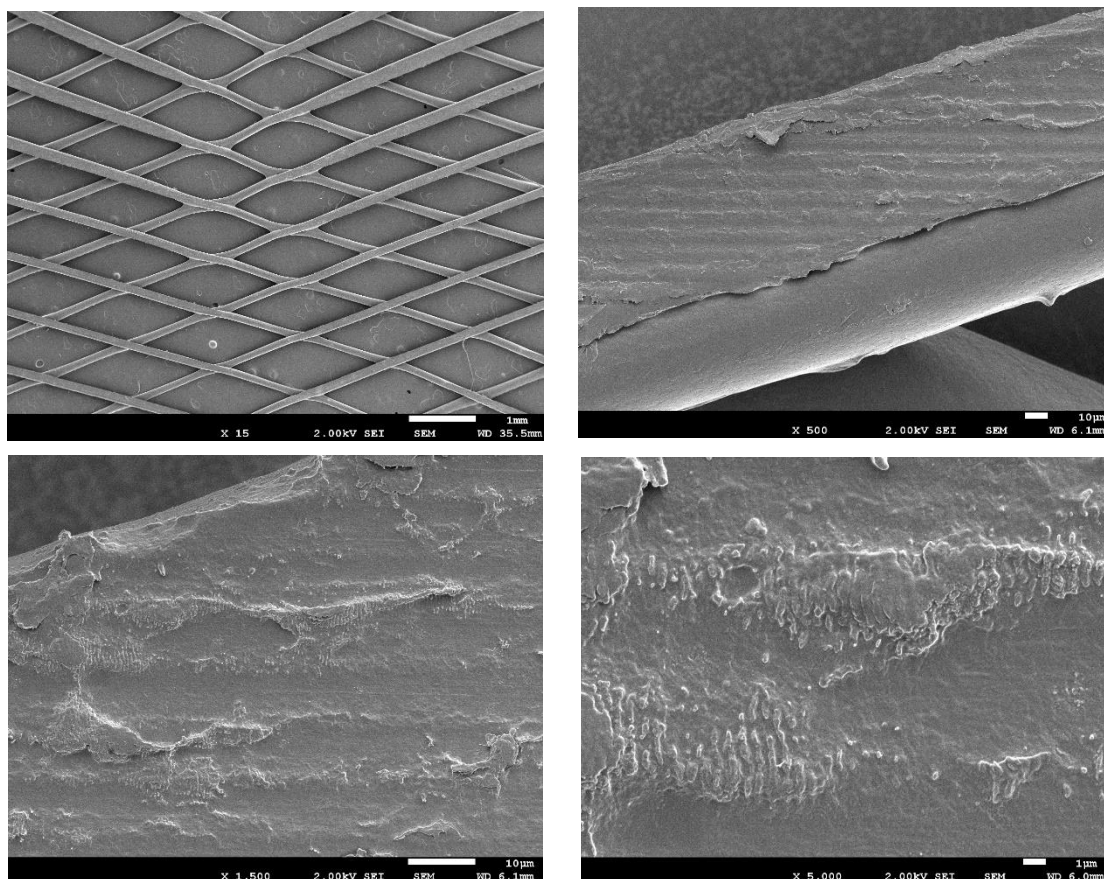


Figure 34. SEM images of perpendicular micropatterning of PLLA stents.

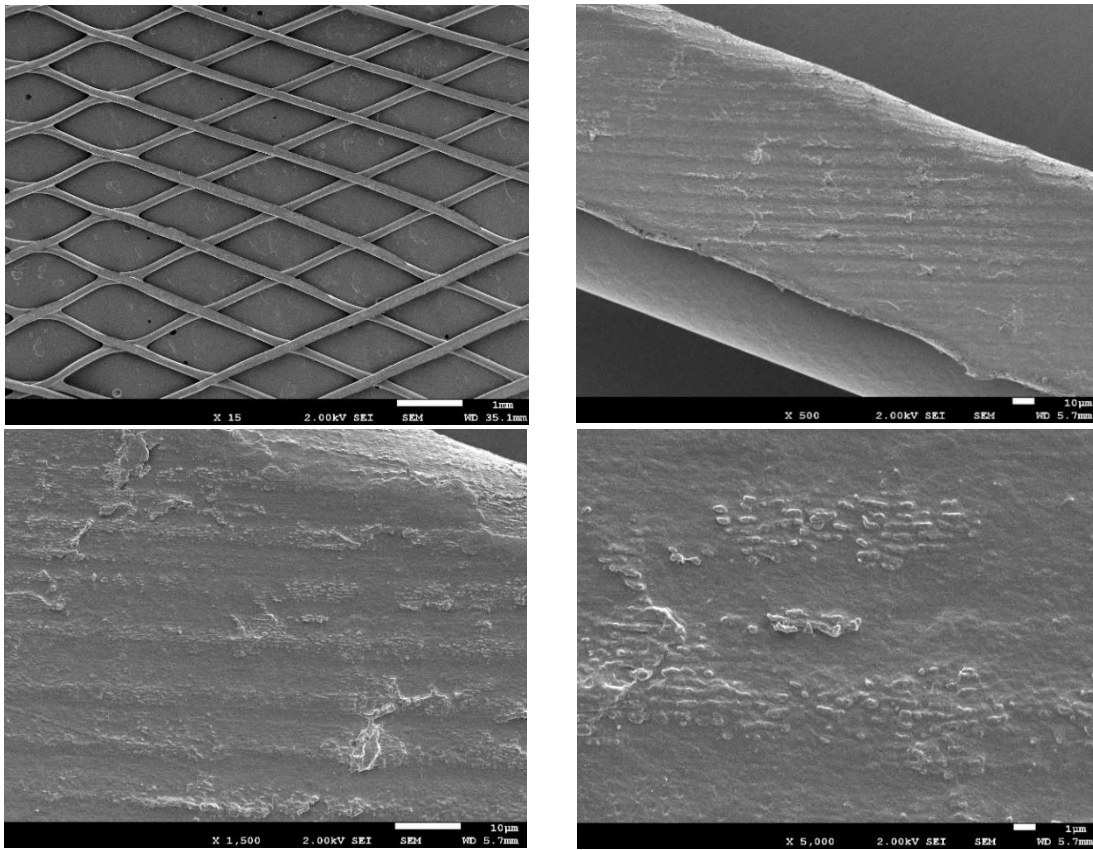


Figure 35. SEM images of parallel micropatterning of PLLA stents.

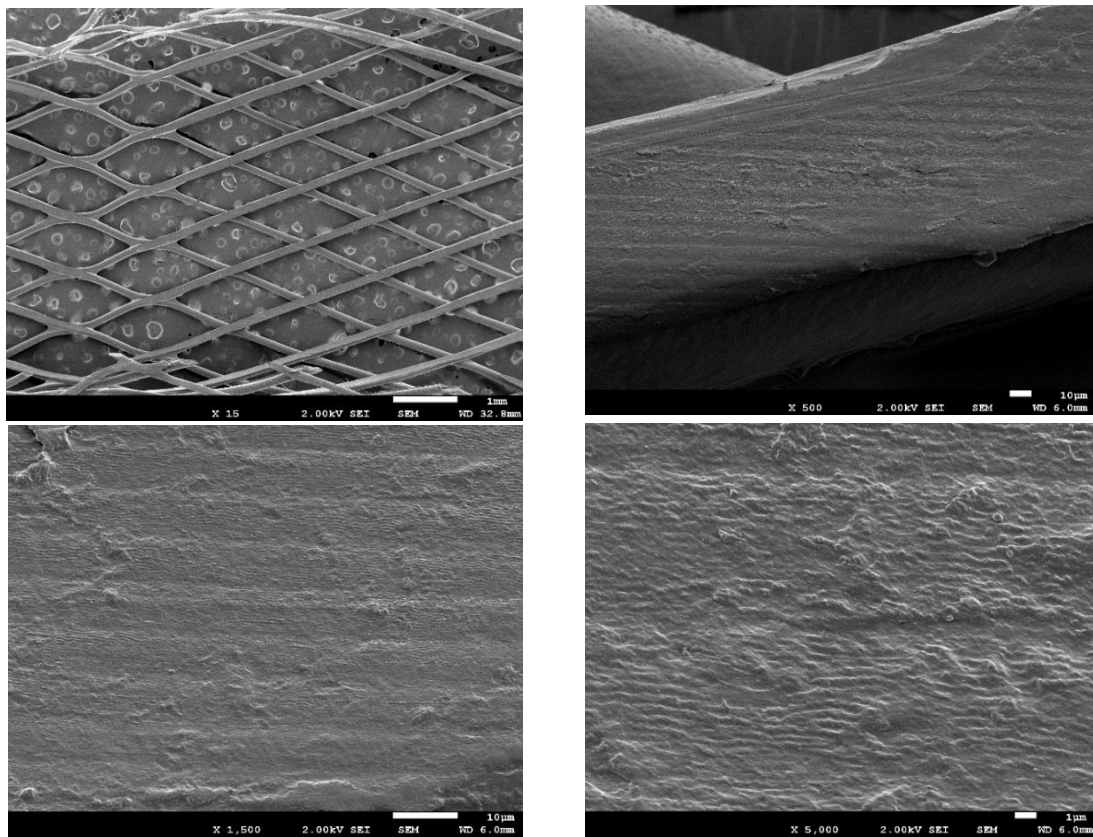


Figure 36. SEM images of parallel micropatterning of PLLA stents, using a solvent trap during 3D printing process.

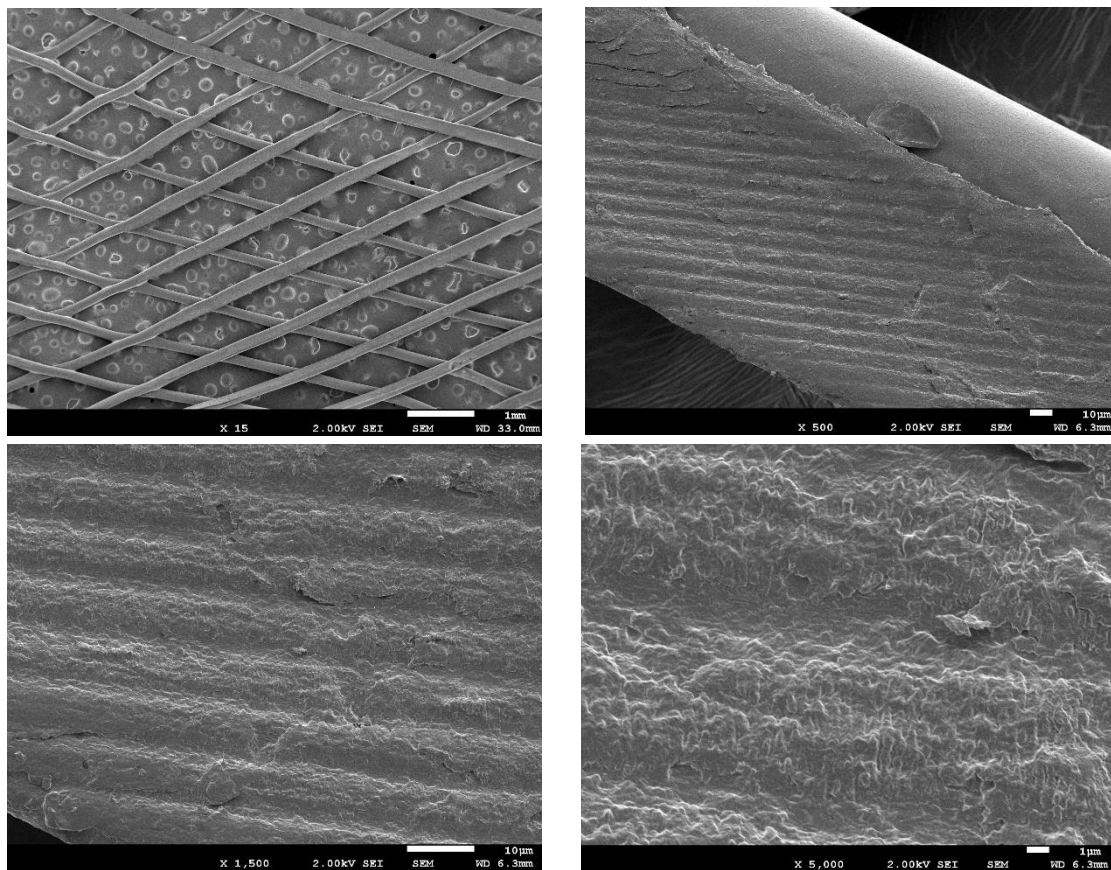


Figure 37. SEM images of perpendicular micropatterning of PLCL stents.

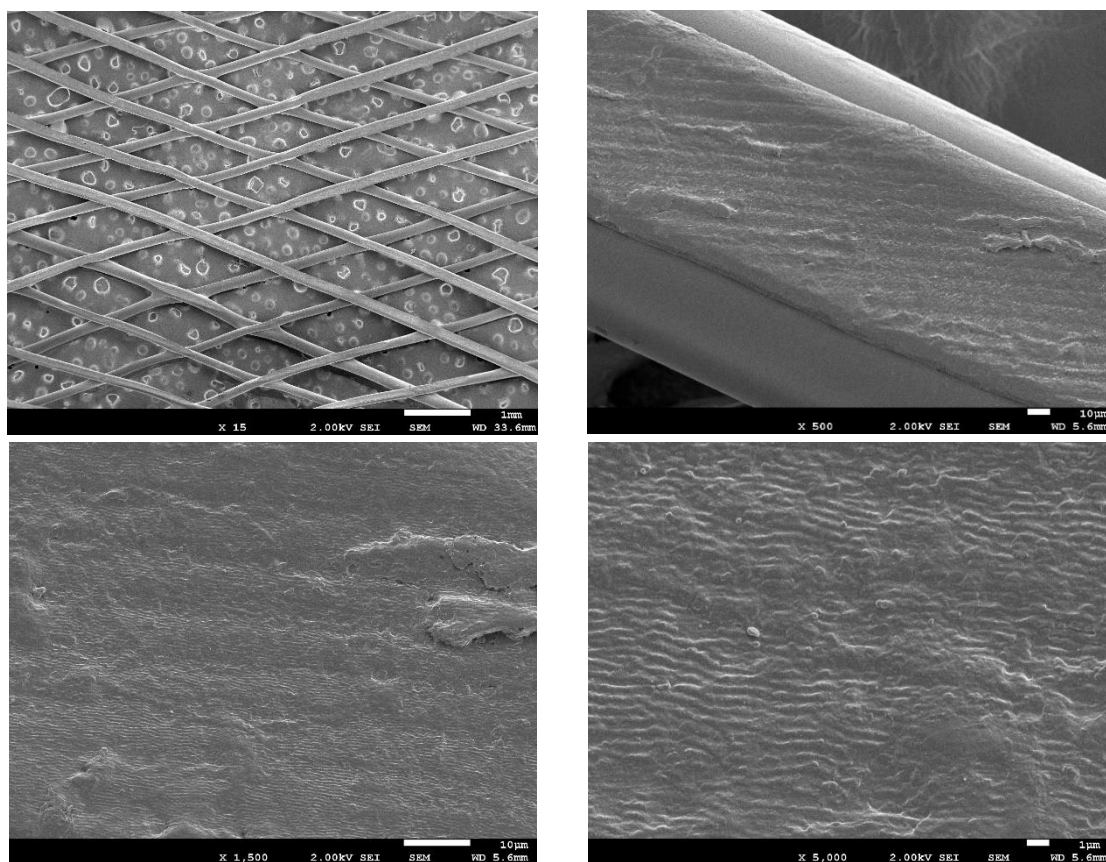


Figure 38. SEM images of parallel micropatterning of PLCL stents.

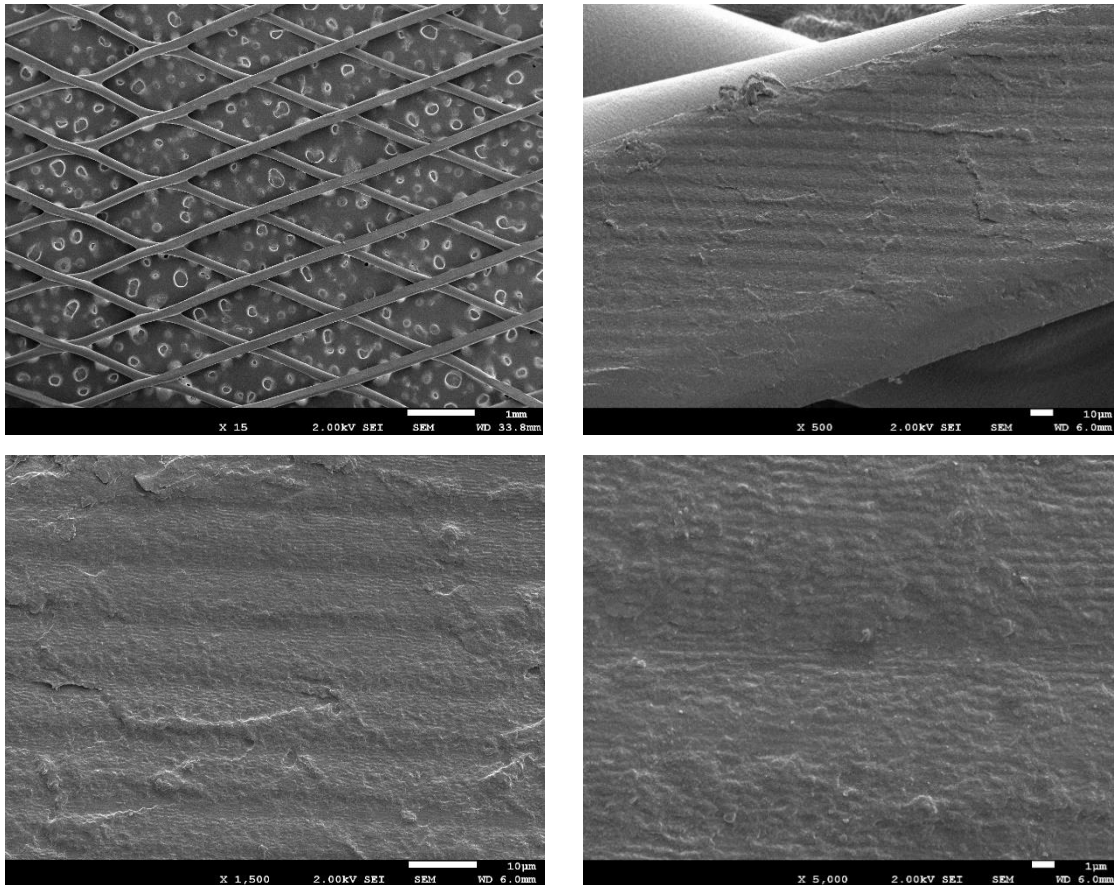


Figure 39. SEM images of parallel micropatterning of PLCL stents, using a solvent trap during the 3D printing process.

4.4. Accelerated degradation study of the stents

4.4.1. Stents appearance

Figure 40 shows stents degradation appearance after 2, 4, 7 and 10 days of degradation time. In general, PLCL stents showed a more reinforced structure in comparison to PLLA stents. Higher differences appeared at day 10. While PLLA presented a more advanced degradation, PLCL kept its structure although some parts of the stents were disintegrated. For both conditions, a reduction in strut thickness is seen as degradation proceeds.

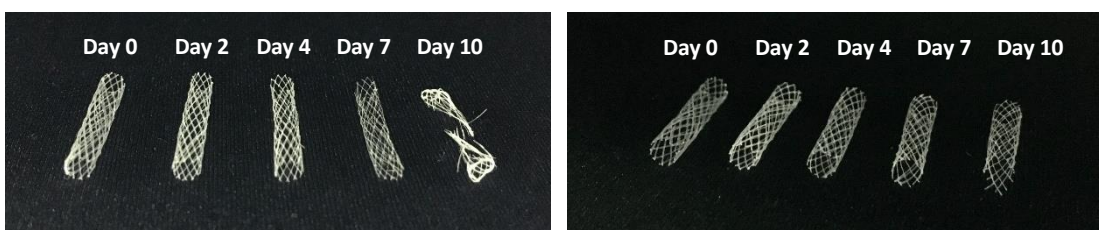


Figure 40. Stents appearance over degradation time. PLLA stents (left) and PLCL stents (right).

4.4.2. Optical Microscope (OM)

Strut thickness of the stents were determined through optical microscope obtaining a gradually decrease for both conditions as can be seen in *Table 8*. A reduction of the strut thickness from day 0 to day 10 of degradation was found for both conditions, a decrease from 120.93 μm to 43.91 μm for PLLA and a decrease from 151.59 μm to 53.31 μm for PLCL.

Table 8. Strut thickness changes over degradation time.

Degradation time (days)	Strut thickness PLLA (μm)	Strut thickness PLCL (μm)
0	120.98 \pm 0.29	151.59 \pm 7.23
2	104.96 \pm 8.51	118.25 \pm 6.52
4	80.25 \pm 2.83	107.84 \pm 1.95
7	54.08 \pm 9.24	98.04 \pm 5.24
10	43.91 \pm 4.05	53.31 \pm 7.50

OM images (*Figure 41*) showed a clear tendency of decrease in strut thickness decrease. The structure of stent remained the same but with thinner struts as the hydrolysis reactions took place. These images show an effect characteristic of surface hydrolysis instead of a bulk hydrolysis, which means that the core of the stents keep without changes while the degradation occurs mainly in the outer layer of the struts, generating the effect observed.

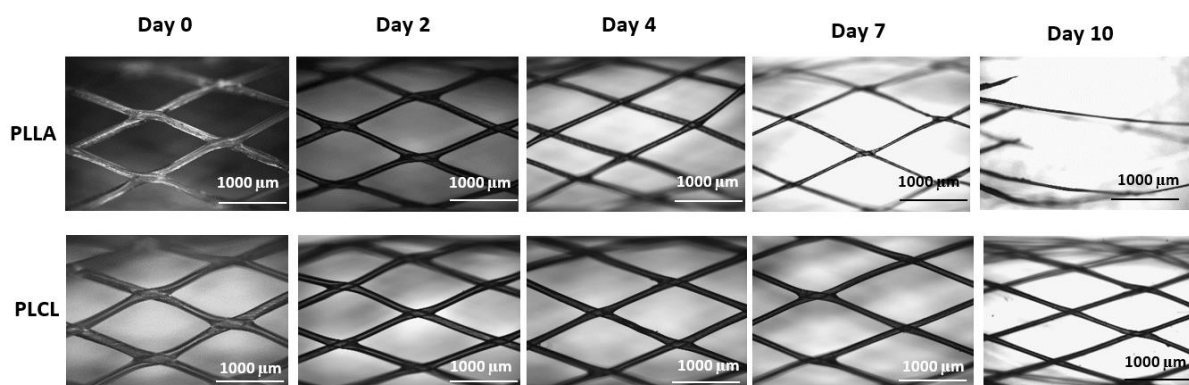


Figure 41. Optical microscope images of PLLA samples (on top) and PLCL samples (down) over degradation time

4.4.3. Scanning electron microscopy (SEM)

Figure 42 and Figure 43 show SEM images of the stents over degradation time at magnifications of x15 and x50.

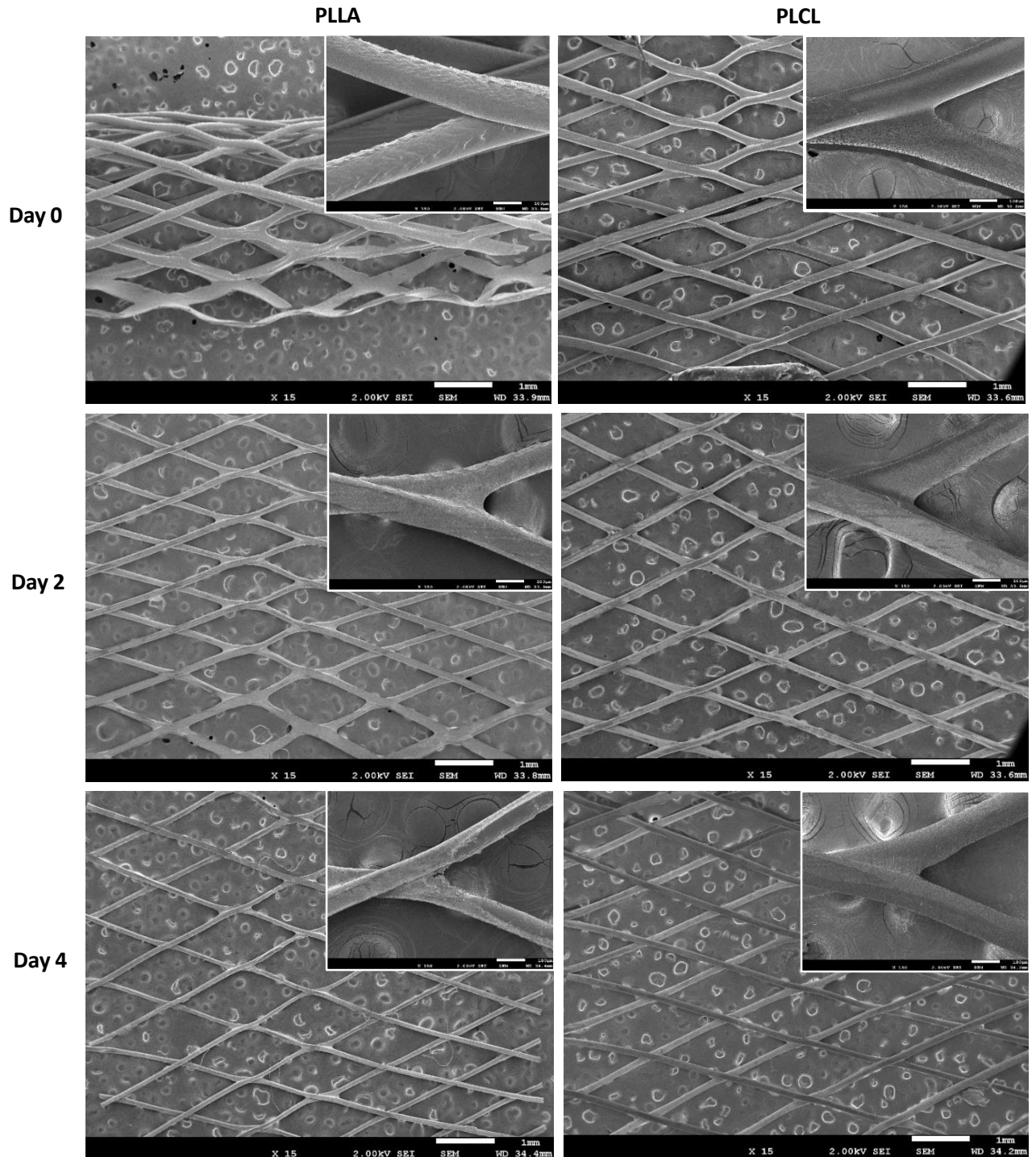


Figure 42. SEM images of PLLA and PLCL stents at 0, 2 and 4 days of degradation.

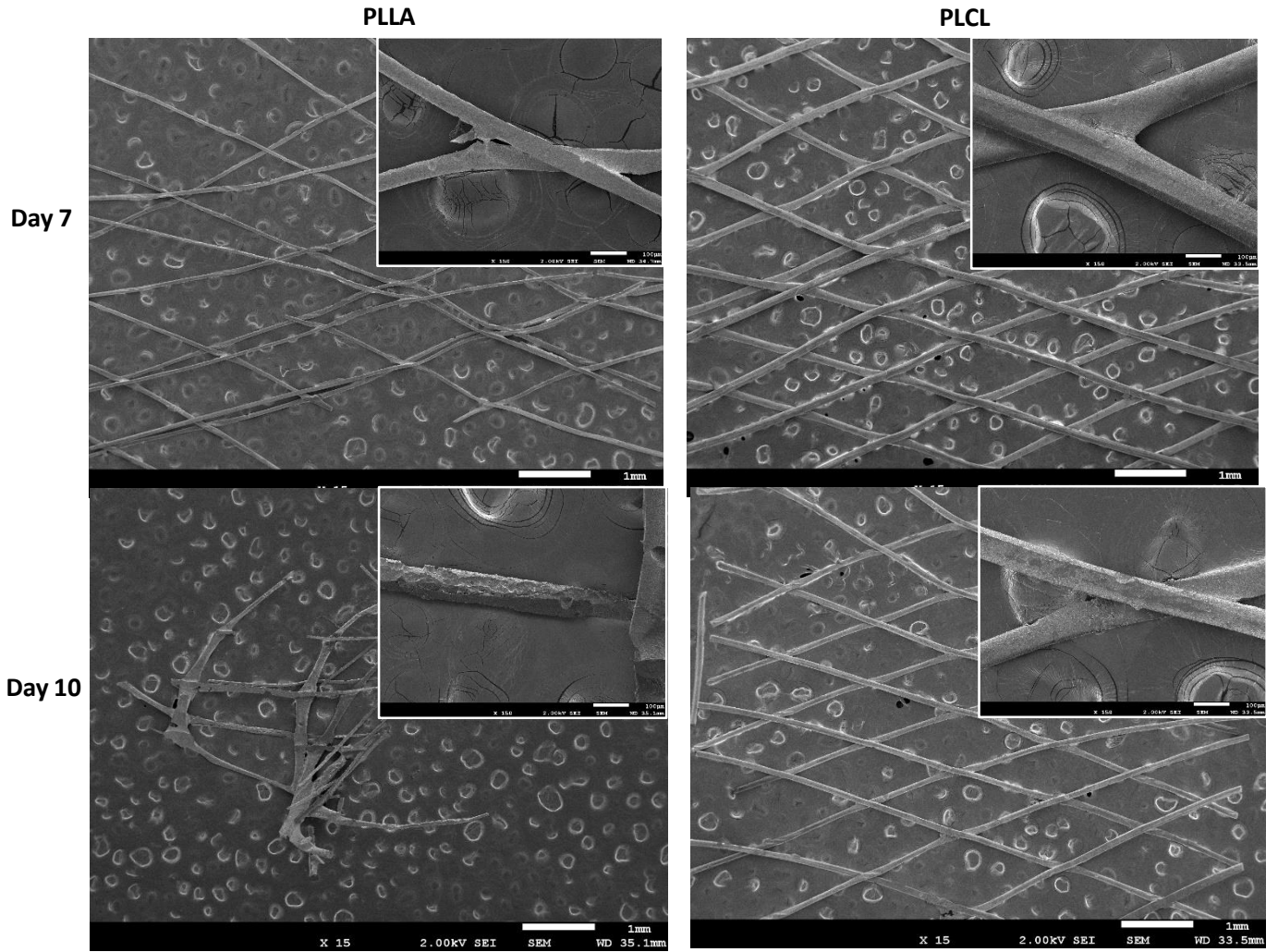


Figure 43. SEM images of PLLA and PLCL stents at day 7 and 10 of degradation.

With these images, it can be seen a thinning effect at the surface of the stents. Therefore, it seems that degradation occurs mainly at the surface where the material is shaved off from the bulk. Although the degradation and decrease on strut thickness, the unions between struts maintained welded, as can be seen at magnification of x150, except for PLLA at day 10 where the high degradation results on the separation of the struts unions. Higher differences between PLLA and PLCL stents are more seen as the degradation proceeded which can be explained for the geometrical factors seen in *Table 8*.

Figures 44 and 45 show cavities as the effect of hydrolysis erosion over degradation with SEM images at magnification of x500

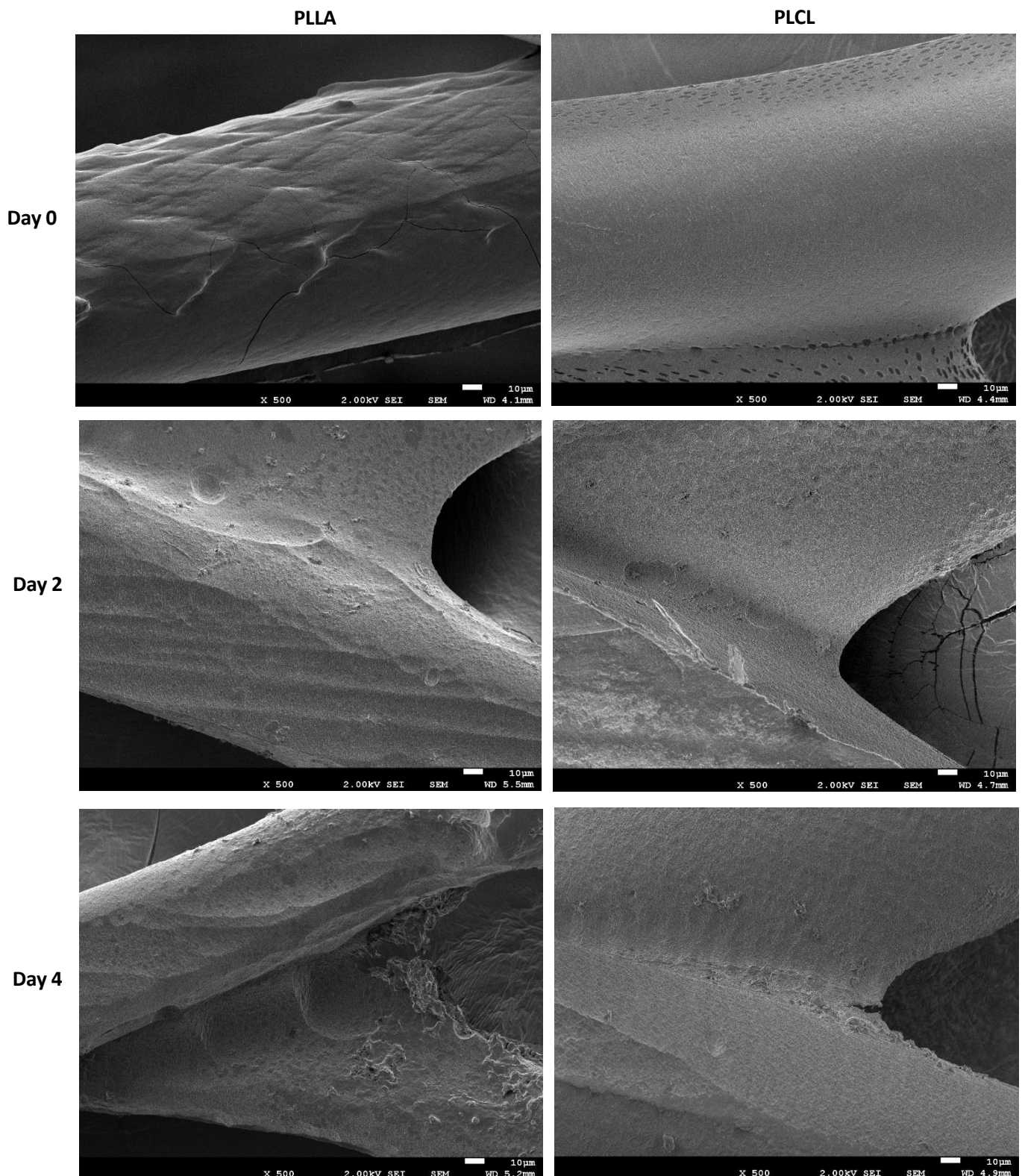


Figure 44. SEM images of stents over degradation time at days 0, 2 and 4 at x500 magnifications.

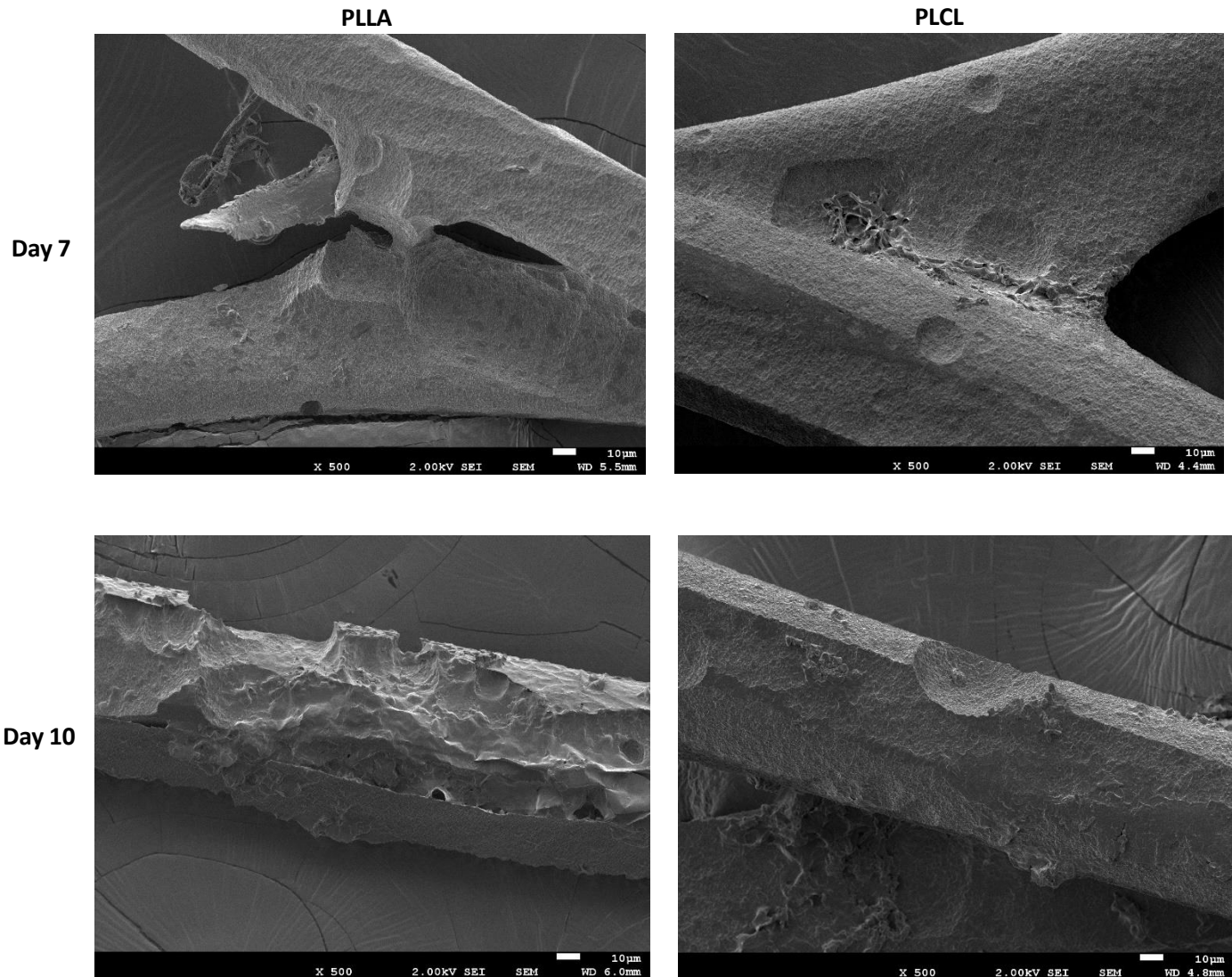


Figure 45. SEM images of stents over degradation time at days 7 and 10 at x500 magnifications.

PLLA stents presented more quantity of cavities in comparison to PLCL stents as the degradation time increased (See Figures 44 and 45). This behaviour was expected due to the PLLA lesser quantity of material. Union between struts are strong enough to keep struts together although the cavities originated due to hydrolysis erosion

4.4.4. pH evolution

The pH of the supernatant of the samples in the accelerated conditions was analysed for each time point (See *Figure 46*) since the degradation of PLLA results in formation of lactic acid and degradation of PLCL results not only in formation of lactic acid but also in caproic acid. pH of the media at time point 0 was around 12.7 (corresponding to the theoretical value of 13), and no variation was seen until day 10, where the solution turned slightly more acidic.

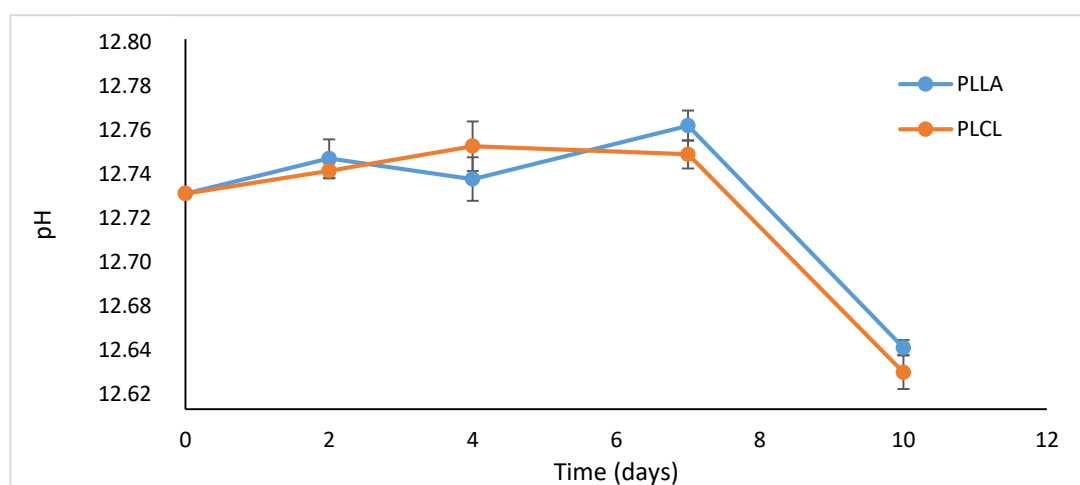


Figure 46. pH changes in the degradation media solution over time.

4.4.5. % of mass loss

Samples were weighed after drying overnight in the oven, before and after the accelerated degradation for each point. *Figure 47* shows the percentage of mass loss with time over 10 days of incubation for samples of PLLA and PLCL. The higher mass loss observed is in accordance with the morphology images seen through OM and SEM. These behavior corresponds to surface hydrolysis mechanisms. PLLA presented higher degradation rate than PLCL at all time points. Significant differences appeared comparing PLLA and PLCL stents of $p < 0.05$ for day 2 and $p < 0.001$ for days 4, 7 and 10. Almost all PLLA stents had been degraded obtaining a considerable standard deviation and an average around 90%, while the structures of PLCL stents were still present in all the samples even though around 75% of the mass was degraded.

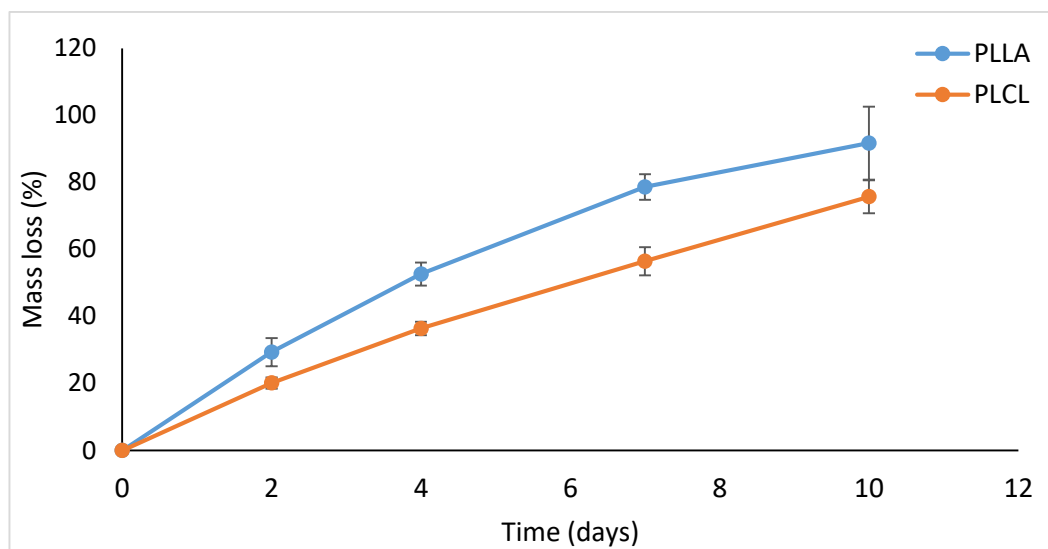


Figure 47. Percentage of mass loss of stents of PLLA and PLCL during the accelerated degradation test.

These results were expected since stents made of PLCL presented higher mass (Table 5). Even though geometrical factors are the main reasons of these results, it is interesting to take into account other possible explanations. PCL presents lower degradation rate than PLLA. Actually, it is used to tune degradation rates of PLLA. Also, PCL presents higher hydrophobicity than PLLA. Then, perhaps all these factors helped to the PLCL to decrease the degradation rate in comparison to PLLA.

4.4.6. Molecular weight

The average molecular weights (M_w and M_n) of PLLA and PLCL stents measured by GPC technique, showed unchanged results over the 10 days of accelerated degradation (See Figure 48). The values of M_n and M_w for PLLA stents are around 273612 and 695210 respectively while lower values for the copolymer of 187316 and 378730 were found. Also similar results of polydispersity index (PDI) were obtained with values of 2.54 and 2.03 for PLLA and PLCL respectively. Thus, these samples did not show monodispersed behaviour ($PDI \neq 1$) which means there are some differences regarding the length of the chains [67]. On the other hand, values around 2 are the expected for condensation polymerization typical of PLLA.

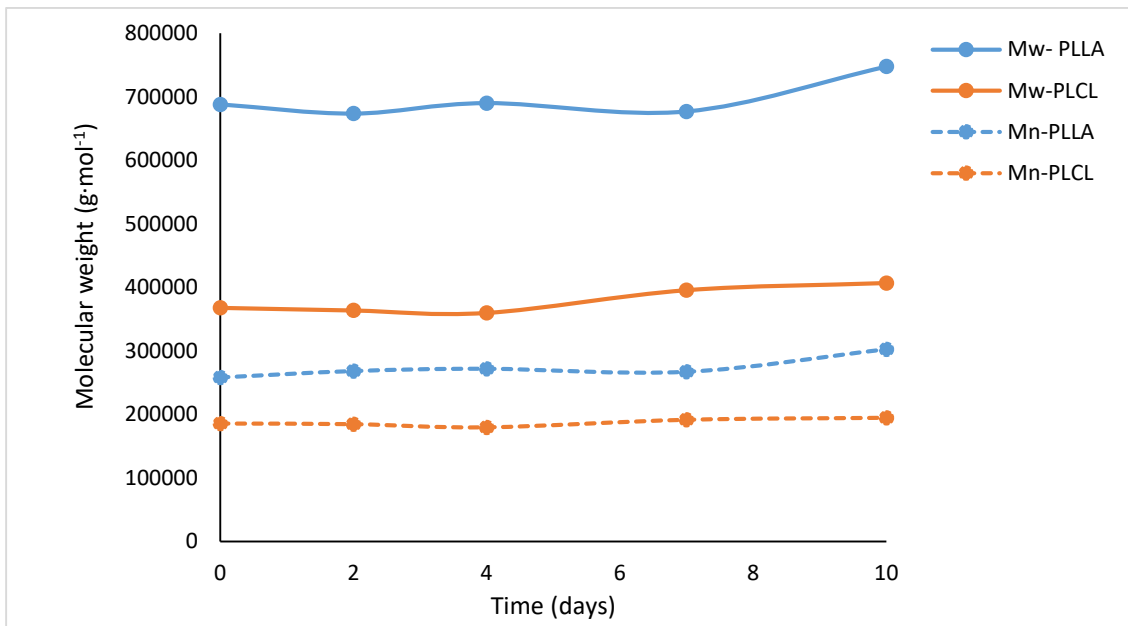


Figure 48. Molecular weight results over degradation time.

While an homogeneous reduction in the molecular weight defines bulk degradation, invariable values would describe surface degradation mechanisms [68]. Then, the unchanged values of M_w correspond to hydrolysis reactions through surface erosion mechanisms which is in consonance with the other results.

4.4.7. Composition change (NMR)

For copolymer stents, a compositional change during degradation was seen indicating which polymer unit degraded faster. These changes were monitored by H-NMR calculating the relative mol % at each time point. NMR spectra showed the same characteristic peaks of PLCL for the different time points of degradation but some variations in the integration peaks were determined. Peaks detected (See Figure 49) were at 1.56 (D, A) (CH₃, PLLA), 5.1 (B,C) (CH, PLLA), 1.35-1.67 (K, M,F,H) (CH₂CH₂CH₂, PCL), 2.39 (I, N) (CH₂CO, PCL) and 4.10 (E, J) (CH₂O, PCL). As an example, these values can be seen in Figure 49 for the case of PLCL without degradation. Note that peaks at 7.25 and 0.0 ppm correspond to the solvent used in the analysis.

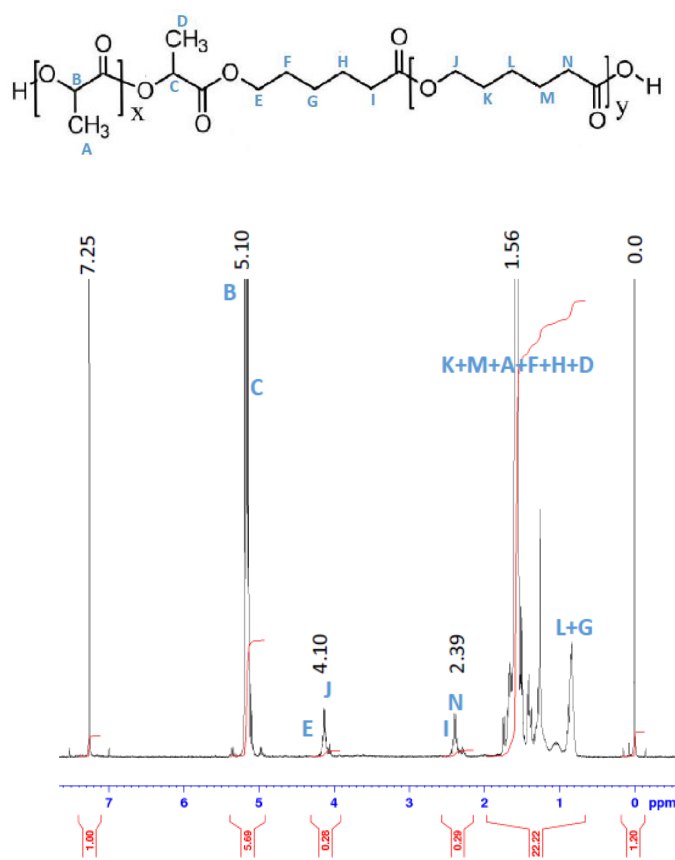


Figure 49. H-NMR spectra for PLCL stents without degradation.

Signals at 2.39, 4.10 and 5.10 correspond to the characteristic LA-CL junctions of a PLCL copolymer which involves transesterification reactions [69].

Using the integration of two characteristic peaks at 5.1 ppm and 4.1 ppm corresponding to the LA units and CL units respectively, LA/CL molar ratio was calculated. *Figure 50* shows the spectra of each signal during degradation assay and *Table 9* shows the complete data of average and standard deviation for molar concentration changes during accelerated degradation.

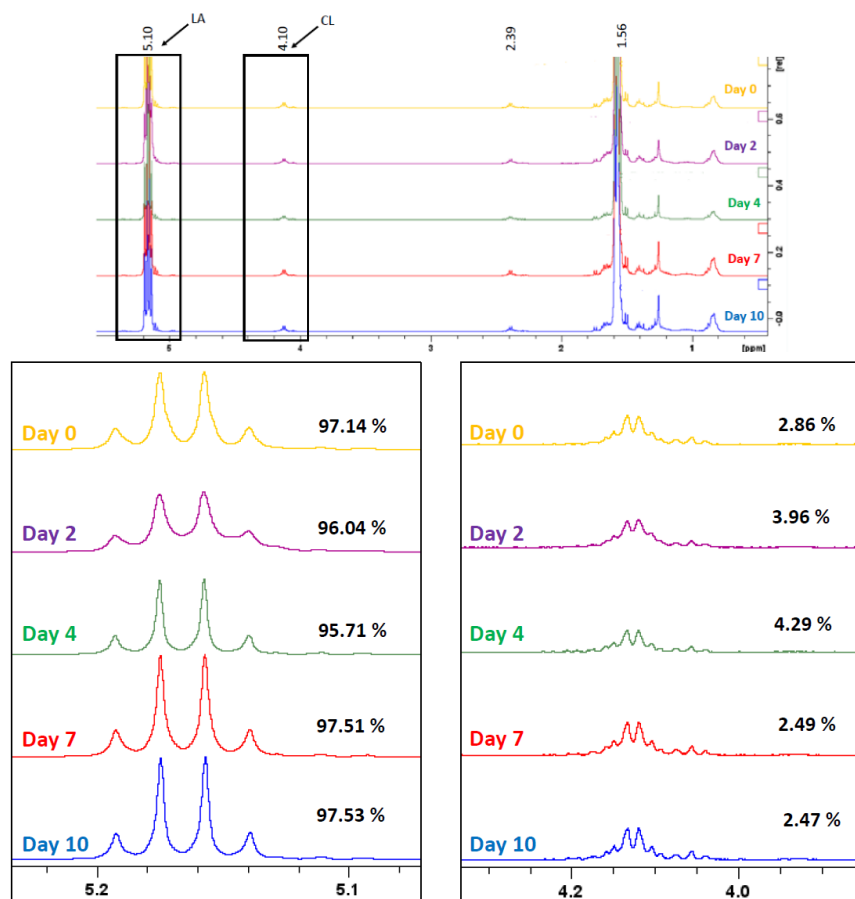


Figure 50. H-NMR spectra at 5.1 ppm corresponding to LA units (left) and at 4.1 ppm corresponding to CL units (right). Percentage of composition change during degradation assay.

Table 9. Composition changes during degradation assay for the copolymer.

Degradation time (days)	LA concentration (%)	CL concentration (%)
0	97.57 ± 0.01	2.43 ± 0.01
2	96.04 ± 0.19	3.96 ± 0.19
4	95.71 ± 0.34	4.29 ± 0.34
7	97.51 ± 0.02	2.49 ± 0.02
10	97.60 ± 0.07	2.40 ± 0.07

LA and CL values did not show significant differences between days 0 with 10, 2 with 4 and 7 with 10. For CL values neither significant differences appeared between day 0 and day 10.

As it can be seen at *Table 9*, first LA units degraded faster than CL units as expected but from day 7 to day 10 molar ratio of LA units started to increase. That means that PCL parts of PLCL started to degrade later than PLLA parts as was expected, and it seems that between day 4 and day 7 is when PCL areas of the copolymer started to degrade through the hydrolysis reactions.

4.4.8. Thermal properties and crystallinity changes

The endothermic peak related to the melting of the crystalline phase remains almost without changes during degradation while the glass transition temperature appears as an exothermic peak due to the enthalpic relaxation of the macromolecules. From day 0 to day 10 the peak becomes slightly less exaggerated as can be seen in *Figure 51* compared with a sharper peak at day 0, which can be attributed to the loss of the amorphous parts of the polymers due to the hydrolysis process. T_g is the temperature in which the physical properties of plastics change from a glassy or crystalline state to a rubber behaviour, which means that above this temperature the molecules of the polymer will have more mobility and they would change from hard and brittle to soft. T_g is only related to amorphous part of semicrystalline polymers, while T_m corresponds to crystalline parts of the polymer [16]. Then, even though the decrease of the T_g is not significant (*See Table 10*) it is clear that the curve of the T_g is gradually disappearing over degradation time since amorphous parts are more degraded.

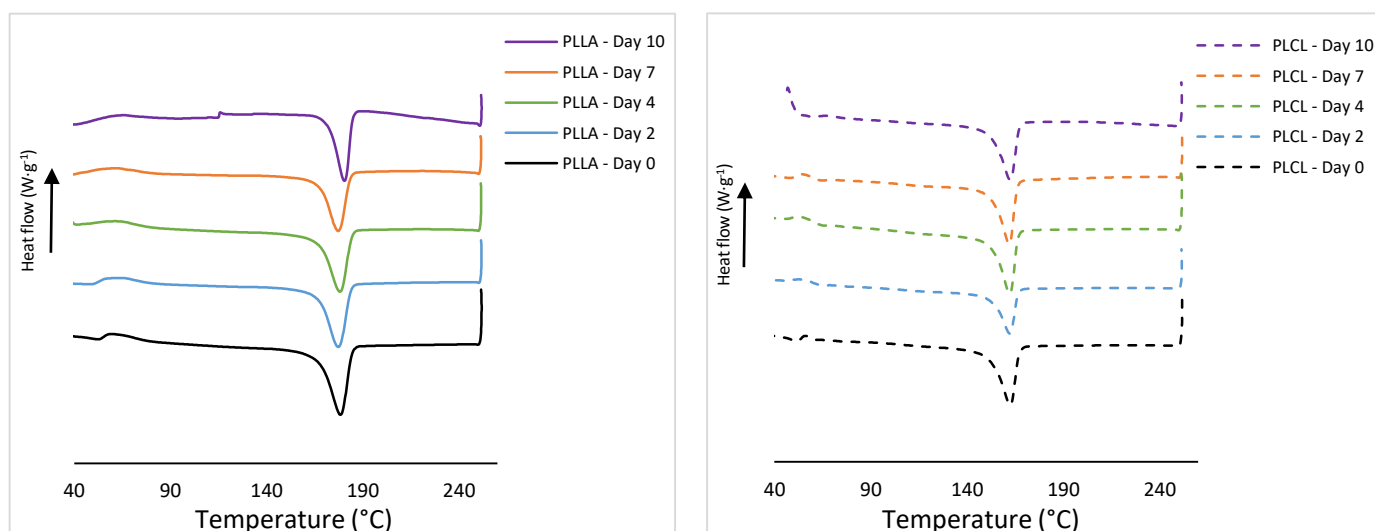


Figure 51. DSC diagrams for thermal changes during accelerated degradation for PLLA (left) and PLCL (right).

No statistically significant differences were seen concerning values of *Table 10* ($p < 0.05$). However, it can be seen a slightly tendency to decrease T_f , ΔH_f or percentage of crystallinity from day 0 to day 4 for PLCL stents. For the same time period it can be also seen a tendency to slightly decrease acid lactic content in the H-NMR analysis (*See Chapter 4.4.7*).

In general, the similar crystallinity values show that the core of the struts remained protected while the degraded chains at the surface of the struts were dispersed into the medium. Therefore, these results are in consonance with last chapters where the hydrolysis reactions showed a surface erosion mechanism.

Table 10. Thermal properties data during degradation.

Degradation time (days)	PLLA				PLCL			
	T_g (°C)	T_m (°C)	ΔH_f (J·g ⁻¹)	Crystallinity (%)	T_g (°C)	T_m (°C)	ΔH_f (J·g ⁻¹)	Crystallinity (%)
0	69.99 ± 2.06	178.70 ± 0.27	24.90 ± 0.70	26.78 ± 0.76	59.88 ± 0.88	162.41 ± 0.34	18.27 ± 2.32	23.60 ± 2.71
2	69.36 ± 0.81	177.85 ± 0.69	26.230 ± 4.40	24.78 ± 1.40	60.21 ± 0.98	162.23 ± 0.10	18.27 ± 0.62	20.64 ± 0.72
4	68.95 ± 0.70	178.20 ± 0.12	24.11 ± 0.05	25.93 ± 0.05	60.12 ± 1.97	162.13 ± 0.13	18.27 ± 0.38	20.64 ± 0.44
7	68.63 ± 2.64	178.40 ± 1.05	23.89 ± 2.29	25.69 ± 2.49	62.94 ± 0.35	161.86 ± 0.02	18.27 ± 0.31	21.28 ± 0.36
10	68.58 ± ./.	172.20 ± ./.	20.18 ± ./.	21.70 ± ./.	60.70 ± 1.27	162.20 ± 0.81	18.27 ± 2.01	22.08 ± 2.34

4.4.9. Mechanical properties

Mechanical properties of the degraded stents were analysed by means of a compression test and data was determined at 25% and 50% of compression of the diameter. It can be seen a tendency to decrease over time with degradation as was expected (*Figures 52 and 53*). It is obvious that mass loss (*See Chapter 4.4.5*) had an influence over the mechanical properties of the stents.

Graphs on *Figure 52* show results of normalizing force by the length of the stents in order to take into account the slightly differences of dimensions of all the stents. No significant differences between PLLA and PLCL stents were found. However, it can be seen a tendency of PLCL to have higher values that is caused by the higher mass as can be contrasted on *Figure 53* where the force is also normalized by mass. High standard deviation is obtained for degraded samples, even more in day 4.

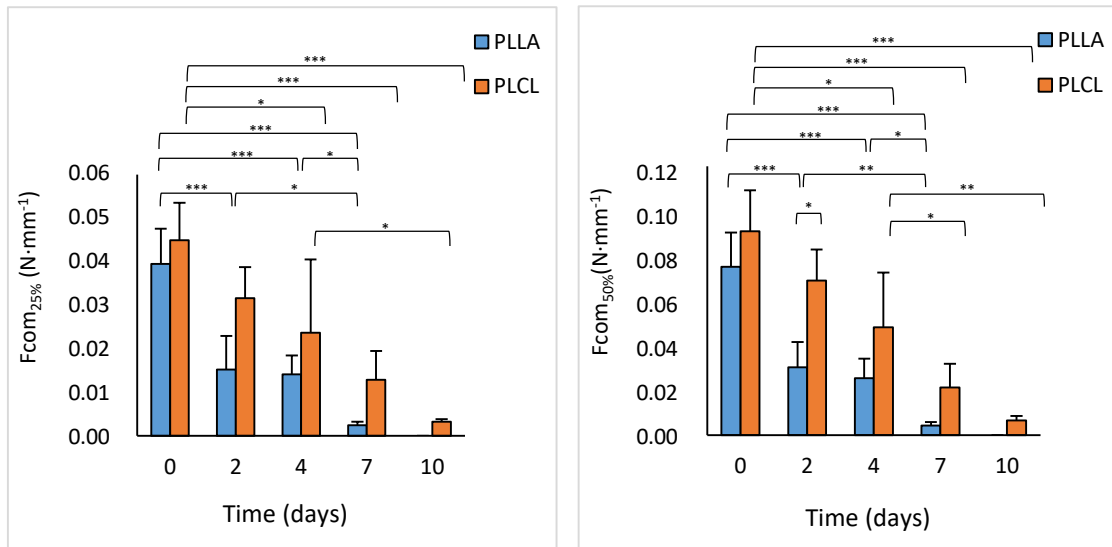


Figure 52. Compression force normalized by length of the stents over degradation time for 50% of compression (left) and 25% of compression (right).

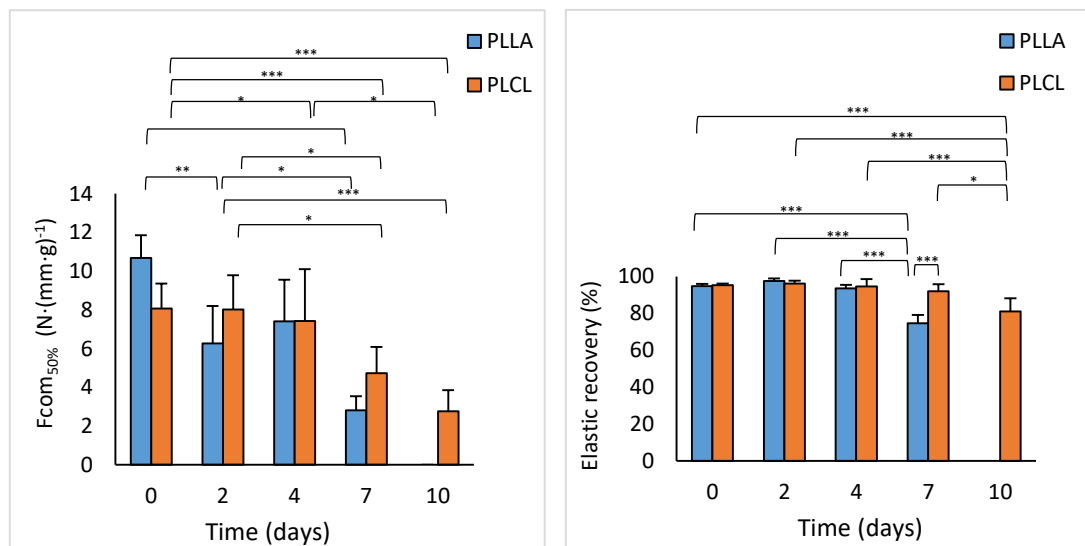


Figure 53. Compression force normalized by weight and length of the stents at 50% of compression (left) and elastic recovery of the stents over degradation time (right).

Also, elastic recovery was computed from initial and final stent diameter obtaining the results of Figure 53. For both types of stents, there is a slightly increase of the elastic recovery from day 0 to day 2, although the high standard deviation it can be related with crystallinity results where there is a decrease of the percentage of crystallinity in both conditions.

Elastic recovery has a tendency to decrease, even though there are not high differences between the conditions. However, while PLLA has a more dramatic decrease, values of PLCL indicates that it takes more time to the polymer to lose its flexibility thanks to its component of PLC or other geometrical factors as higher content of mass in the stents.

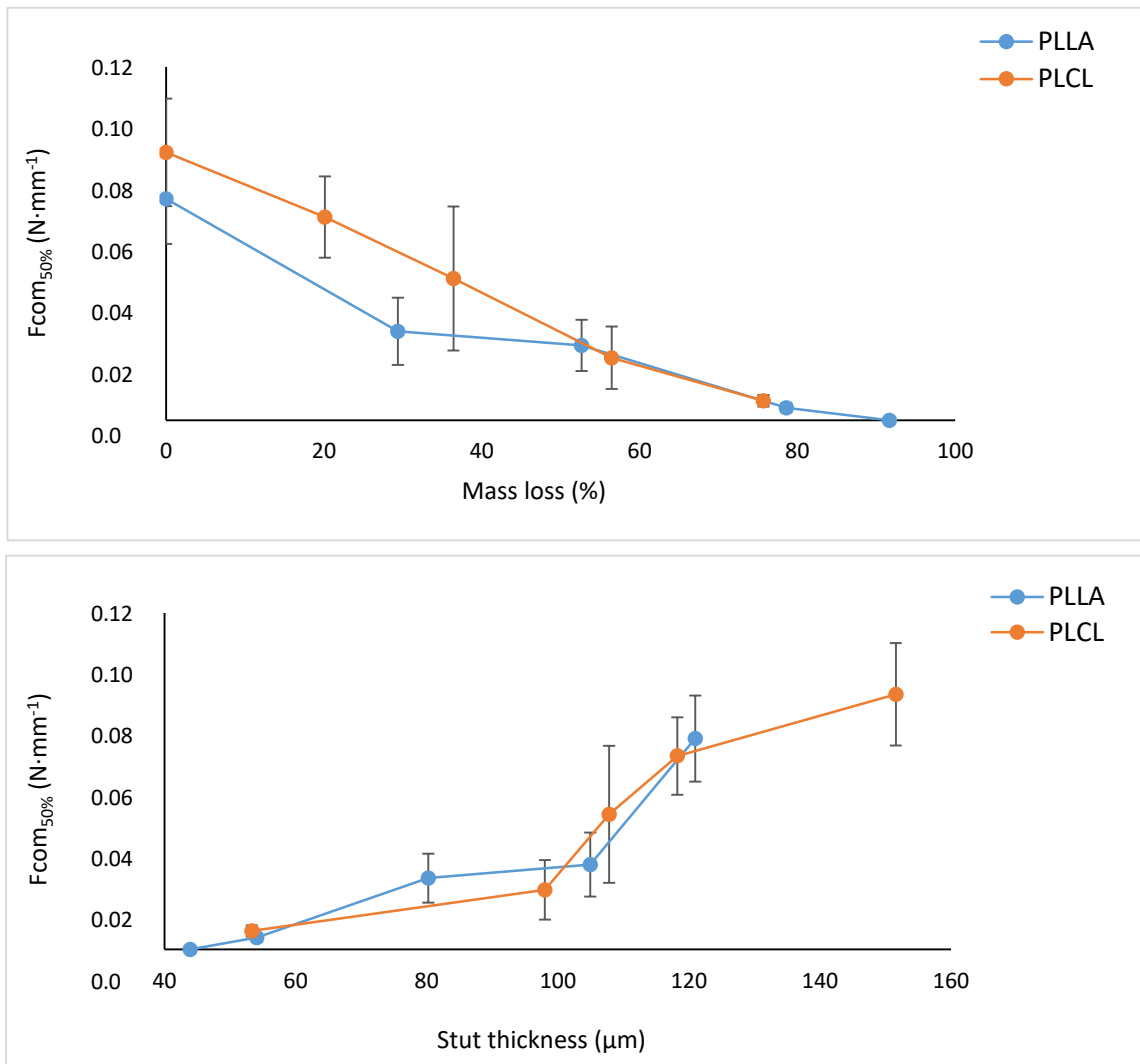


Figure 54. Force at a 50% diameter compression vs % mass loss or strut thickness.

Figure 54 shows force at a diameter compression of 50% normalized by length versus two different variables: mass loss or strut thickness. It can be clearly seen the force decrease as mass loss increased and strut thickness decreases.

With all the results from the accelerated degradation assay, the mechanisms that took place during the hydrolysis reactions can be analysed. PLLA can degrade through bulk or surface degradation

mechanisms. The experimental effects of morphology changes, mechanical changes and thermal properties will indicate which one prevailed to the other in the degradation assays. Values obtained in the accelerated degradation assay showed a thinning effect on the morphology images, significant mass loss, unchanged molecular weight, insignificant differences on the crystallinity and slightly decrease of compression force while decreasing strut thickness. All these results are in consonance with each other and verify that surface degradation is the pathway that occurs in the present study. The reason of that is the use of the alkaline medium for achieving the accelerated conditions corresponding to previous studies [22]. When the degradation was taking place, the scission chains with lower molecular weight at the surface of the struts of the stents were gradually dispersed into the medium, while the core of the struts remained protected and without changes in the molecular weight. The stents analysed would have therefore the remainders of crystalline regions still attached to the stent core at the surface. *Figure 55* shows the process.

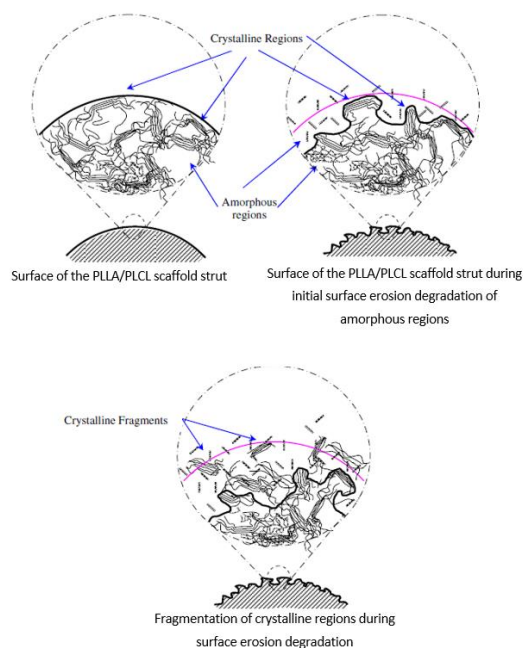


Figure 55. Schematic visualization of how crystalline fragmentation could have taken place. Picture extracted and modified from [22].

4.5. Stents sterilization technique evaluation

4.5.1. Fourier transformed infrared spectroscopy (ATR-FTIR)

The chemical identity of the stents after EtO sterilization was analysed by FTIR-ATR as can be seen in *Figure 56*. The spectra determined the typical resonance for PLA, peaks at around 2911 cm^{-1} and 1270 cm^{-1} for CH_3 groups, 1754 cm^{-1} for C=O groups and 1087 cm^{-1} for carboxyl group. No changes after sterilization were found between control samples and ethylene oxide sterilized samples.

These results showed that none of the two conditions modified the chemical composition of the material. It is important to identify if there is any remaining residual. With this results there is no signal of EtO peaks at 3020 cm^{-1} or at 1125 cm^{-1} which confirmed that the protocols of aeration of the sterilized samples in order to remove possible residual EtO were properly done [70][71].

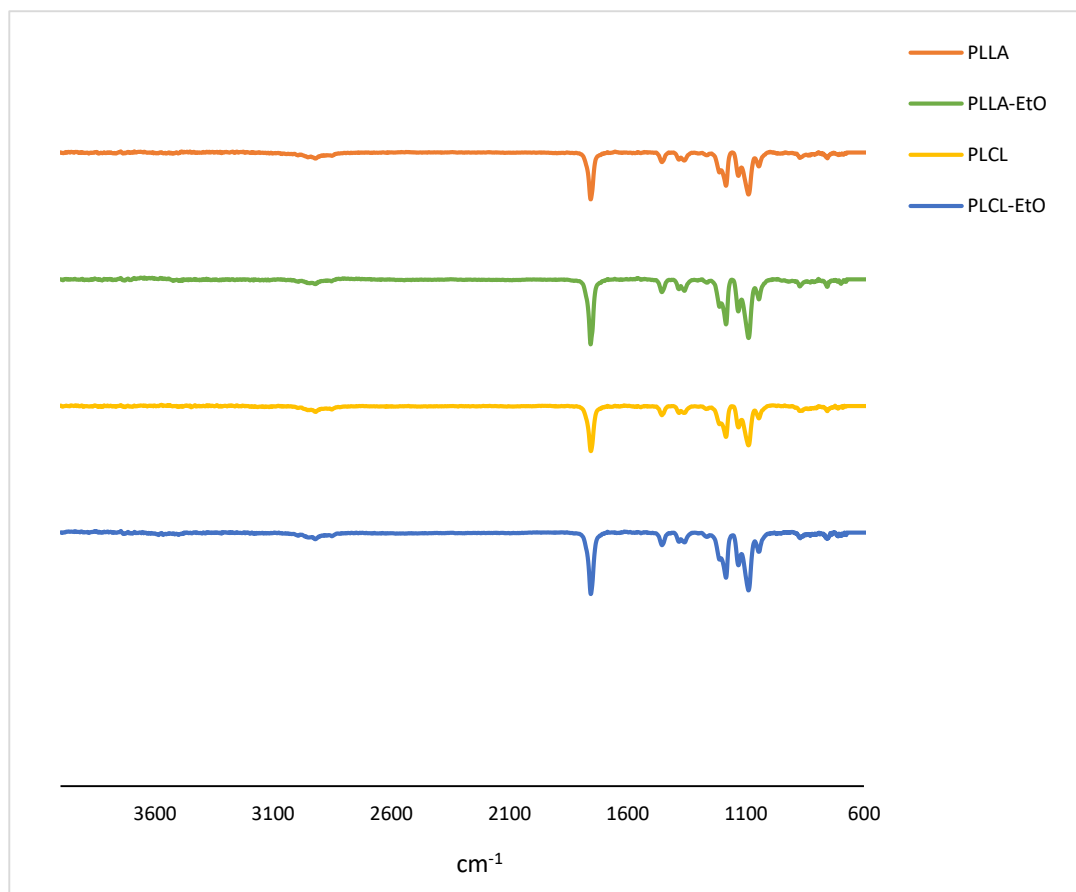


Figure 56. FTIR spectra of control samples (PLLA and PLCL) and sterilized samples with ethylene oxide.

4.5.2. Thermal properties changes

Table 11 shows the results of thermal properties after sterilization of the stents. While conditions sterilized with EtO presented unchanged results, huge changes of percentage of crystallinity was found for gamma sterilization with a value of 40.52% for PLLA samples and 28.64 % for PLCL samples. Also the intensity on the DSC curves for the melting peak of gamma sterilization samples increased considerably as can be seen on Figure 51 while EtO sterilization remained the same. Regarding T_g , gamma radiation conditions exhibited a slightly decrease compared with control samples.

Table 11. Thermal properties changes of PLLA and PLCL stents after sterilization.

Condition	T_g (°C)	T_m (°C)	ΔH_f (J·g ⁻¹)	Crystallinity (%)
PLLA	69.99 ± 2.06	178.70 ± 0.27	25.40 ± 0.46	27.32 ± 0.49
PLLA γ	66.85 ± 0.17	178.85 ± 0.77	37.68 ± 1.03	40.52 ± 1.11
PLLA EtO	69.19 ± 1.13	179.28 ± 0.48	24.74 ± 0.32	26.60 ± 0.34
PLCL	59.88 ± 0.88	162.52 ± 0.28	18.27 ± 1.11	20.90 ± 1.27
PLCL γ	58.26 ± 0.85	167.04 ± 0.13	25.04 ± 0.07	28.64 ± 0.08
PLCL EtO	60.44 ± 0.51	163.47 ± 0.16	18.70 ± 0.60	21.39 ± 0.68

Milicevic et al. [72] reported the increase in degree of crystallinity of a PLLA sample with absorbed dose up to 50 kGy. It was attributed to the scission of strained tie molecules which produced growth of new thin crystal lamellar and then, there is an increase in lamellar thickness. In higher doses, they concluded that the crystallinity decreases due to radiation-induced crystallinity damage which introduces crystal defects and decrease in crystal size. Thus, results obtained of higher value of crystallinity in both polymers and higher intensity in the melting peaks (See Table 11 and Figure 57) when irradiating with gamma irradiation are according the literature since less dose than 50 kGy was used. For the same reasons, decrease in T_g and increase in T_m is obtained by gamma irradiation (See Table 11). A higher difference of T_m for PLLA γ samples in comparison to PLCL γ samples was obtained. Perhaps PCL component on the copolymer helped the system to reorganize in a different way than PLLA.

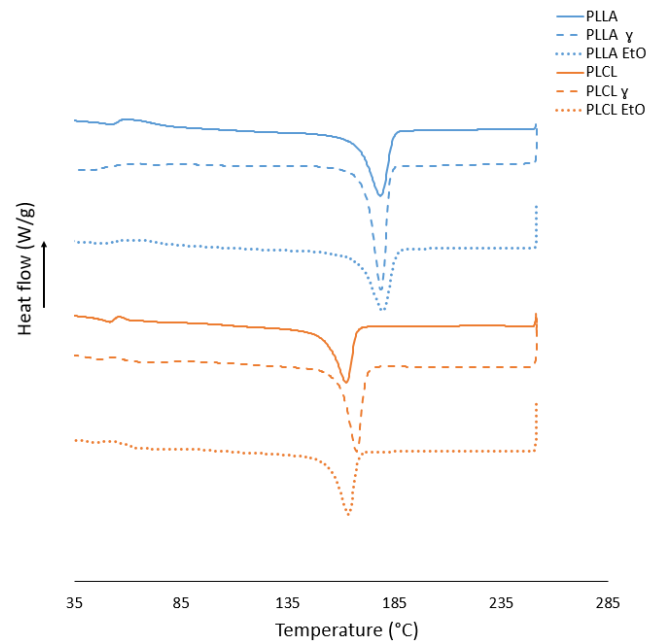


Figure 57. DSC curves of stents at different conditions of sterilization.

On the other hand, it is reported in the literature that EtO can increase the crystallinity of PLLA but does not alter the molecular structure or molecular weight of PLLA [39]. However, EtO sterilization showed in general less thermal variations for both types of stents. It can be easily seen through DSC curves (Figure 57) that none differences of the intensity of the peaks regarding T_m was found, as well as none differences of the values of T_g , T_m and percentage of crystallinity has been determined (Figure 58). Therefore, EtO values showed positive results since no huge differences have been found comparing samples in both conditions before and after sterilization process.

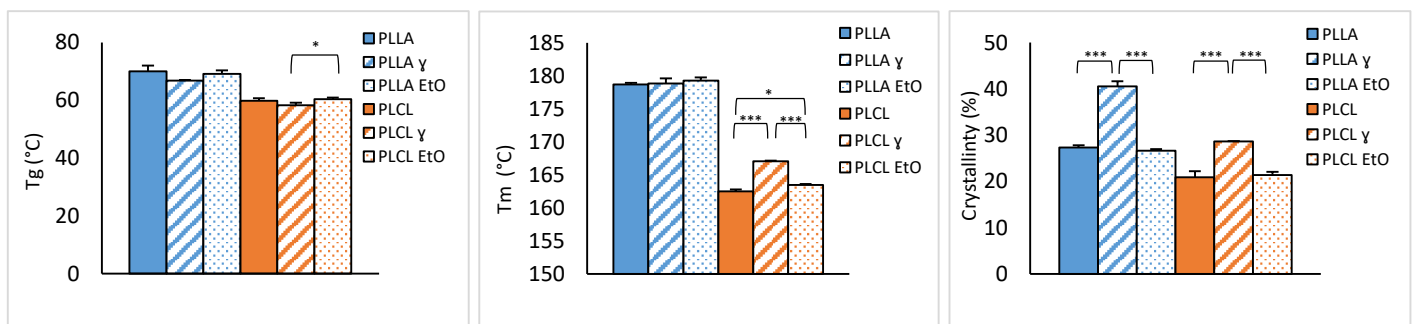


Figure 58. Thermal variations of PLLA and PLCL stents for glass transition temperature (T_g), melt temperature (T_m) and percentage of crystallinity.

These results correspond with the literature. Zada et al. [40] studied PLCL balloons sterilized with gamma irradiation and EtO and concluded that material's properties suffered a considerably decrease after gamma radiation sterilization while EtO did not change polymer properties. On the other hand, Conrad et al. [73] compared different gamma radiation on 3D-printed PLA samples at different radiation doses reporting that tensile strength properties changes were seen mainly beyond 50kGy.

4.5.3. Molecular weight

The average molecular weights (M_w and M_n) of PLLA and PLCL stents were analysed through GPC. Values for EtO sterilization showed unchanged results for PLLA and PLCL (See figure 59). While gamma radiation showed a dramatic decrease of M_n and M_w for both conditions. For PLLA, M_w decreased from 688050 to 186900. For PLCL, M_w decreased from 367840 to 171300. Values of M_n decreased from 258210 to 119220 and from 185690 to 198430 for PLLA and PLCL respectively.

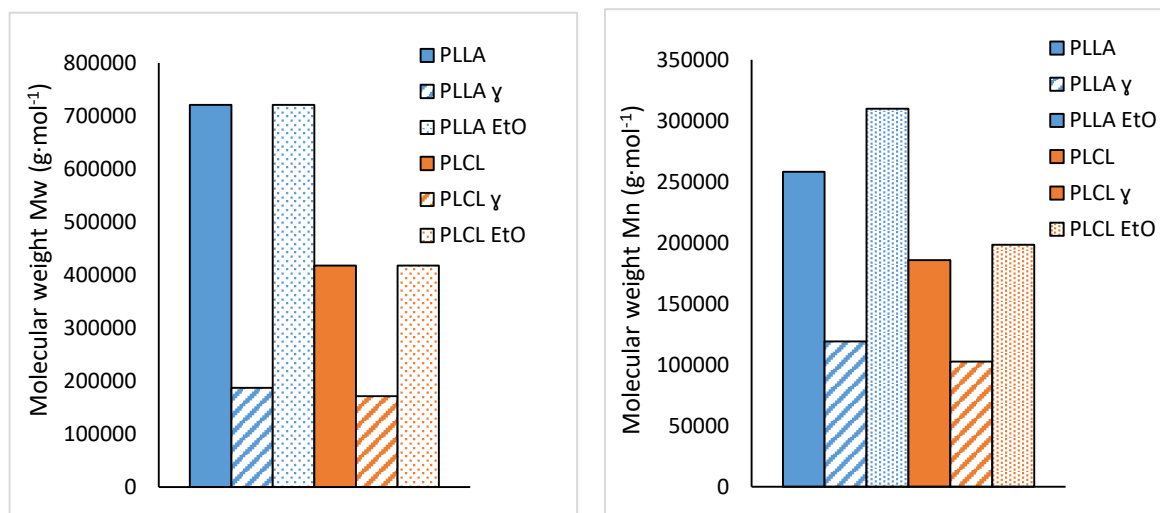


Figure 59. Molecular weight changes through GPC results.

These results show that after gamma radiation all the samples experienced polymer degradation while with ethylene oxide sterilization there is no significant degradation.

4.5.4. Mechanical properties

Mechanical properties were analysed for samples before and after sterilization and results are shown in the next graphs (Figure 60 and 61). In general, big variability has been observed for results of all conditions. No significant differences were observed ($p > 0.05$) for values of force. Regarding elastic recovery, significant differences between PLLA with PLLA γ ($p < 0.05$) or with PLLA EtO ($p < 0.001$) were found.

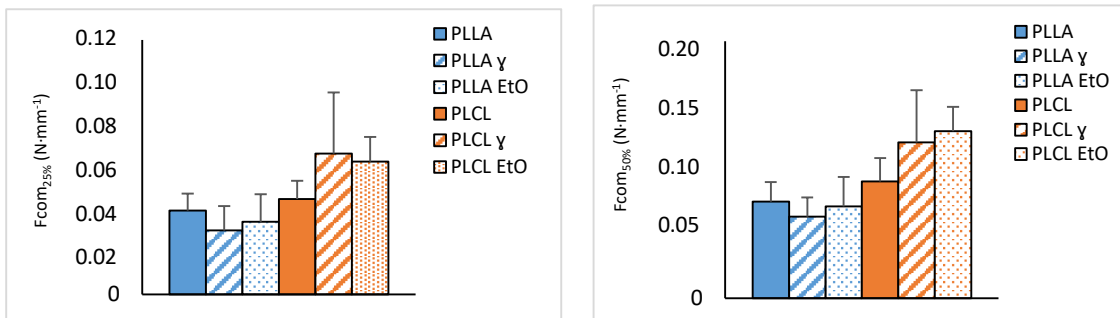


Figure 60. Compression force normalized by length for each sterilization technique.

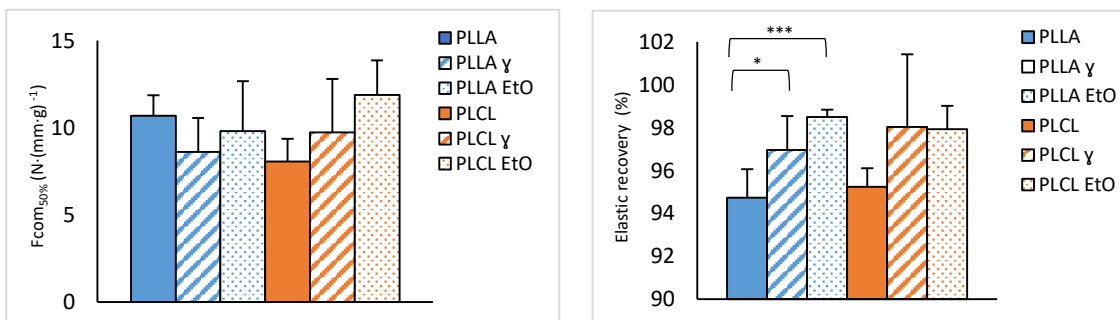


Figure 61. Compression force normalized by weight and length (left) and elastic recovery results (right) for each sterilization technique.

What can be surely said is that gamma radiation produces higher deviation on the results which shows that chain scission and crystallinity changes discussed in Chapter 4.5.2 induces more heterogeneous values in mechanical properties than EtO. None of the conditions broke in the compression test but with these results it can be concluded that EtO sterilization affects less to the materials properties than gamma radiation.

To sum up, results obtained for gamma sterilization processes showed significant differences on crystallinity, decrease on molecular weight and higher standard deviation of mechanical properties. On the other hand, ethylene oxide sterilization did not show any significant change. The increase on percentage of crystallinity for irradiated samples is attributed to the scission of the tie molecules. This effect is corroborated with GPC analysis, which shows a high decrease on molecular weight as a cause of the polymer degradation.

Tie molecules keep the distance of the amorphous areas of the polymer. When there is scission of the tie molecules, there is a growth of the crystal lamellar areas. Thus, increasing percentage of crystallinity of the polymer as seen in the present study.

Nuutinen et al. [39] also reported that EtO did not markedly affect the mechanical properties of the samples after PLLA samples sterilization compared with gamma irradiation and electron beam which corresponds with the present study.

5. CONCLUSIONS

The main objective of this project was the production of PLLA or PLCL BRSs with micropatterning by means of 3D printing through solvent-cast direct-writing (SC-DW). To improve micropatterning surface definition, a solvent trap was designed and built as an accessory for the 3D Printer in order to reduce solvent evaporation while printing. Furthermore, the study of stent properties under degradation conditions was carried out. Properties of the stents before and after different sterilization process were also evaluated.

PLLA and PLCL inks showed non-Newtonian results after injectability evaluation. Different rheological curves for each ink were obtained. PLLA showed a higher viscosity compared with PLCL as was expected due to its higher molecular weight.

The fabrication of PLLA and PLCL biodegradable stents with micropatterning by 3D printing was successfully achieved. SEM images of micropatterned stents' topography showed that the addition of a solvent trap improved PLLA behaviour. More micropatterning definition was achieved in comparison to stents manufactured without the 3D printer accessory. PLCL stents showed good behaviour on both conditions, with and without patterning, since it presented lower solvent evaporation rate while printing in comparison to PLLA.

On the other hand, accelerated degradation of the stents through alkaline medium was successfully performed. Morphology analysis showed a thinning effect of the stents over degradation time since surface erosion took place. Afterwards, the material was shaved off from the bulk which resulted in intact molecular weight and high mass loss. NMR analysis of PLCL showed monomer relation ratio over degradation. Results revealed that LA monomer degraded faster than CL monomer. Thermal analysis did not show dramatic differences over degradation time. Crystallinity studies revealed a slightly decrease over degradation due to hydrolysis reactions. Thermogram curves showed a gradual loss of the glass transition temperature peak as a result of the degradation of the amorphous parts of the polymer. Mechanical properties showed a good behaviour since none of the samples broke and a gradual decrease was formed as a result of decreased strut thickness. However, compression of PLLA at day 10 of degradation could not be performed since the material was highly degraded.

As a matter of a fact, results of characterization studies of degraded stents provide strong evidence to support that the hydrolysis mechanism performed in this project was surface degradation.

On the other hand, stent evaluation after a process of gamma or ethylene oxide sterilization was carried out. Thermal values presented unchanged results for the ethylene oxide process while there is a dramatic increase of crystallinity after gamma radiation. Big changes on the glass transition temperature and the melting temperature for gamma radiation sterilization were obtained, while no significant differences after ethylene oxide sterilization appeared. It is clear that gamma radiation damaged the polymer's structure corresponding to the scission of the strained tie molecules according to literature. Concerning mechanical properties after sterilization, huge differences were seen between the different sterilization processes. Samples subjected to gamma radiation had a higher variability in comparison with the samples sterilized through ethylene oxide. However, none of the samples broke in compression testing showing positive results. Regarding molecular weight changes, a dramatic decrease on M_w after gamma sterilization confirmed the degradation of the polymer after the irradiation processes.

In conclusion, ethylene oxide sterilization did not show any effect to the material's properties while huge differences on M_w and crystallinity were found in gamma radiation. Therefore, ethylene oxide should be the preferred method for the sterilization of the stents.

6. FUTURE WORKS

The obtention of micropatterned stents give rise to the next future goal: biological characterization. In previous works, patterned and biofunctionalized PLLA films were characterized obtaining improved cell migration. Therefore, the next step should be to functionalize the micropatterned stents produced in the present work with the improved printing efficiency conditions.

The obtained results on the accelerated degradation assay opens a new window of research. Since surface hydrolysis has been obtained in alkaline conditions, a comparison of a new accelerated assay showing bulk degradation would be interesting. Increasing the temperature instead of using an alkaline medium would be an easy way to accelerate hydrolysis through bulk mechanisms. Although it would take more time than in alkaline conditions, a more similar behaviour to the real mechanisms that occur in the body would be obtained according to literature. Also, the degradation rate could be evaluated with the linearity relationship between molecular weight and time degradation characteristic of bulk degradation. In addition, a non-accelerated degradation assay at long-term could be done. Therefore, a comparison between accelerated and non-accelerated conditions would be analysed.

Sterilization evaluation confirms that for future *in vivo* studies, ethylene oxide sterilization would have to be performed. However, even though FTIR analysis did not show any presence of residual ethylene oxide, a cytotoxicity assay would be needed in order to be sure that sterilized stents are completely able to be placed into the body without producing any damage.

With GPC analysis, a significant reduction in molecular weight has been seen in comparison to the theoretical raw material M_w . Actually, a GPC analysis of the raw materials is currently in process in order to understand if the polymer degradation came from the raw materials or during the manufacturing process of the stents.

In general, 3D printing process for bioresorbable stents, opens up new possibilities in research for the rapid production of customised medical solutions patient-specific, combined with a low price manufacturing process.

7. COSTS

The present section shows the global cost of this project. It includes the time equipment used, human resources as well as material costs. The reference price has been obtained from specific price quotes and from the Research Center in Multiscale Science and Engineering website. The total cost of the project estimation is 17432.23 euros.

RAW MATERIALS			
DESCRIPTION	QUANTITY	PRICE	COST (€)
PLLA PL65	0.0055 kg	1878.30 €/kg	10.33
PLCL PLC9538	0.0075 kg	5904 €/kg	44.28
Chloroform (≥99.5%)	0.115 L	108 €/5L	2.48
NaOH pellets	0.04 kg	35.19 €/kg	1.41
PET sheet 5mm 50x60	2	25.55 €/1 uts	51.10
Adhesive Plasteceys Blister	1	3.65 €/1 uts	3.65
TOTAL			113.25
CHARACTERIZATION TECHNIQUES			
DESCRIPTION	QUANTITY	PRICE	COST (€)
OM	3	9 €/h	27
FE-SEM	2.5	187.50 €/h	468.75
GPC	14 samples	530 €/14 samples	530
NMR	3	90 €/h	270
FTIR	2	22.50 €/h	45
Technical Assistance	4.5	80 €/h	360
TOTAL			1700.75
STERILIZATION			
DESCRIPTION	QUANTITY	PRICE	COST (€)
Gamma	1 box	65 €/1 box	65
Ethylene Oxide	1 box	./.	./.
TOTAL			65
LABORATORY MATERIAL			
DESCRIPTION	QUANTITY	PRICE	COST (€)
Speed mixer PP recipient 25mL	26 uts	28 €/100 uts	7.28
24-well plate	2 uts	46.50 €/50uts	1.86
5 ml pipette	26 uts	32 €/250uts	3.33
Capillary tip Ø410µm blue Nordson	6 uts	58.94 €/1box	3.54
Nozzle pink tip Ø250µm Nordson	26 uts	60.76 €/1box	15.80
Parafilm	3m	18 €/38 m	1.42
Common lab equipment, paper, pliers, gloves...	./.	./.	100
Office material	./.	./.	20
TOTAL			153.23
SPECIALIZED PERSONNEL (5 months)			
DESCRIPTION	QUANTITY	PRICE	COST (€)
Project Chief Engineer (Thesis director)	10h/month	40 €/h	2000
Senior Engineer (PhD Student)	70h/month	20 €/h	7000
Junior Engineer (Author)	160h/month	8 €/h	6400
TOTAL			15400

8. REFERENCES

- [1] E. Wilkins, L. Wilson, K. Wickramasinghe, and P. Bhatnagar, "European Cardiovascular Disease Statistics 2017," *Eur. Hear. Netw.*, pp. 94–100, 2017, [Online]. Available: www.ehnheart.org.
- [2] C. McCormick, "Overview of cardiovascular stent designs," in *Functionalised Cardiovascular Stents*, Elsevier, 2018, pp. 3–26.
- [3] A. Taki, A. Kermani, S. M. Ranjarnavazi, and A. Pourmodheji, "Overview of Different Medical Imaging Techniques for the Identification of Coronary Atherosclerotic Plaques," in *Computing and Visualization for Intravascular Imaging and Computer-Assisted Stenting*, 1st ed., Elsevier, 2017, pp. 79–106.
- [4] P. Manning and E. H. Awtry, "Unstable Angina: Presentation, Diagnosis, and Management," in *Encyclopedia of Cardiovascular Research and Medicine*, Elsevier, 2018, pp. 606–615.
- [5] X. Wang, J. L. Rutkowsky, and G. Z. Feuerstein, "Imaging and molecular biomarkers of vulnerable atheromatous plaques," *Biomark. Med.*, vol. 1, no. 1, pp. 23–35, Jun. 2007, doi: 10.2217/17520363.1.1.23.
- [6] J. L. Anderson and D. A. Morrow, "Acute Myocardial Infarction," *N. Engl. J. Med.*, vol. 376, no. 21, pp. 2053–2064, May 2017, doi: 10.1056/NEJMra1606915.
- [7] P. José *et al.*, "Original Article Stent versus Coronary Artery Bypass Surgery in Multi-Vessel and Left Main Coronary Artery Disease : A Meta-Analysis of Randomized Trials with Subgroups Evaluation," pp. 511–523, 2018, doi: 10.5935/abc.20190027.
- [8] B. Tomberli, A. Mattesini, G. I. Baldereschi, and C. Di Mario, "Breve historia de los stents coronarios," *Rev. Española Cardiol.*, vol. 71, no. 5, pp. 312–319, May 2018, doi: 10.1016/j.recesp.2017.11.016.
- [9] D. Buccheri, D. Piraino, G. Andolina, and B. Cortese, "Understanding and managing in-stent restenosis: A review of clinical data, from pathogenesis to treatment," *J. Thorac. Dis.*, vol. 8, no. 10, pp. E1150–E1162, 2016, doi: 10.21037/jtd.2016.10.93.
- [10] K. D. Rizas and J. Mehili, "Stent polymers: Do they make a difference?," *Circ. Cardiovasc. Interv.*, vol. 9, no. 6, pp. 1–13, 2016, doi: 10.1161/CIRCINTERVENTIONS.115.002943.
- [11] D. Capodanno, "Bioresorbable Scaffolds in Coronary Intervention: Unmet Needs and Evolution," *Korean Circ. J.*, vol. 48, no. 1, p. 24, 2018, doi: 10.4070/kcj.2017.0194.
- [12] W. A. Omar and D. J. Kumbhani, "The Current Literature on Bioabsorbable Stents: a Review," *Curr. Atheroscler. Rep.*, vol. 21, no. 12, p. 54, Dec. 2019, doi: 10.1007/s11883-019-0816-4.
- [13] S. McMahon *et al.*, "Bio-resorbable polymer stents : a review of material progress and prospects," *Prog. Polym. Sci.*, vol. 83, pp. 79–96, 2018, doi: 10.1016/j.progpolymsci.2018.05.002.
- [14] O. Avinc and A. Khoddami, "Part I : Production ,properties , performance , environmental impact and end-use applications of Poly (lactic acid)fibres," in *Overview of poly(lactic acid) (PLA) fibre*, vol. 41, no. 6, 2009, pp. 16–25.

- [15] C. M. Pistor, M. Atif Yardimci, K. J. Jasiak, and S. I. Guceri, *Thermal conductivity of composite materials*, vol. 28. Elsevier Inc., 1996.
- [16] W. W. li, T. P. Web, A. Polymerization, and C. Polymerization, "Introduction to Plastics and Elastomers," in *Chemical Resistance of Thermoplastics*, W. A. W. and S. Ebnesajjad, Ed. 2012, pp. xxi–xxxiv.
- [17] J. Fernández, A. Etxeberria, and J.-R. Sarasua, "Synthesis, structure and properties of poly(L-lactide-co-caprolactone) statistical copolymers," *J. Mech. Behav. Biomed. Mater.*, vol. 9, pp. 100–112, May 2012, doi: 10.1016/j.jmbbm.2012.01.003.
- [18] S. McMahon *et al.*, "Bio-resorbable polymer stents: a review of material progress and prospects," *Prog. Polym. Sci.*, vol. 83, pp. 79–96, Aug. 2018, doi: 10.1016/j.progpolymsci.2018.05.002.
- [19] A. C. Vieira, J. C. Vieira, R. M. Guedes, and A. T. Marques, "Experimental Degradation Characterization of PLA-PCL, PGA-PCL, PDO AND PGA fibers," *Mater. Sci. Forum*, vol. 636, no. 637, pp. 825–832, 2010, [Online]. Available: http://scholar.google.com/citations?view_op=view_citation&hl=en&user=MTV5c-4AAAAJ&citation_for_view=MTV5c-4AAAAJ:d1gkVwhDpl0C.
- [20] G. Gorrasi and R. Pantani, "Hydrolysis and Biodegradation of Poly(lactic acid)," no. May, pp. 119–151, 2017, doi: 10.1007/12_2016_12.
- [21] A. C. Vieira, J. C. Vieira, J. M. Ferra, F. D. Magalhães, R. M. Guedes, and A. T. Marques, "Mechanical study of PLA-PCL fibers during in vitro degradation," *J. Mech. Behav. Biomed. Mater.*, vol. 4, no. 3, pp. 451–460, 2011, doi: 10.1016/j.jmbbm.2010.12.006.
- [22] C. X. F. Lam, M. M. Savalani, S. H. Teoh, and D. W. Hutmacher, "Dynamics of in vitro polymer degradation of polycaprolactone-based scaffolds: Accelerated versus simulated physiological conditions," *Biomed. Mater.*, vol. 3, no. 3, 2008, doi: 10.1088/1748-6041/3/3/034108.
- [23] N. A. Weir, F. J. Buchanan, J. F. Orr, and G. R. Dickson, "Degradation of poly-L-lactide. Part 1: In vitro and in vivo physiological temperature degradation," *Proc. Inst. Mech. Eng. Part H J. Eng. Med.*, vol. 218, no. 5, pp. 307–319, 2004, doi: 10.1243/0954411041932782.
- [24] C. Humberto Valencia, "Hydrolytic degradation and in vivo resorption of poly-L-lactic acid-chitosan biomedical devices in the parietal bones of Wistar rats," *J. Int. Med. Res.*, vol. 47, no. 4, pp. 1705–1716, Apr. 2019, doi: 10.1177/0300060519828935.
- [25] S. Li, H. Garreau, and M. Vert, "Structure-property relationships in the case of the degradation of massive poly(α -hydroxy acids) in aqueous media - Part 3 Influence of the morphology of poly(L-lactic acid)," *J. Mater. Sci. Mater. Med.*, vol. 1, no. 4, pp. 198–206, 1990, doi: 10.1007/BF00701077.
- [26] N. D. Miller and D. F. Williams, "The in vivo and in vitro degradation of poly(glycolic acid) suture material as a function of applied strain," *Biomaterials*, vol. 5, no. 6, pp. 365–368, 1984, doi: 10.1016/0142-9612(84)90037-1.
- [27] J. Ferreira, A. Gloria, S. Cometa, J. F. J. Coelho, and M. Domingos, "Effect of in vitro enzymatic degradation on 3D printed poly(ϵ -caprolactone) scaffolds: Morphological, chemical and mechanical properties," *J. Appl. Biomater. Funct. Mater.*, vol. 15, no. 3, pp. e185–e195, 2017, doi: 10.5301/jabfm.5000363.
- [28] N. A. Weir, F. J. Buchanan, J. F. Orr, D. F. Farrar, and G. R. Dickson, "Degradation of poly-L-lactide. Part 2: Increased temperature accelerated degradation," *Proc. Inst. Mech. Eng. Part H J. Eng. Med.*, vol. 218, no. 5, pp. 321–330, May 2004, doi: 10.1243/0954411041932809.

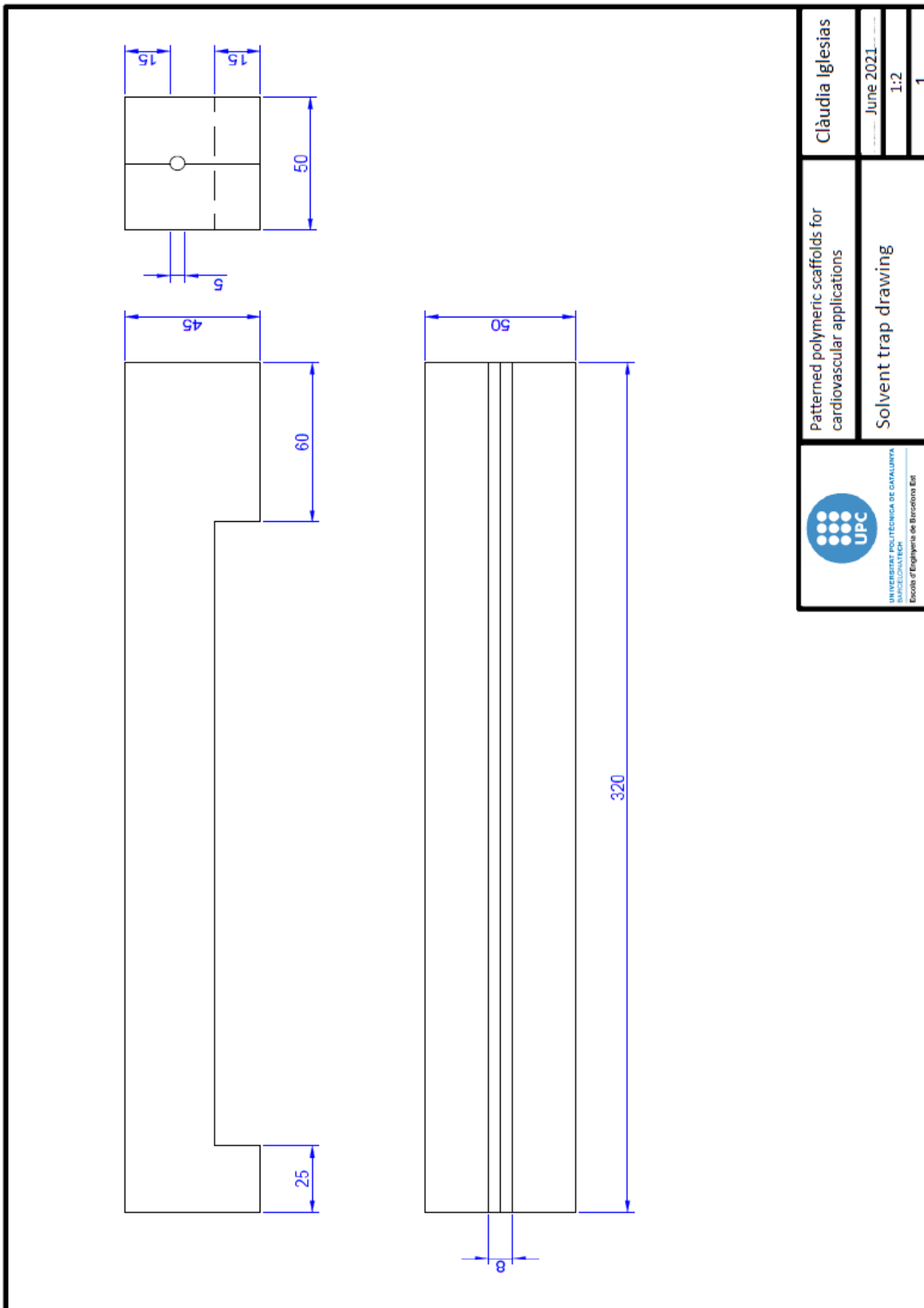
- [29] L. N. Woodard and M. A. Grunlan, "Hydrolytic Degradation of PCL-PLLA Semi-IPNs Exhibiting Rapid, Tunable Degradation," *ACS Biomater. Sci. Eng.*, vol. 5, no. 2, pp. 498–508, 2019, doi: 10.1021/acsbmaterials.8b01135.
- [30] A. Guerra, A. Roca, and J. de Ciurana, "A novel 3D additive manufacturing machine to biodegradable stents," *Procedia Manuf.*, vol. 13, pp. 718–723, 2017, doi: 10.1016/j.promfg.2017.09.118.
- [31] A. J. Guerra Sánchez, "Contribution to Bioabsorbable Stent Manufacture With Additive Manufacturing Technologies," p. 239, 2019, [Online]. Available: <https://www.tdx.cat/handle/10803/667867#page=1>.
- [32] S.-Z. Guo, F. Gosselin, N. Guerin, A.-M. Lanouette, M.-C. Heuzey, and D. Therriault, "Solvent-Cast Three-Dimensional Printing of Multifunctional Microsystems," *Small*, vol. 9, no. 24, pp. 4118–4122, Dec. 2013, doi: 10.1002/sml.201300975.
- [33] C. S. Chen, M. Mrksich, S. Huang, G. M. Whitesides, and D. E. Ingber, "Micropatterned Surfaces for Control of Cell Shape, Position, and Function," vol. 7938, no. 98, pp. 356–363, 1998.
- [34] S. Jana, "Endothelialization of cardiovascular devices," *Acta Biomater.*, vol. 99, pp. 53–71, 2019, doi: 10.1016/j.actbio.2019.08.042.
- [35] Y. Shen, G. Wang, L. Chen, H. Li, P. Yu, and M. Bai, "Investigation of surface endothelialization on biomedical nitinol (NiTi) alloy : Effects of surface micropatterning combined with plasma nanocoatings," *Acta Biomater.*, vol. 5, no. 9, pp. 3593–3604, 2009, doi: 10.1016/j.actbio.2009.05.021.
- [36] Y. E. Saleh, M. A. Gepreel, and N. K. Allam, "Functional Nanoarchitectures For Enhanced Drug Eluting Stents," *Nat. Publ. Gr.*, pp. 1–12, 2017, doi: 10.1038/srep40291.
- [37] S. Choudhary, M. Berhe, K. M. Haberstroh, and T. J. Webster, "Increased endothelial and vascular smooth muscle cell adhesion on nanostructured titanium and CoCrMo," *Int. J. Nanomedicine*, vol. 1, no. 1, pp. 41–50, Jan. 2006, doi: 10.2147/nano.2006.1.1.41.
- [38] Z. Dai, J. Ronholm, Y. Tian, B. Sethi, and X. Cao, "Sterilization techniques for biodegradable scaffolds in tissue engineering applications," *J. Tissue Eng.*, vol. 7, p. 204173141664881, Jan. 2016, doi: 10.1177/2041731416648810.
- [39] J. P. Nuutinen, C. Clerc, T. Virta, and P. Törmälä, "Effect of gamma, ethylene oxide, electron beam, and plasma sterilization on the behaviour of SR-PLLA fibres in vitro," *J. Biomater. Sci. Polym. Ed.*, vol. 13, no. 12, pp. 1325–1336, 2002, doi: 10.1163/15685620260449723.
- [40] M. Haim Zada, A. Kumar, O. Elmalak, G. Mechrez, and A. J. Domb, "Effect of Ethylene Oxide and Gamma (γ -) Sterilization on the Properties of a PLCL Polymer Material in Balloon Implants," *ACS Omega*, vol. 4, no. 25, pp. 21319–21326, 2019, doi: 10.1021/acsomega.9b02889.
- [41] S. Lerouge, "Sterilization and cleaning of metallic biomaterials," in *Metals for Biomedical Devices*, 2nd ed., Elsevier, 2019, pp. 405–428.
- [42] N. P. Tipnis and D. J. Burgess, "Sterilization of implantable polymer-based medical devices: A review," *Int. J. Pharm.*, vol. 544, no. 2, pp. 455–460, 2018, doi: 10.1016/j.ijpharm.2017.12.003.
- [43] F. Hasanain, K. Guenther, W. M. Mullett, and E. Craven, "Gamma sterilization of pharmaceuticals - A review of the irradiation of excipients, active pharmaceutical ingredients, and final drug product formulations," *PDA J. Pharm. Sci. Technol.*, vol. 68, no. 2, pp. 113–137, 2014, doi: 10.5731/pdajpst.2014.00955.


- [44] R. Schieber *et al.*, "Direct Laser Interference Patterning of CoCr Alloy Surfaces to Control Endothelial Cell and Platelet Response for Cardiovascular Applications," *Adv. Healthc. Mater.*, vol. 6, no. 19, pp. 1–14, 2017, doi: 10.1002/adhm.201700327.
- [45] T. Committee and ISO/TC 198, "ISO11137 Sterilization of health care products — Radiation," p. 41.
- [46] T. C.: I. 198, "ISO 11135:2014 Sterilization of health-care products — Ethylene oxide — Requirements for the development, validation and routine control of a sterilization process for medical devices." p. 78, [Online]. Available: <https://www.iso.org/standard/56137.html>.
- [47] M. Barczewski and O. Mysiukiewicz, "Rheological and processing properties of poly(lactic acid) composites filled with ground chestnut shell," *Polym.*, vol. 42, no. 2, pp. 267–274, 2018, doi: 10.7317/pk.2018.42.2.267.
- [48] Z. Zhang and S. G. Hatzikiriakos, "Entry pressure correlations in capillary flow," *Phys. Fluids*, vol. 32, no. 7, p. 073106, Jul. 2020, doi: 10.1063/5.0017922.
- [49] A. M. F. R. Pinto, V. B. Oliveira, and D. S. Falcão, "Experimental methods of characterization," in *Direct Alcohol Fuel Cells for Portable Applications*, Elsevier, 2018, pp. 113–155.
- [50] H. Garbacz and A. Królikowski, "Corrosion resistance of nanocrystalline titanium," in *Nanocrystalline Titanium*, Elsevier, 2019, pp. 145–173.
- [51] D. Sun, M. O. R. Siddiqui, and K. Iqbal, "Specialty testing techniques for smart textiles," in *Smart Textile Coatings and Laminates*, Elsevier, 2019, pp. 99–116.
- [52] H. U. of Berlin, "Investigation of Polymers with Differential Scanning Calorimetry," *Adv. Lab DSC Investig. Polym.*, pp. 1–17, 2009.
- [53] R. Xu, J. Xie, and C. Lei, "Influence of melt-draw ratio on the crystalline behaviour of a polylactic acid cast film with a chi structure," *RSC Adv.*, vol. 7, no. 63, pp. 39914–39921, 2017, doi: 10.1039/c7ra05422j.
- [54] D. Cam, S. hyu Hyon, and Y. Ikada, "Degradation of high molecular weight poly(l-lactide) in alkaline medium," *Biomaterials*, vol. 16, no. 11, pp. 833–843, 1995, doi: 10.1016/0142-9612(95)94144-A.
- [55] S. Sánchez-González, N. Diban, and A. Urriaga, "Hydrolytic degradation and mechanical stability of poly(ϵ -Caprolactone)/reduced graphene oxide membranes as scaffolds for in vitro neural tissue regeneration," *Membranes (Basel)*, vol. 8, no. 1, 2018, doi: 10.3390/membranes8010012.
- [56] R. Naseem, L. Zhao, S. K. Eswaran, and H. Willcock, "Characterization of biodegradable poly(l-lactide) tube over accelerated degradation," *Polym. Eng. Sci.*, vol. 60, no. 7, pp. 1430–1436, 2020, doi: 10.1002/pen.25390.
- [57] O. Dragostin and L. Profire, "Molecular weight of polymers used in biomedical applications," in *Characterization of Polymeric Biomaterials*, Elsevier, 2017, pp. 101–121.
- [58] P. H. Geil, "Polymer Characterization," in *Modern Textile Characterization Methods*, CRC Press, 2017, pp. 9–143.
- [59] C. Causserand and P. Aimar, "Characterization of Filtration Membranes," in *Comprehensive Membrane Science and Engineering*, vol. 1, Elsevier, 2010, pp. 311–335.
- [60] J. M. Anderson and G. Voskerician, "The challenge of biocompatibility evaluation of biocomposites," in *Biomedical Composites*,

Elsevier, 2010, pp. 325–353.

- [61] Rajendra P. Chhabra, “Non-Newtonian Fluids: An Introduction,” in *Rheology of Complex Fluids*, vol. 53, no. 9, 2013, pp. 1689–1699.
- [62] S. Z. Guo, F. Gosselin, N. Guerin, A. M. Lanouette, M. C. Heuzey, and D. Therriault, “3D Printing: Solvent-cast three-dimensional printing of multifunctional microsystems,” *Small*, vol. 9, no. 24, pp. 4118–4122, 2013, doi: 10.1002/sml.201300975.
- [63] K.Sungsanit, “Rheological and Mechanical Behaviour of Poly (Lactic Acid)/Polyethylene Glycol Blends,” no. March, pp. 1–305, 2011.
- [64] J. F. Cortes, “3D printing of patient specific bioresorbable cardiovascular stents,” 2017, doi: <http://resolver.tudelft.nl/uuid:ad6e95ffe466-451e-a2e9-bac2eee487d2>.
- [65] A. Sakamoto, H. Jinnouchi, S. Torii, R. Virmani, and A. V. Finn, “Understanding the impact of stent and scaffold material and strut design on coronary artery thrombosis from the basic and clinical points of view,” *Bioengineering*, vol. 5, no. 3, pp. 1–19, 2018, doi: 10.3390/bioengineering5030071.
- [66] Goremedical, “Mechanical Properties of Nitinol Stents and Stent-Grafts: Comparison of 6mm Diameter,” *Devices .L. Gore Assoc. Inc.*, 2011.
- [67] A. Shrivastava, “Polymerization,” in *Introduction to Plastics Engineering*, S. C. Ameta, P. B. Punjabi, R. Ameta, and C. Ameta, Eds. Elsevier, 2018, pp. 17–48.
- [68] A. Göpferich and J. Tessmar, “Polyanhydride degradation and erosion,” *Adv. Drug Deliv. Rev.*, vol. 54, no. 7, pp. 911–931, 2002, doi: 10.1016/S0169-409X(02)00051-0.
- [69] 2 NEERAJ KUMAR1 KALPNA GARKHAL, SHALINI VERMA, 1 S. JONNALAGADDA, “Fast Degradable Poly(L-lactide-co-ε-caprolactone) Microspheres for Tissue Engineering: Synthesis, Characterization, and Degradation Behavior,” *J. Polym. Sci. Part A Polym. Chem.*, vol. 46, no. April, pp. 7207–7224, 2007, doi: 10.1002/pola.
- [70] N. I. of S. and Technology, “Ethylene Oxide,” *Libro del Web de Química del NIST, SRD 69*, 2021. <https://webbook.nist.gov/cgi/cbook.cgi?ID=75-21-8&Type=IR-SPEC&Index=QUANT-IR,1#IR-SPEC>.
- [71] M. Savaris, V. dos Santos, and R. N. Brandalise, “Influence of different sterilization processes on the properties of commercial poly(lactic acid),” *Mater. Sci. Eng. C*, vol. 69, pp. 661–667, 2016, doi: 10.1016/j.msec.2016.07.031.
- [72] D. Milicevic, S. Trifunovic, S. Galovic, and E. Suljovrujic, “Thermal and crystallization behaviour of gamma irradiated PLLA,” *Radiat. Phys. Chem.*, vol. 76, no. 8–9, pp. 1376–1380, 2007, doi: 10.1016/j.radphyschem.2007.02.035.
- [73] C. West, R. McTaggart, T. Letcher, D. Raynie, and R. Roy, “Effects of gamma irradiation upon the mechanical and chemical properties of 3D-printed samples of polylactic acid,” *J. Manuf. Sci. Eng. Trans. ASME*, vol. 141, no. 4, 2019, doi: 10.1115/1.4042581.
- [74] A. Agüero *et al.*, “Study of the influence of the reprocessing cycles on the final properties of polylactide pieces obtained by injection molding,” *Polymers (Basel)*, vol. 11, no. 12, 2019, doi: 10.3390/polym11121908.

9. ANNEX



 UNIVERSITAT POLITÈCNICA DE CATALUNYA BARCELONATECH Escola d'Enginyeria de Barcelona Est	Patterned polymeric scaffolds for cardiovascular applications	Clàudia Iglesias
	Solvent trap drawing	June 2021
		1:2
		1